Silica-based composite nanoparticles as pH-responsive drug carriers and their application in contact lens drug delivery

by

Xin Fan

A thesis submitted to the Graduate Faculty of
Auburn University
in partial fulfillment of the
requirements for the Degree of
Doctor of Philosophy

Auburn, Alabama
August 5, 2017

Key words: silica sol-gel encapsulation, pH-responsive polymers, controlled drug delivery, contact lens drug delivery

Copyright 2017 by Xin Fan

Approved by

Dr. Allan E. David, Chair, Assistant Professor of Chemical Engineering
Dr. W. Robert Ashurst, Committee Member, Associate Professor of Chemical Engineering
Dr. Elizabeth Lipke, Committee Member, Associate Professor of Chemical Engineering
Dr. Arthur Yang, Committee Member, President of ISTN, Inc

Abstract

Controlled drug delivery from contact lenses is an attractive method to treat ocular disease, like glaucoma, as it overcomes the deficiencies of traditional eye drops, such as poor patient adherence and low bioavailability. With controlled delivery from contact lenses, drug molecules have a longer residence time in the post-lens tear film, which ultimately leads to a higher drug flux through the cornea and a lowered possibility of toxic side effects. The goal of this project is to design a novel contact lens device with integrated pH-responsive nanocomposite particles that trigger drug release under physiological pH conditions.

Biocompatible drug carriers, with the ability to control delivery of therapeutic agents, are a promising way to overcome the limitations of conventional therapies. Among all types of carriers, silica-based nanocomposites have emerged as a promising candidate because of its biocompatibility and high physical and chemical stability. Moreover, silica-based, pH-responsive nanocomposite materials can be produced by encapsulation of natural or synthetic pH-responsive polymers, such as alginate, chitosan, poly (methacrylic acid) and poly (acrylic acid). In this work, silica-alginate composite materials were prepared with different structures, such as alginate beads loaded with silica nanoparticles, silica-alginate monolithic gels, and silica-alginate nanoparticles. All of them showed a pH-responsive release of rhodamine B, which was used as a model drug.

In this dissertation, the focus was on pH-responsive silica-based composite nanoparticles synthesizes using silica sol-gel chemistry and formed in a water-in-oil microemulsion system. Different polymer (alginate, poly(methacrylic acid)) solutions were used as the water phase for the formation of silica-polymer nanoparticles. Nano-sized particles between 20-80 nm were detected by transmission electron microscopy. Silica-alginate composite nanoparticles showed no significant pH-responsive release of timolol maleate, which is a commonly used drug for glaucoma treatment. However, silica-PMAA nanoparticles displayed encouraging pH-responsive release of timolol maleate with only a fraction of drug released at low pH and then continuous, sustained release at physiological pH. These particles demonstrated the concept of ON/OFF triggered release with < 15% drug released under pH 2.5 and a long, sustained release of drug in simulated tear fluid.

The inclusion of nanoparticles did not adversely affect important properties of contact lens like optical clarity and water content. Encouraging pH-responsive release profiles were also observed for silica-PMAA nanoparticles incorporated contact lenses. Those lenses showed limited release of timolol maleate in low pH buffer solution and much higher release of timolol maleate in simulated tear fluid. This promising pH-responsive release performance of silica-PMAA nanoparticles incorporated contact lens shows the potential of a good candidate for commercial contact lens drug delivery vehicles.

Acknowledgments

First, I would first like to thank my advisor Dr. Allan E. David for his motivation and mentorship throughout the culmination of my PhD project and in the preparation of this dissertation. Dr. David has always been available when needed. I have learned a lot from him, not only in scientific research skills but also in how to be a better person in life. Without his encouragement and guidance, this dissertation would not have been possible.

I would like to acknowledge my committee members, Dr. W. Robert Ashurst, Dr. Elizabeth Lipke, and Dr. Arthur Yang for their insightful comments and support. I would like to thank Dr. Maria Soledad Peresin as my university reader. I would also like to thank Dr. Virginia Davis, Dr. Maria Lujan Auad and Dr. Sushil Adhikari for the help of TGA characterization. I would like to thank Dr. Christopher Roberts, Dr. Rui Xu, and David Roe for the help of BET. I would like to thank Dr. Michael Miller for the help of TEM.

My sincere thanks also go to everyone at ISTN, Inc and Lynthera. Thanks for the expertise and support from Jeff Yang, Dr. Arthur Yang, Dr. Roman Domszy, and Dr. Naiping Hu.

I thank all the members of the David Lab, Dr. Young Suk Choi, Tareq Anani, Hunter Rogers, Alex Kelly, Alan Hanley, Prachi Sangle, Richard Cullum, Ricky Whitener, Barry Yeh, Camille Hanot, Chelsea Harris, Marjan Azadi. I would also like to thank Adam Milton, Evan Miler, Colton Martinez, Kelsie Williams, and Jessica Pinkston for their assistance with many

aspects of this work. I would also like to thank my friends who help me adjust the life in here and support me throughout this journey: Wenjian Guan, Peng Cheng, Shu Fang, Jingran Duan, Pengfei Zhao, Zixiu Wang, Chen Zhou, Jie Zhong, Xinquan Cheng, Pengcheng Li, Yuling Han, Nan Shi, Rong Zhao. I would also like to acknowledge the help from Dr. Mario Eden, Karen Cochran and Elaine Manning from chemical engineering department.

Last but not the least, this would not have been possible without the support and encouragement of my family. I would like to express the highest levels of gratitude to my parents and sister, for their relentless love and support over this PhD journey and my life in general.

Table of Contents

List of Tables

List of Figures

List of Abbreviations

TEOS	Tetraethoxysilane
TMOS	Tetramethoxysilane
THEOS	Tetrakis(2-hydroxyethyl) orthosilicate
PMAA	Poly (methacrylic acid)
AOT	Sulfosuccinic acid bis (2-ethylhexyl) ester sodium salt
NP-5	Polyoxyethylene (5) nonylphenyl ether
PLL	Poly-L-lysine
TEM	Transmission electron microscopy
SEM	Scanning electron microscope
TGA	Thermogravimetric analysis
IPN	Interpenetrated polymer networks

Chapter 1 Introduction

Glaucoma is one of the leading causes of irreversible blindness worldwide. In 2010, there were 60 million people had glaucoma, and this number may increase to 80 million by 2020.[1] Glaucoma is a group of ocular disorders that can result in optic nerve degeneration, often associated with increased intraocular pressure in the eye.[2] Even with proper treatment, approximately 10 % of glaucoma patients still experience vision loss.[3] There are two main types of glaucoma: open-angle and angle-closure. Open angle glaucoma is the most common form, which affects approximately 2.2 million people in American.[4]

Currently, all treatments for glaucoma mainly focus on reducing intraocular pressure. The most common method is the prescription of eye drops, which is required to be taken properly and regularly.[5] However, eye drop treatment has poor patient adherence and is very inefficient. For example, the persistence rates for glaucoma patients prescribed eye drops are generally lower than 50 % after the first year, which is largely associated with the inconvenience of tedious dosing regimen.[6] In addition, drug release from eye drops is characterized by a burst dosage upon administration, followed by a relatively short period of effective therapeutic concentration, and then a prolonged period of insufficient concentration. This profile results in poor drug absorption of only 5-10 %, with the remainder lost due to canalicular drainage, epiphora dilution, and poor patient technique.[7]

Developments in nanotechnology provide promising improvements for the drug delivery to the eye. Ocular drug delivery research has increasingly focused on the encapsulation of drugs into nanoparticles, liposomes, nanomicelles, nanosuspensions, and dendrimers that can target the

eye.[8] Drug loaded contact lens has also been an active area of research to develop an extended ocular drug delivery platform. Delivered from contact lens, drug molecules have a longer residence time in the post-lens tear film, which ultimately leads to higher drug flux through the cornea. Incorporating transport barriers into contact lenses for further sustained elution of drugs has been reported to give prolonged therapeutic levels of various drugs.[9] Storage stability is a major reason why this technology has been limited to commercialization. More specifically, while sustained release for up to a month has been demonstrated, all the lenses studied to date continue to release encapsulated drugs even while in their packaging, which limits commercial feasibility and provides unacceptable variability in efficacy. Drug loaded contact lens combined with nanoparticle provide an alternative way for the glaucoma treatment. This nanoparticle loaded contact lens can be used as a targeted, extended and controlled ocular drug delivery platform. The nanoparticles inside the contact lens can be engineered to control release the drug molecules base on different environment changing, such as temperature, pH, light, or enzyme.

The work presented in this dissertation focuses on the creation of a novel contact lens device that integrates pH-responsive nanoparticles to overcome many of these limitations mentioned above. First, in chapter 3, the pH-responsive control release ability of silica-alginate materials was tested by rhodamine B as a drug model. Secondly, in chapter 4, the synthesis and characterization of silica-alginate nanoparticles were studied. Next, in chapter 5, *in vitro* release studies were performed for silica-alginate nanoparticles with rhodamine B and timolol maleate, respectively. In chapter 6, silica-PMAA nanoparticles were also tested for *in vitro* release study of timolol maleate. In the end, how silica-based nanoparticle affected the contact lens properties, such as optical clarity and water content, was studied in chapter 7.

Chapter 2 Background

2.1 Silica-based nanocomposite materials

Nanocomposites are multiphase materials with one or more phases in nanosize dimension to enhance properties, such as thermal, mechanical, electrical, optical, or catalytic, relative to either of the single homogeneous constituents.[10] Among all types of nanocomposites, silica-based nanocomposites have attracted immense attention due to their attractive physicochemical properties. For example, silica material has been widely studied due to its high physical and chemical stability, silica also shows acceptable biocompatibility for biomedical applications.[11] Moreover, silica does not absorb light or interfere with magnetic fields, which retains original optical or magnetic properties of combined components.[12] Finally, hydroxyl groups on silica surface allow facile chemical modifications to other functional groups, including amines, thiols, and carboxyls, to develop diverse structures.[13] In addition, composite materials could combine the advantages of each single component and enhance their properties compared to that of individual component. For example, with the addition of stimuli-responsive polymer, this type of silica-polymer composite materials can be used as “smart” delivery vehicles. Silica provides effective solid support, and stimuli-responsive polymer controls the release of bioactive molecules. Silica sol-gel technique is a promising method to prepare silica-based nanocomposites materials, especially for silica-based composite nanoparticles.

2.1.1 Silica sol-gel process

The term “sol-gel” was first used in 1864 from Graham’s study about silica gels.[14] Sol is a stable liquid suspension of colloidal particles or polymers. Gel is a three-dimensional liquid matrix, in which cross-linked rigid colloidal particles or polymers form the submicrometer pores size network.[15] Silica sol-gel process refers to the transition from a colloidal silica sol suspension to a continuous silica gel network of interconnected solid particles with a liquid phase entrapped. This transition results from the hydrolysis and polycondensation of a silica sol-gel precursor, usually a silicon alkoxide, such as tetraethoxysilane (TEOS) or tetramethoxysilane (TMOS).[16] As shown in Figure 2.1, when most of the entrapped liquid is extracted as a gas phase from gel network under hypercritical condition like supercritical drying, the silica network does not collapse and a low density aerogel is produced. However, if most of the entrapped liquid is removed at or near ambient pressure by thermal evaporation, shrinkage of the gel network occurs, and xerogel is obtained in the end.[17]

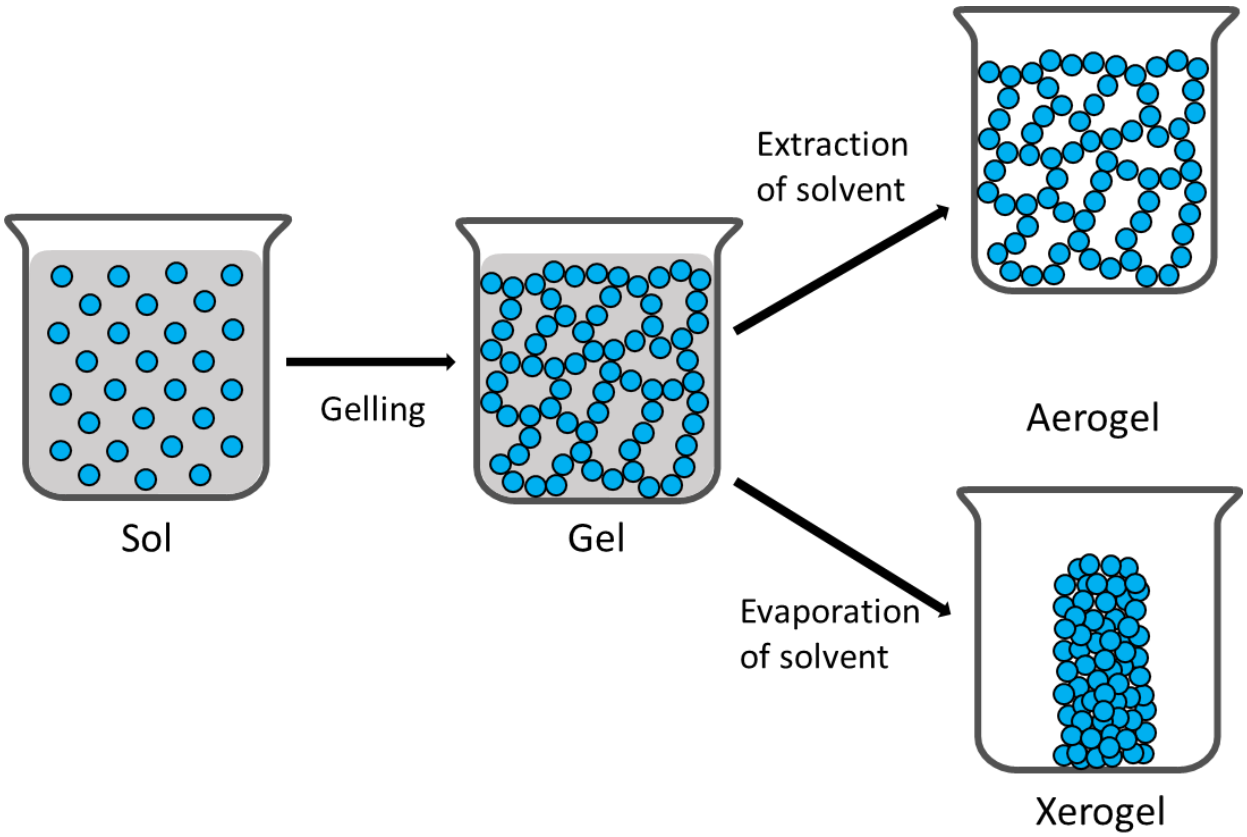

Figure 2.1 Illustration of the various stages of the sol-gel process.

There are three mainly studied silica sol-gel precursors. Silicic acid, sodium silicate, and silicon alkoxides.

Silicic acid

Silicic acid, $Si(OH)_4$, is the fully hydrolyzed product by silicon alkoxide. It can be made through ion exchange method from sodium silicate. However, at room temperature silicic acid is not stable, and it enters easily into polycondensation reactions to form a silica gel. Therefore, silicic acid requires to be freshly prepared every time. This time-consuming process restricts its use. [18]

Sodium silicate

Sodium silicate (Na_2SiO_3), also known as water glass, is another type of silica sol-gel precursor. Usually, hydrochloric acid is needed for the sol-gel processes of sodium silicate. A sol-gel transition is observed when the pH drops below 7. The chemical reaction of this transition is shown as below:

$$Na_2SiO_3 + 2HCl + (x-1)H_2O \longrightarrow SiO_2 \cdot xH_2O + 2NaCl$$

However, this produced could cause some compatibility issue, especially for the sol-gel encapsulation of some biomolecules, due to the addition of hydrochloric acid. Moreover, sodium silicate has a high ionic strength, which may be problematic, and the gel must be extensively washed to remove the considerable amount of salt.[19]

Silicon alkoxides

Silicon alkoxides, $Si(OR)_4$, are silicon esters with the general formula of the silicon atom linked to organic groups through an oxygen bridge. The most commercially used silicon alkoxide is tetraethoxysilane (TEOS). However, there are still some limitations on the sol-gel process with TEOS. Especially in the application of entrapment for biopolymers. As ethanol, produced during the sol-gel process, can affect the compatibility with biopolymers. For example, most polysaccharides precipitate when the ethanol is present in their aqueous solution, proteins are also sensitive to the presence of ethanol, which can cause unfolding and result in a denaturing effect.[20]

Among all three main types of silica precursors, silicon alkoxides are the most used due to their high purity and flexibility of the organic groups. Most of the silica nanoparticles are made by silicon alkoxides *via* Stöber process or microemulsion method.

Most silicon alkoxides are not water soluble, therefore, a mutual solvent, generally ethanol, is required for the hydrolysis reaction. For example, the sol-gel process of TEOS can be described as follows:

Hydrolysis

$$Si(OC_2H_5)_4 + H_2O \rightarrow Si(OC_2H_5)_x(OH)_{4-x} + C_2H_5OH$$

Condensation

$$\equiv Si - OC_2H_5 + \equiv Si - OH \rightarrow \equiv Si - O - Si \equiv + C_2H_5OH$$

$$\equiv Si - OH + \equiv Si - OH \rightarrow \equiv Si - O - Si \equiv + H_2O$$

This process can be divided into three stages: (1) Partial hydrolysis of TESO after mixing with water, which leads to the formation of silanols; (2) condensation reactions between either two silanols or a silanol and an ethoxy group to form a siloxane (Si-O-Si) network with releasing water or ethanol; (3) sol nanoparticles transit to gel network by crosslinking.[17]

However, the overall sol-gel process is a slow reaction. This is due to the low polarity of the Si-O bond in silicon alkoxides will inhibit hydrolysis and condensation rates. Therefore, a catalyst is usually needed to increase the hydrolysis and condensation rates. Mineral acids or ammonia are generally used as catalysts in silica sol-gel process, other known catalysts are acetic

acid, potassium hydroxide, amines, hydrofluoric acid, titanium alkoxides, and vanadium alkoxides.[21] The hydrolysis and condensation reaction rates are also pH dependent. In acidic conditions, the relative rate of hydrolysis reaction is faster than condensation reaction. At pH 5 the two reactions have the same relative rates and under basic conditions, the condensation reaction is faster than the hydrolysis reaction.[22]

For the silica sol-gel mechanism under acidic condition as shown in Figure 2.2, for hydrolysis reaction, an alkoxy group bonded to Si atom is rapidly protonated, which makes Si atom more electrophilic and attractable to a water molecule, followed by formation of a positively charged five-coordinate transition state which can transfer to inversion of the silicon tetrahedron and release an alcohol. Then, condensation reaction proceeds *via* a rapid formation of a charged intermediate by reaction with a proton, followed by a slow attack of a second neutral silicon species on this intermediate. More specifically, in acidic condition the transition state is positively charged and stabilized by electron donating alkoxy groups, therefore less substituted $(RO)_3SiOH$ condense faster than $(RO)_2Si(OH)_2$, which condenses faster than $ROSi(OH)_3$ and $Si(OH)_4$. This means that for acid catalyzed reaction, the first step of hydrolysis is the fastest, and the product of this first step undergoes the fastest condensation. Consequently, an open network initially forms, followed by further hydrolysis and cross-condensation reactions. In the end, silica gels with a texture closer to that of polymeric gels derived from organic chemistry are obtained.[24]

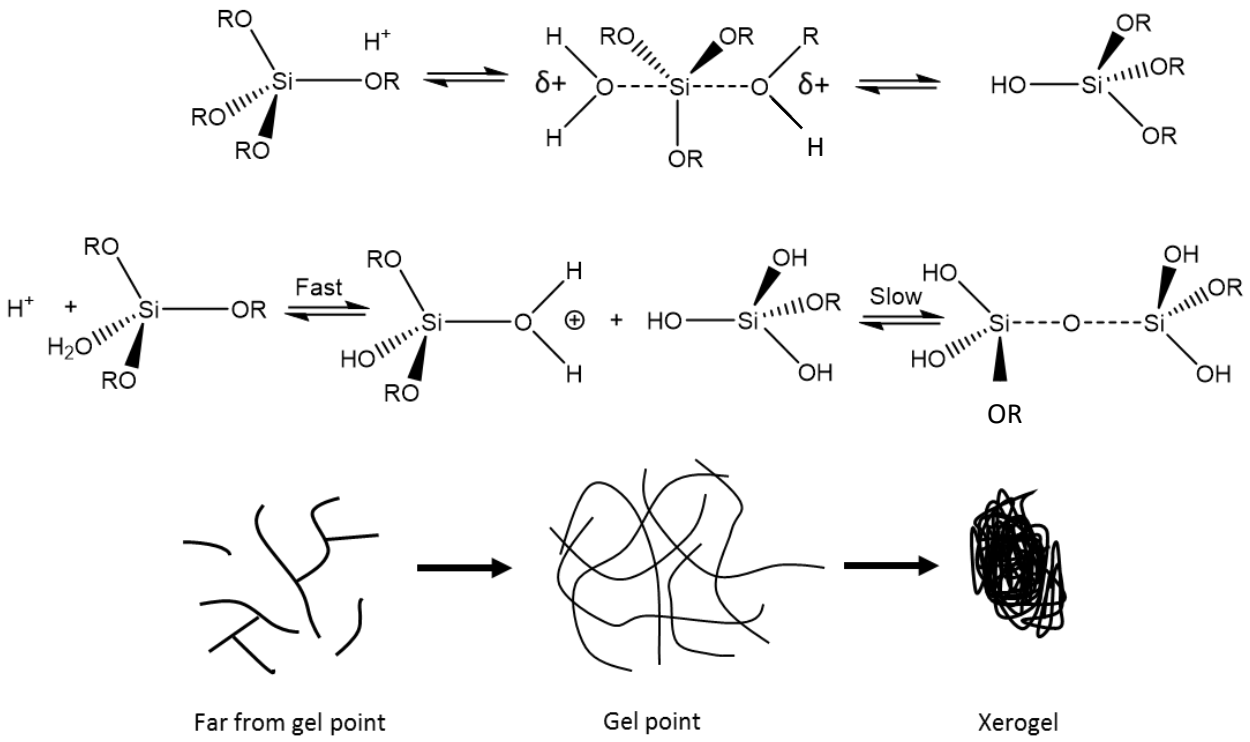

Figure 2.2 Hydrolysis and condensation of silicon alkoxide under acidic condition.[17]

In basic condition as shown in Figure 2.3, for hydrolysis reaction, water first rapidly dissociates to produce nucleophilic hydroxyl anions. The hydroxyl anion then attacks the silicon atom to form a negatively charged five-coordination transition state. In base catalyzed condensation, the negatively charged transition state becomes more stable as more hydroxyl groups replace the electron donating alkoxy groups. Thus, successive hydrolysis sept occurs increasingly rapidly, and the most hydrolyzed species undergoes the fastest condensation reactions. Therefore, the most substituted $Si(OH)_4$ condense faster than $ROSi(OH)_3$, which condenses faster than $ROSi(OH)_2$ and $(RO)_3SiOH$. As a consequence, in base catalyzed reactions

highly cross-linked large sol particles are interconnected particles, which favors the formation of denser colloidal silica particles and colloidal gels.[24]

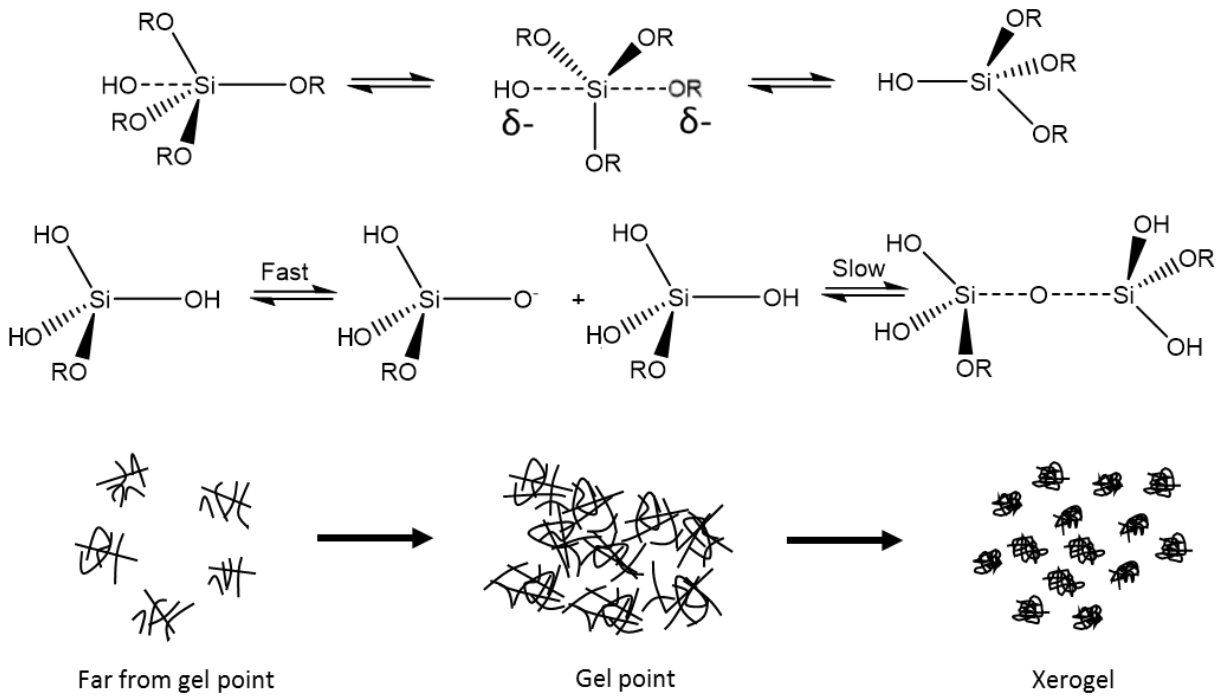

Figure 2.3 Hydrolysis and condensation of silicon alkoxide under basic condition.[17]

2.1.2 Silica sol-gel encapsulation

Besides of making pure silica materials, silica sol-gel method is also widely used to make silica composites materials with encapsulating other organic or inorganic materials in silica matrix. Dopant molecules can be entrapped in the inner porosity of a silica-based matrix by simple adding the dopant molecules during the silica sol-gel process:[25]

$$Si(OR')_4 + RSi(OR')_3 + dopant + H_2O \xrightarrow{cosolvent} dopant@\left[RSiO_nH_m(OR')_q\right]_p$$

A wide variety of biopolymers, including proteins, enzymes, and antibodies, have been encapsulated within silica matrix by silica sol-gel method. In 1955, Dickey first studied the possibility of enzyme stabilization by a silica matrix, but the experiments were unsuccessful.[26] Johnson and Whateley first developed a silica sol-gel procedure for enzyme immobilization in 1971. The entrapped trypsin was not released from the silica matrix by washing, demonstrating the sol-gel encapsulation can increase trypsin stability.[27] Later, Avinr et al. performed successful sol-gel entrapment experiments with various enzymes, such as b-glucosidase, alkaline phosphatase, chitinase, and aspartase.[28] Then the application of sol-gel encapsulation for biopolymers has grown rapidly. Multiple biopolymers, such as arabinogalactan, alginate, carboxymethyl cellulose, chitosan, cyclodextrin, starch, and albumin, have been used in silica sol-gel encapsulation. [29-31]

One of the commonly used methods for silica sol-gel encapsulation of biopolymers is a two-stage procedure.[18] The first stage is producing a stable sol solution of silica sol-gel precursor, such as TEOS. At the second stage, first a buffer solution is used to change the pH to neutral region. Then biopolymers are added for encapsulation by the condensation reactions. As

a result, the biopolymers encapsulated into the three-dimensional network by cross-linked sol nanoparticles. This two-stage procedure avoids the detrimental effect of acid, but it still produces alcohol during the hydrolysis and condensation reactions. Alcohol can cause unfolding of the biomacromolecules and denaturation of enzymes. To improve the biocompatibility of this procedure, alcohol can be removed from the sol solution in the first stage by rotary evaporation under vacuum. The other method for silica sol-gel encapsulation is a one-stage approach based on an ethylene glycol-containing precursor, tetrakis(2-hydroxyethyl) orthosilicate (THEOS).[32] This silica sol-gel precursor is water soluble, so there is no need to add any organic cosolvent. Furthermore, THEOS produces ethylene glycol instead of alcohol during the hydrolysis and condensation reactions. Moreover, ethylene glycol is a biocompatible organic solvent for biopolymers. Therefore, the hydrolytically generated ethylene glycol would not cause stability issues of biopolymers during the sol-gel process.

Silica sol-gel encapsulation can also be used for drug delivery application. It can provide homogeneous encapsulation of drug molecules within silica materials. Magdalena Prokopowicz et, al. encapsulated doxorubicin in base catalyzed mesoporous silica xerogel materials. They investigated the effect of aging time on the physical and structural properties and sorption-desorption of drug. The results revealed increasing aging time led to more drug sorption and less release.[33] Barbe et al. combined sol-gel technology with emulsion chemistry to make silica particle from 10 nm to 100 μm. The release profile of small molecules, such as Orange II or Rhodamine 6G, can be controlled by the internal structure of the particles, such as pore volume, pore size, tortuosity and surface chemistry.[34] The limitation of silica materials for drug delivery is that release rate is only controlled by diffusion. However, in biological applications, stimuli-responsive property is more and more important for controlled release. Therefore, silica

materials can be modified with stimuli-responsive polymers to enhance the release ability of silica. Silica-based nanoparticles have several advantages than the bulk gels in drug delivery application. As nanoparticles have much higher surface area for binding of active ingredient, which can be used as multifunction targeting vehicles. Furthermore, silica-based nanoparticle is good candidate for contact lens related application, as the low light absorbance and small size, which can maintain the optical clarity of contact lens even with silica-based nanoparticles inside.

2.2 pH-responsive polymers in drug delivery application

Stimuli-responsive polymers, also called smart, intelligent or environmentally responsive polymers, are capable of changing their physical or chemical properties in exposure to a number of external stimuli as shown in Table 2.1. These responsive property alternations include changes in conformation, solubility, hydrophilic/hydrophobic balance, or a combination of responses at the same time.[35]

Table 2.1 External stimuli that induce various responses of stimuli-responsive polymers

External Stimuli	Example of changes	Reference
Physical	temperature, electric fields, light, pressure, sound, magnetic fields and ultrasound irradiation	[36-40]
Chemical and biological	pH, ionic strength, chemical agents, redox, glucose level, enzyme, and DNA	[41-45]

pH-responsive polymers have gained great attention due to their various application potentials, such as drug delivery, gene delivery, sensors, membranes, and chromatography.[41, 46, 47] Especially in biomedical field, different organs, tissues, and cellular compartments have large variations of pH, which makes pH-responsive a suitable stimulus.[37] pH-responsive polymers usually have weak acidic or basic groups, such as carboxyl, amines, sulfonic, and

pyridine, either accept or release protons depends on the variation of pH. This leads to polymer property changes, such as surface activity, chain conformation, solubility or configuration.[35]

Both synthetic and natural polymers have been widely studied as pH-responsive polymers. Some of the examples are listed in Table 2.2 and Table 2.3. In general, synthetic polymers can be made with high purity and easy to modify. Whereas natural polymers are more biocompatible and biodegradable. In this chapter, alginate as a natural polymer and poly (methacrylic acid) (PMAA) as a synthetic polymer are discussed.

Table 2.2 Examples of pH-responsive synthetic polymers

Synthetic polymers	Functional groups	Reference
Poly(acrylic acid)(PAA)	Carboxylic groups	[48]
Poly(methacrylic acid) (PMAA)	Carboxylic groups	[49]
Poly[(2-dimethylamino) ethyl acrylate] (PDMAEA)	Tertiary amine groups	[50]
Poly[(2-diethylamino) ethyl methacrylate] (PDEA)	Tertiary amine groups	[51]
Poly(acryloymorpholine) (PAM)	Morpholino	[52]
Poly(N-ethylpyrrolidine methacrylate)(PEPyM)	Pyrrolidine	[53]

Table 2.3 Examples of pH-responsive natural polymers

Synthetic polymers	Functional groups	Reference
Alginate	Carboxylic groups	[54]
Hyaluronic acid	Carboxylic groups	[55]
Guar gum	Carboxylic groups	[56]
Carboxymethyl cellulose	Carboxylic groups	[57]
Chitosan	Primary amine groups	[58]

2.2.1 Alginate

Alginate, also named as algin or alginic acid, is an anionic polysaccharide extracted from the cell wall of brown algae. It is also produced by two bacterial genera Pseudomonas and Azotobacter, which played a major role in the unraveling of its biosynthesis pathway.[59] Alginate is a copolymer composed of poly-β-1,4-Dmannuronic acid (M units) and α-1,4-L-glucuronic acid (G units) in varying proportions as shown in Figure 2.4, and it is renewable, water soluble, odorless, non-toxic and biodegradable.[60] Alginic acid has been widely used as an additive in food products. In addition, it has been applied in biotechnology as support of enzyme- and cell-based biocatalysts as well as bioreactors. Alginate hydrogels have also been studied in wound healing applications, artificial organs, and drug delivery system due to its biocompatible, biodegradable, and non-toxic properties.[61]

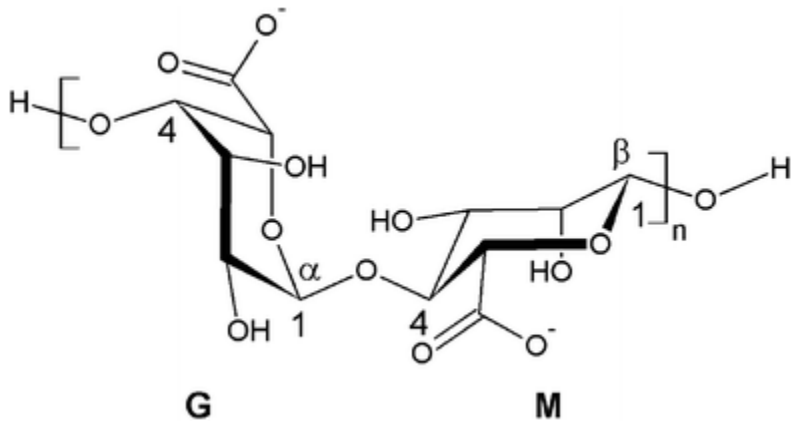

Figure 2.4 Chemical structure of a repeating unit of alginate.

Alginate aqueous solution can become to a hydrogel form with the presence of divalent cations (except Mg^{2+}). So far, Ca^{2+} is the most studied cross-linker due to its non-toxic property for *in vivo* application. Alginate hydrogel can show pH-dependent swelling, the pKa of alginate

is around 3.2, and it shrinks at acidic condition and swells in neutral or base condition. This pH-responsive behavior is because of to the -COO- groups of the alginate convert to -COOH groups in acidic solutions, which strengthens the hydrogen bonding interaction among hydrophilic groups to limit the swelling of alginate hydrogel. However, in the biological condition (pH value is around 7.4), the hydrogen bonding interaction among hydrophilic groups is broken, and the electrostatic repulsion among polymer chains is increased, in the end alginate hydrogel show further swell.[60, 62]

However, the alginate hydrogel formed by Ca^{2+} has a low stability in a solution containing monovalent ion such as Na^{+} or K^{+}. In this condition, an equilibrium exists between the $(Alg\text{-}Ca^{2+})_{gel}$ and $(Alg\text{-}Na^{+})_{solution}$ will lead to the redissolution of alginate hydrogel.[63] One method to overcome this issue is to coat the alginate hydrogel with a cationic polymer, such as poly-L-lysine (PLL) or chitosan.[64] In this case, a polyelectrolyte complex layer is formed on the surface that stabilizes the alginate hydrogel in biological buffers with Na^{+} or K^{+}. In addition, the development of sol-gel technology and hybrid material synthesis open a new route to use inorganic materials to enhance the stability of alginate materials. By combining the flexibility of silica sol-gel chemistry and the intrinsic chemical and physical properties of alginate, a wide variety of composites materials have been synthesized and characterized.[61]

Alginate and silica are both negatively charged at neutral pH condition, so they can be mixed in solution with no phase separation. There are mainly three methods of synthesizing silica-alginate composite materials. (1) Hybrid materials by the formation of alginate gel coated with silica source; (2) Interpenetrated polymer networks (IPN) structure materials by the gelation of a mixture of alginate and silica source simultaneously; and (3) Composite hydrogel by adding

silica particles into alginate solution then gelation by introducing Ca^{2+}. The resulting composite materials can be beads, bulk gels, films or fibers.

The composite approach

Fukushima et al. proposed the first example of silica-alginate composite materials in 1988.[65] This method was based on the preparation of a mixture of alginate and colloidal silica solution following by dropping into a calcium chloride solution to form alginate-silica composite beads. SEM characterizations revealed that colloidal silica particles were homogeneously dispersed inside the alginate hydrogel. This method was later extended to the use of silica nanotubes as well as mesoporous silica nanoparticles.[66, 67]

The hybrid approach

Heichal-Segal et al.[68] studied a hybrid approach for the silica-alginate composite materials. In this method, alginate beads were first prepared and then immersed in a solution of TMOS in hexane. TMOS hydrolysis occurred at the interface between the organic solvent and the hydration water surface of alginate beads. These hydrolysis products diffused into the alginate hydrogel with a certain extent. The condensation reactions that occurred at the same time led to increasingly larger silica oligomers and particles. In the end, most of the silica was coated on outer surface of the alginate beads, and some of the silica was stayed inside the beads.

The IPN approach

Interpenetrated polymer networks (IPN) approach is based on the gelation of a mixture of the alginate solution and silica sol-gel precursor. This method can be used to overcome the

limitation that silica polymerization mainly occurs on the surface of alginate material. Kawakami et al.[69] first used this method to make silica-alginate composites. In this study, TMOS, as the sol-gel precursor, was first hydrolyzed under acidic condition and then mixed with alginate solution. In the following step, calcium chloride solution was added to the mixed solution to form a composite hydrogel. However, there was phase separation between silica and alginate under the SEM characterization. Another formation method without adding the calcium chloride solution was studied using THEOS, a water-soluble silicon alkoxide, as silica sol-gel precursor. In this method, there was no phase separation in the silica-alginate composites materials.[29]

Alginate is widely used for controlled drug release application due to is pH-responsive ability. For example, Ya-Ni Dai et al.[70] investigated the swelling behavior and *in vitro* release of nifedipine from alginate-chitosan hydrogel beads. Alginate-chitosan mixed beads and alginate-chitosan coated beads were prepared by ionic gelation method. The swelling ability of these beads and *in vitro* release of nifedipine were dependent on the pH as well as the presence of the polyelectrolyte complex between chitosan and alginate. The results suggested that the coated beads could hold drugs better at low pH than the mixed beads. Therefore, the alginate-chitosan coated beads could be a suitable polymeric carrier for drug delivery in the intestinal tract. A.M Rabasco et al. prepared alginate-chitosan particles by ionic gelation to test the release of sodium diclofenac. pH-responsive release profiles were observed with limited release of sodium diclofenac at acidic pH, while the release was complete in a few minutes when pH is raised up to 6.4 and 7.2. The ratio of alginate and chitosan and the gelation condition of the particles also controlled the release rate.[71]

However, organic delivery systems suffer from limitations, such as poor thermal and chemical stability, and rapid elimination by the immune system. Therefore, the combination of silica and alginate will open a new door for the control release application. For example, Siling Wang et al. used alginate coated mesoporous silica nanoparticles as drug carriers for indomethacin, a poorly water-soluble drug. The results showed that sustained release of indomethacin due to the blockage effect from the coated alginate.[72]

2.2.2 Poly (methacrylic acid)

Poly (methacrylic acid) (PMAA) is an ionizable hydrophilic polymer made from methacrylic acid. It is often used as its sodium salt, as shown in Figure 2.5 (B). PMAA is one of the most commonly studied pH-responsive ionic polymers. Other well studied polymers include poly(acrylamide) (PAAm), poly(acrylic acid) (PAA), poly(diethylaminoethyl methacrylate) (PDEAEMA), and poly(dimethylaminoethyl methacrylate) (PDMAEMA).[73]

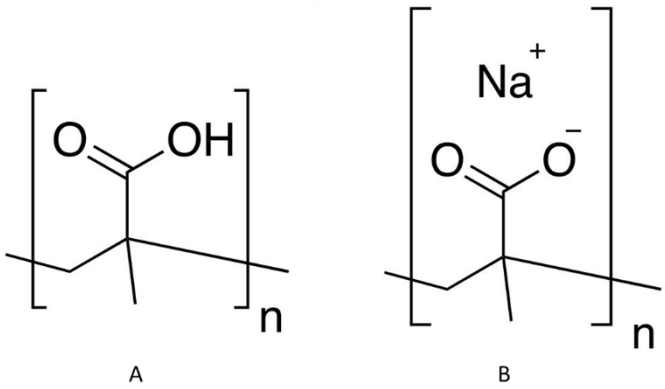

Figure 2.5 Chemical structure of (A) poly (methacrylic acid) and (B) poly (methacrylic acid) sodium salt.

PMAA has shown promising application in cosmetics,[74] pharmaceutics,[75] drug testing,[76] and biomedical technology,[77] due to its pH-induced conformational transition. This conformational response to pH has been studied by different methods such as viscosimetry,[78] Raman spectroscopy,[79] small angle X-ray scattering,[80] potentiometric titration,[81] analytical ultracentrifugation,[82] fluorescence spectroscopy,[83] and dynamic light scattering.[84] The results from these different techniques have shown that PMAA undergoes a hypercoiling transition and collapses into a tight globule at pH < 4, because of the hydrophobic

interaction of the methyl groups and the hydrogen bonding between carboxylic acid groups. At pH 6, PMAA chain stretches to an open structure due to electrostatic repulsion between carboxylate groups.[82, 84, 85]

Cross-linked PMAA hydrogel exhibits a great pH-dependent swelling behavior due to the ionization/deionization transition of carboxylic acid groups as shown in Figure 2.6. At low pH, usually lower than 5.5 (the pKa of PMAA) the carboxyl groups accept protons to an uncharged state, hydrophobic interaction of the methyl groups and hydrogen bonding between carboxylic acid groups keep hydrogel with compact structure. However, at high pH, carboxyl groups lose protons to an ionized state, electrostatic repulsion between the charged carboxylate groups leads to the further swelling of PMAA hydrogel.[86, 87]

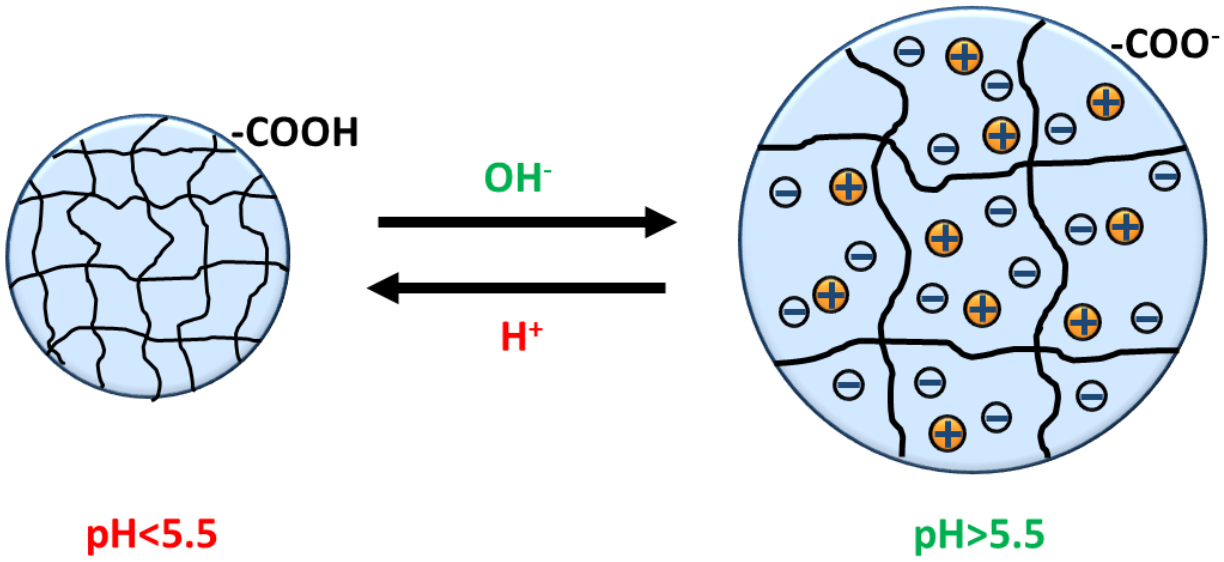

Figure 2.6 Illustration of pH-dependent swelling of PMAA hydrogel.

PMAA based materials have been widely studied in pH-responsive controlled drug delivery application due to the physiological pH variations in the body. For example, this system can be designed to target delivery drug molecules to gastrointestinal tract as the inside pH variation, and to tumor tissues as most solid tumors with a measured tumor extracellular pH value range from 6.5 to 7.2, which is lower than the normal tissues.[88, 89] Most of the PMAA based pH-responsive drug delivery vehicles have been developed by PMAA copolymer system or PMAA-silica hybrid system.

PMAA copolymer system

Xu group synthesized pH-response PMAA-b-PEG-b-PMAA triblock copolymers, which can self-assemble into spherical nanolevel micelles with an average size range from 18 to 89 nm. The results showed a 67.75 % encapsulation efficiency of prednisone in the micellar core and implied a control drug release behavior for the small intestine of various hydrophobic drugs.[90] Peppas group made pH- and temperature-sensitive PMAA/PNIPAAm interpenetrating polymer networks by a sequential UV polymerization method. These hydrogels were shown to exhibit relatively independent swelling transition at a temperature range of 31-32 °C, the LCST of the PNIPAAm network, and a pH value of approximately 5.5, the pKa of PMAA. Both pH and temperature showed great influence on the model drug permeability. A hypothesis mechanism had been proposed to explain the phenomena that the model drug has the highest permeability at the physiological state of 37 °C and pH 7.4, which was desirable in the membrane and drug delivery applications.[87]

PMAA-silica hybrid system

Liu group developed PMAA-grafted hollow silica vesicles by grafting PMAA brushes on the surface via atom-transfer radical polymerization. This PMAA surface brushes had a lower ionization degree and a low solubility in pH 3.4, but a higher ionization degree and solubility when the pH was higher than 7. This provided a pH-triggered release property renders PMAA-g-hollow silica vesicles, in which either calcein blue or FITC-labelled dextran could be encapsulated in the interiors of PMAA-g-hollow silica vesicles, and were released at pH 7.4.[91] Sun group developed a "smart" mesoporous silica-PMAA hybrid nanoparticles drug delivery system by coating PMAA onto amino-modified mesoporous silica nanoparticle surface. Ibuprofen was used as a model drug to evaluate the performance of this system. The results showed drug release from drug loaded silica-PMAA nanoparticles was pH-dependent with an increasing tendency with the increase of pH value.[92]

2.3 Silica-based composite nanoparticles prepared by microemulsion

Microemulsion is a system comprising a mixture of water, oil, and amphiphile compounds, which is a macroscopically homogeneous, optically isotropic, and thermodynamically stable liquid solution.[93] There are two types of microemulsion, dispersed and bicontinuous. Dispersed microemulsion is further subdivided into water-in-oil (W/O) and oil-in-water (O/W) structures. In W/O microemulsion, a low volume fraction of water results in water droplets dispersed in continuous oil phase; while O/W microemulsion, with a low volume fraction of oil, formed when oil droplets are dispersed in continuous aqueous phase. In system where the amounts of water and oil are similar, a bicontinuous microemulsion may form. In all those types of microemulsion, the interface is stabilized by an appropriate combination of surfactant and sometimes cosurfactant.[94]

Microemulsion has numerous advantages compared to the conventional emulsion. The key differences are shown in Table 2.4.[94] Microemulsion droplets can serve as nanoreactors for the preparation of nanoparticles with different particle properties such as particle size, geometry, morphology, and homogeneity.[96] Therefore, it is suitable to assist the silica sol-gel technique to encapsulate other materials for making silica-based composites nanoparticles.

Table 2.4 Comparison of microemulsion with conventional emulsion

Property	Microemulsion	Emulsion
Appearance	Transparent (or translucent)	Cloudy
Optical Isotropy	Isotropic	Anisotropic
Interfacial tension	Ultra-low	High
Microstructure	Dynamic (interface is continuously and spontaneously fluctuating)	Static
Droplet size	20-200 nm	>500 nm
Stability	Thermodynamically stable, long shelf-life	Thermodynamically unstable (kinetically stable), will eventually phase separate
Phase	Monophasic	Biphasic
Preparation	Facile preparation, relatively lower cost for commercial production	Require a large input of energy, higher cost

2.3.1 Microemulsion formation

There have been several theories to explain the formation of microemulsion. Here lists the interfacial or mixed film theory and thermodynamic theory as examples.

Mixed film theory

In 1955, Bowcott and Schulman[97] considered that there was an interfacial film in equilibrium with both the oil and water phases in microemulsion, and this third phase had its own spreading pressure (π). The total droplet interfacial tension γ_T for microemulsion might be:

$$\gamma_T = \gamma_{O/W} - \pi$$

where $\gamma_{O/W}$ is the water and oil interfacial tension in the presence of a surfactant. According to this equation, when π is equal or greater than $\gamma_{O/W}$, γ_T becomes zero or negative. This results in a spontaneous increase in the interfacial area that leads to the formation of microemulsion. [98]

When a cosurfactant presents in the microemulsion system, Prince modified the above equation to:[99]

$$\gamma_T = (\gamma_{O/W})_a - \pi$$

where $(\gamma_{O/W})_a$ is the water and oil interfacial tension in the presence of a cosurfactant, this cosurfactant can further reduce the interfacial tension. This leads to a more favorable situation of π value equal or greater than the water and oil interfacial tension. In the end, γ_T tends to be zero or negative favoring formation of thermodynamically stable microemulsion.[100]

Thermodynamic theory

The immiscibility of water and oil is due to the high interface tension, which thermodynamically can be described as $\gamma = (\delta G/\delta A)$ at constant pressure and temperature. Since γ is always positive, so the Gibbs free energy change is also positive, therefore water and oil could not be mixed homogeneously. The addition of surfactant and cosurfactant can change the surface tension of the interface of oil and water to a very low value to make the free energy change negative. The free energy of microemulsion formation can be considered as below,[101]

$$\Delta G_f = \Delta H + \gamma \Delta A - T\Delta S$$

where ΔG_f is the Gibbs free energy change, ΔH is the enthalpy change, γ is the surface tension of the oil and water interface, ΔA is the change in interfacial area, ΔS is the change in entropy of the system which is effectively the dispersion entropy, and T is the temperature. The enthalpy change is negligible when immiscible oil and water are mixed. The change in ΔA is very large due to the formation of numerous small droplets. For the change in entropy, one is the very large dispersion entropy arising from the mixing of one phase in the other in the formation of small droplets, the other one is arising from other dynamic processes such as surfactant diffusion into the interfacial layer and monomer-micelle surfactant exchange. Thus, a negative free energy of formation can be achieved when a large reduction in surface tension is achieved by adding surfactant and cosurfactant. In such cases, microemulsion is spontaneous and thermodynamically stable.

2.3.2 Synthesis of silica-based nanoparticle in miceormulsion

Water-in-oil microemulsion is a colloidal nanodispersion of water droplets in oil phase stabilized by surfactant and cosurfactant. These thermodynamically stable dispersions not only can be considered as nanoreactors, which can be used for nanoparticle formation, but also as steric barriers to prevent the aggregation of nanoparticles. For the synthesis of nanomaterials, the reaction occurs in the water drop pool as shown in Figure 2.7. The radius of the droplet is depended on the mole ratio of water and surfactant ([H_2O]/[surfactant]). At a constant surfactant amount, increases water amount leads to larger droplets.[102]

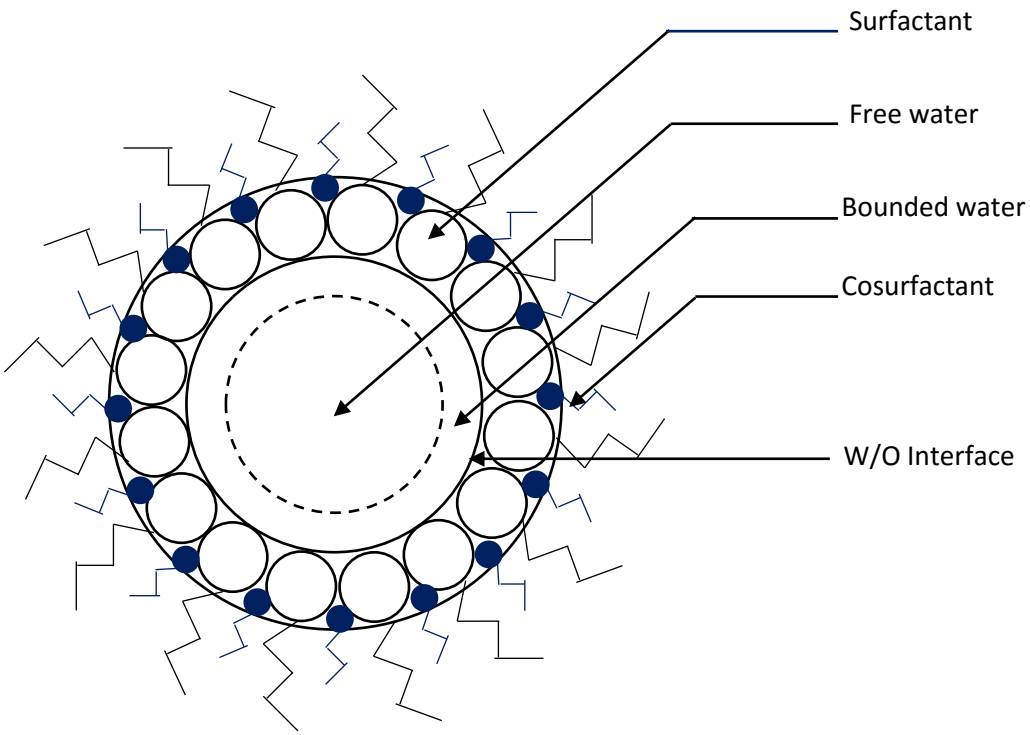

Figure 2.7 Schematic representation of a water droplet form a four-component water-in-oil microemulsion system.

Water-in-oil microemuslion has been used to make silica nanoparticles from various silica sol-gel processors. Several factors can affect the particle size and size distribution, such as the type of surfactant molecules, the concentrations of precursors and catalysts, the water to surfactant molar ratio, cosurfactant to surfactant molar ratio, even the different types of organic solvent. [103] [104] Water-in-oil microemulsion method has also been used to make silica-based nanocomposites particles. In 1994, Chang et al.[105] made silica-CdS nanocomposites with different structures in reverse microemulsions by controlling the hydrolysis of TEOS and the coprecipitation of CdS. Since then more and more studies have been focused on preparation and application of silica-based nanocomposites by water-in-oil microemulsions. Such as silica magnetic nanocomposites,[106] CdTe@SiO2 core-shell structured spheres,[107] dye doped silica particles.[108] And those particles can be used as catalysts or biomedical imaging and theranostic applications. However, little studies showed the silica-based nanocomposites particles using for the controlled drug delivery area, especially for the silica-polymer nanocomposites.

2.4 Contact lenses for ophthalmic drug delivery

Effective treatment for eye diseases like glaucoma, cataract, age-related macular degeneration has been a major challenge due to the unique anatomy and physiology of the eye. Eye drops treatment accounts for 90% of all ophthalmic formulations, however, there are several limitations for this treatment method. First, it is extremely inefficient. Almost 95% of the eye drops administered mix with tears flows away from the target tissue and drain into the nasal cavity, then flow through the blood stream to other organs, in the end cause undesirable side effects. In addition, dosage through eye drops is inconsistent and usually needs high frequency of administration, which leads to a lower patient compliance. Moreover, most of the drugs are released in an initial burst of concentration and have a short residence time of about 2 min in the tear film.[109] Current ophthalmic drug delivery methods are even more inconvenient for animals such as cats, dogs, bovines and horses. To overcome these problems, researchers have been studying the application of controlled release devices, such as conjunctival inserts, puncta plugs, subconjunctival devices and contact lenses. Among all of these devices, contact lenses are ideally suited for delivering drugs to the cornea due to the location of the contact lens in the eye.[110]

2.4.1 Contact lenses interactions with tear film

Tear film has a highly specialized structure, which covers the anterior conjunctiva and the cornea. The total tear volume is around 7 μL, with a thickness about 6 to 10 μm. The composition of tear film is usually described as a three-layer film as shown in Figure 2.8. Tear film plays a number of roles to maintain the health and function of the eye.[111] The lipid layer is mainly composed of cholesterol esters and ester waxes, this layer can decrease the surface tension of air to tear film interface, reduce water evaporation, and stabilize the tear film against rupture. The aqueous layer contains water, electrolytes, and proteins, such as antibodies, lipocalin, lactoferrin, lysozyme, and lacritin. This layer has the functions with bacteriostasis, debris flushing, and maintenance of epithelial hydration. The mucin of the mucus layer comes from the conjunctival goblet cells or glands of moll and krasse. This layer provides the hydrophilic of the epithelial surface for aqueous to wet.

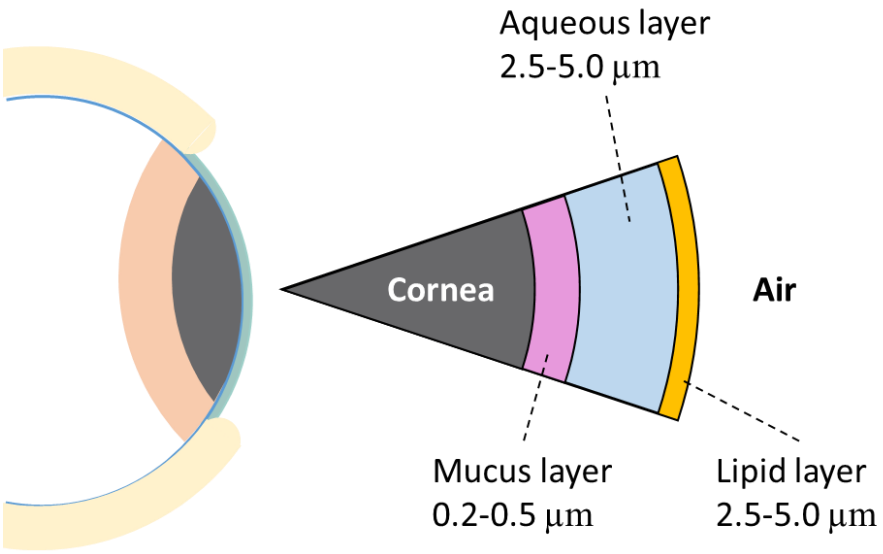

Figure 2.8 The classical three-layer viewpoint for the pre-corneal tear film with typical thicknesses.

When contact lens is placed on the eye, it causes several changes to tear film due to the interaction between the contact lens and tear film. This complex and dynamic interaction influences several aspects of ocular physiology as well as patient safety, vision, and comfort. Contact lens first divides the tear film into two layers: a pre-lens tear film and a post-lens tear film as shown in Figure 2.9. The pre-lens tear film is more associated with wearing comfort while the post-lens tear film more with lens fit and movement. Moreover, the pre-lens tear film also needs to act like the pre-corneal film, in order to protect the lens surface from drying and deposition.[112]

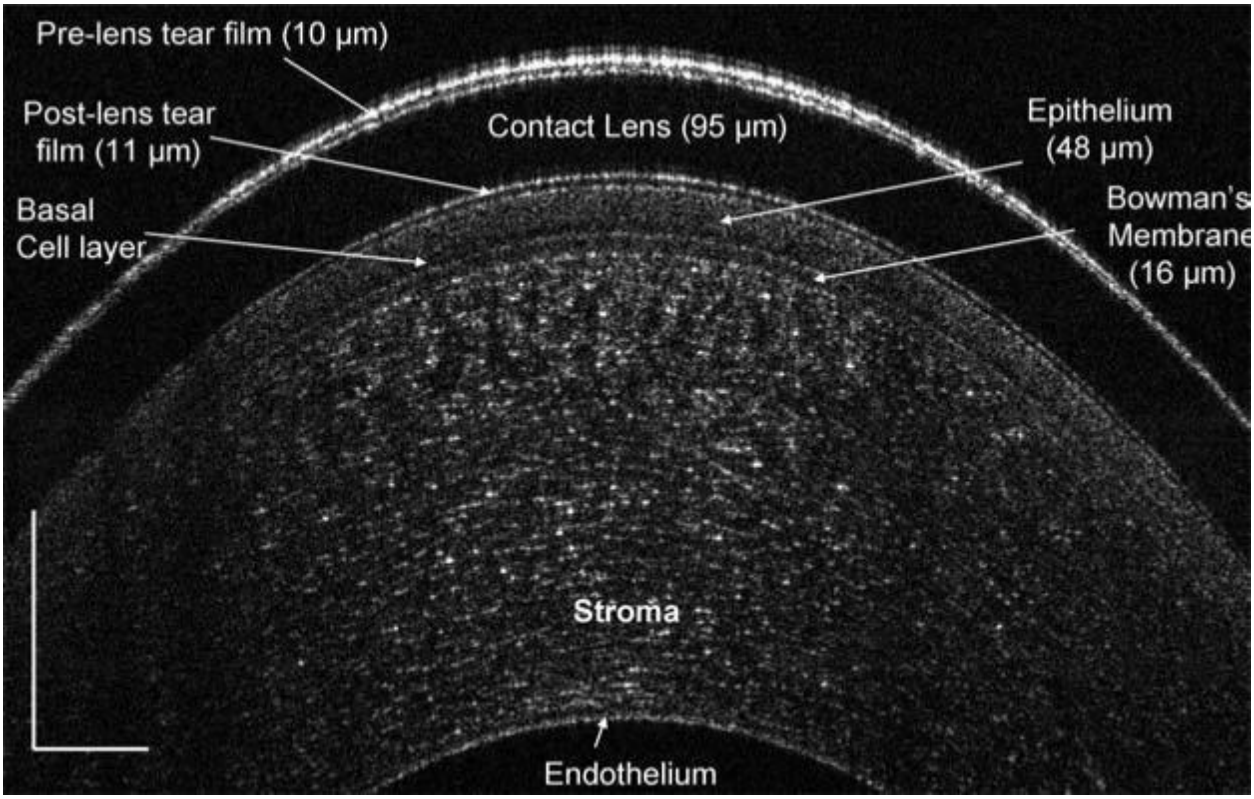

Figure 2.9 The central cornea with a PureVision lens after instillation of artificial tears. Reproduced with permission from [113]

Contact lens wearing can also change the tear production. There is higher rate of reflex tearing during the wear of rigid gas permeable lenses compared to soft lenses. However, due to technological limitations, no consistent research has confirmed the alteration of the tear production during contact lens wear. Further study and more test methods are needed for a better understanding of tear production changing by wearing contact lenses.[114] Tear pH is another key physiochemical property may be changed by contact lens wearing. A variety of tear pH values (5.2-8.6) are listed in the literature with an average value of 7.7. [115, 116]. It has been observed that the tear pH showed very little changes during continuous contact lens wear, possibly due to the buffering capability of the tear film.[117, 118]

Furthermore, the contact lenses can cause two types of alteration for the biochemical and biophysical properties of tear film. First, the lens can reduce or remove some specific components in the tear film, and the lens can also stimulate the influx of new components or increase the concentration of existing components. For example, the lipid components are most likely to immobilize on the lens surface, which results in the increasing autoxidative degradation of the lipid. This lipid oxidation phenomenon is the main reason for the discomfort of the symptomatic contact lens patients. In addition, the lens leads to complexity influence on tear proteins. First, lower molecular weight proteins show strong absorption with the lens matrix. At the same time, the lens can stimulate cascade or upregulation processes, which can result in either increasing the concentration of existing components or generating additional proteins and peptides.[119]

2.4.2 Contact lenses as drug delivery vehicles

Contact lenses have some unique advantages over other devices for delivering drugs to the cornea due to its location in the tear film. Drug released from the posterior surface of the contact lens is trapped in post-lens tear film between the cornea and the lens, which leads to an extended period longer than 30 min, compared with 2-5 min from the eye drops treatment.[120] This enhanced residence time leads to significant increase in the bioavailability due to more drug uptake by the cornea, which reduces the toxic side effects by eye drop overdosing.[110]

The focus on using contact lenses for drug delivery has increased considerably in the last decade. It was, however, a few decades ago when contact lenses were first tried for delivering drugs, primarily to glaucoma treatment. Some of the studies focused on soaking hydrophilic lenses in commercial drug solution followed by insertion into the eye.[121, 122] However, it is not a viable option to modify the parameters of drug-soaked commercial contact lenses to control release drugs. In recent years, several methods have been proposed to increase the drug loading capacity and extend the release kinetics of soft contact lenses. For example, molecular imprinting technique is widely used to increase the interaction with the polymer network to increase drug loading capacity and delay the release.[123-126] However, all of the imprinting studies focused on hydrophilic hydrogel based contact lenses, which are not suitable for extended wear due to limited oxygen permeability. Vitamin E can also be used as a diffusion barrier to extend the drug release from contact. This vitamin E barrier can force drug molecules to diffuse through a long tortuous path.[109] However, although this method increases the drug release durations from contact lenses, it could not stop the drug release during packing and storage.

Contact lens incorporated with drug loaded nanoparticle is another strategy for ocular drug release. In this method, the drug release process will be determined by the diffusion from nanoparticles and then from the contact lens. The ability to modify of these particles allows greater control over the release kinetics and possibly targeting of the ideal rate for a particular application. For example, Chauhan et al.[127] incorporated highly cross-linked nanoparticles containing covalently bonded timolol maleate into a hydrogel contact lens; the ester linkage was hydrolyzed at a faster rate at physiological temperature with the timolol release occurring up to 4 weeks. Hydrolysis still occurred at ambient storage conditions at a slow rate and this methodology may not be applicable to other types of therapeutics. Dean Ho et al.[128] incorporated nanogels into a hydrogel contact lens. These nanogels were composed of nanodiamonds with an enzyme-cleavable chitosan and timolol maleate. Lysozyme in the ocular tear fluid triggered slow release of timolol maleate over 24 hours. However, the optical transmission of the contact lens decreased from 93.7 % to 84.5 % with 0.2 wt% of nanogels embedded in the lens. Therefore, the ideal condition is that the contact lens can protect the drug activity through the processing conditions including autoclaving and shelf storage, and only release the drug in tear film condition. In addition to this controlled release ability, the other challenge is the drug eluting contact lens can still maintain good critical lens properties such as water content, ion and oxygen permeability, modulus, transparency.

2.5 Mathematical modeling of drug release

The mathematical modeling of drug transport in controlled delivery systems can be highly useful. It predicts drug release kinetics through the design parameters, such as geometry, dimensions and dosage preparation procedure.[129-131] In addition, it provides a deeper insight into the mass transport mechanisms that are involved in the control of drug release process.[132-135] One or more of the following mass transport processes could be involved in the control of drug release.[136-140] For example, the surface wetting process by water; the penetration of water into the system; drug dissolution; drug diffusion out of dosage form; pore changing due to polymer swelling; hydrostatic pressure created within the system; polymer matrix erosion; change in device geometry due to shear forces and other processes. In general, the mathematical analysis of drug release can be simplified according to the slowest mass transport rate-limiting mechanism.[141] Diffusion, swelling, and erosion are the most important rate-limiting mechanisms of controlled release systems.[142]

A number of models have been studied, including empirical/semi-empirical models as well as mechanistic realistic ones. Empirical models are easy to use to help explain the mass transport mechanisms. Mechanistic models can determine system-specific parameters for a better understanding of the release mechanisms.

2.5.1 Empirical/semi-empirical mathematical models

Higuchi equation

The most famous used mathematical Higuchi equation was proposed in 1961 to describe drug release from a thin ointment film into the skin.[143] The assumptions for Higuchi equation include: (1) initial drug concentration in the system is much higher than the drug solubility; (2) it is a one-dimension diffusion process and edge effect must be negligible; (3) drug particle size is much smaller than the system thickness; (4) negligible swelling or dissolution of the system; (5) constant drug diffusivity; (5) perfect sink conditions, drug concentration can be considered to be negligible outside the carrier.[144]

The basic equation for Higuchi model is:

$$\frac{M_t}{A} = \sqrt{D(2c_0 - c_s)c_s t}$$

where M_t is the cumulative amount of drug released in time t, A is the surface area of the release vehicle, D is the drug diffusivity in the matrix carrier, c_0 is the initial drug concentration, and c_s is the solubility of drug in the matrix media. However, the most common used Higuchi equation is the simplify model:

$$\frac{M_t}{M_\infty} = kt^{1/2}$$

where M_∞ is the cumulative amount of drug released at infinite time, and k is Higuchi dissolution constant.

Peppas equation

Peppas equation, also called Korsmeyer-Peppas equation, Ritger-Peppase equation, or power law, is another easy-to-apply model to describe drug release process.[145]

$$\frac{M_t}{M_\infty} = k_1 t^n$$

where M_t is the cumulative amount of drug released in time t, M_∞ is the cumulative amount of drug released at infinite time, k is a constant related to device structure and geometry, and n is the release exponent to characterize the release mechanism as shown in Table 2.5. Fickian diffusion is the drug diffusion due to a chemical potential gradient. Whereas, non-Fickian Case-II transport associates with the polymer swelling and the drug release is zero-order. Anomalous transport is between these two extreme cases. In general, Peppas equation is valid for $\frac{M_t}{M_\infty} < 0.6$. For the sphere system, the release exponent n depends on the width of the particle distribution.

Table 2.5 Release mechanisms based on release exponent n

Release exponent n			Drug release mechanism
Thin film	Cylinder	Sphere	
0.5	0.45	0.43	Fickian diffusion
$0.5 < n < 1.0$	$0.45 < n < 0.89$	$0.43 < n < 0.85$	Anomalous transport
1.0	0.89	0.85	Case-II transport

Peppas-Sahlin equation

This equation developed by Peppas and Sahlin by decoupling Fickian diffusion and Case-II transport as below:[146]

$$\frac{M_t}{M_\infty} = k_1 t^m + k_2 t^{2m}$$

where M_t is the cumulative amount of drug released in time t, M_∞ is the cumulative amount of drug released at infinite time, $k_1 t^m$ is Fickian diffusion contribution (F). $k_2 t^{2m}$ is Case-II relaxational contribution (R), and m is the purely Fickian diffusion exponent for any geometrical shape device which exhibits controlled release. The ratios of both contributions can be expressed as:

$$\frac{R}{F} = \frac{k_2 t^m}{k_1}$$

2.5.2 Mechanistic realistic models for diffusion controlled system

For diffusion controlled system, Fick's second law of diffusion can be used to quantify diffusional mass transport as given below:[141]

$$\frac{\partial C}{\partial t} = D\left(\frac{\partial^2 C}{\partial x^2} + \frac{\partial^2 C}{\partial y^2} + \frac{\partial^2 C}{\partial z^2}\right)$$

where C is the drug concentration, D is the diffusion coefficient, and t is ti me. The initial and boundary conditions are based on the drug delivery system and release conditions. In general, the following assumptions are considered for simplifying mathematical modeling: (1) diffusion is the rate-limiting step; (2) diffusion coefficient of drug is constant; (3) perfect sink condition is maintained; (4) mass transfer resistance at the surface is negligible; (5) No significantly swelling and degradation of the release device. Table 2.6 lists different types of systems including: reservoir systems with a drug release rate controlling barrier membrane; the monolithic system with drug molecules are homogeneously distributed inside the system. In addition, the initial drug concentration (c_{ini}), drug solubility (c_s) and geometry of the drug delivery system all play important roles as shown in Table 2.6.

Table 2.6 Diffusion mathematical models for drug release

Diffusion system		Expression[141]
Reservoir systems	Non-constant activity sources $c_{ini} < c_s$	$Slab$: $\frac{M_t}{M_\infty} = 1 - \exp(-\frac{ADKt}{VL})$ $Sphere$: $\frac{M_t}{M_\infty} = 1 - \exp(-\frac{3R_0DKt}{R_i^2R_0 - R_i^3})$ $Cylinder$: $\frac{M_t}{M_\infty} = 1 - \exp\left[-\frac{(R_iH + R_0H + 2R_iR_0)DKt}{R_i^2R_0 - R_i^3}\right]$
	Constant activity sources $c_{ini} > c_s$	$Slab$: $M_t = \frac{ADKc_st}{L}$ $Sphere$: $M_t = \frac{4\pi DKc_sR_iR_0t}{R_0 - R_i}$ $Cylinder\ (Only\ radial\ diffusion)$: $M_t = \frac{2\pi HDKc_st}{ln(R_0/R_i)}$
Matrix systems	Monolithic solutions $c_{ini} < c_s$	$Slab$: $\frac{M_t}{M_\infty} = 1 - \frac{8}{\pi^2}\sum_{n=0}^{\infty}\frac{exp[-D(2n+1)^2\pi^2t/L^2]}{(2n+1)^2}$ $Sphere$: $\frac{M_t}{M_\infty} = 1 - \frac{6}{\pi^2}\sum_{n=0}^{\infty}\frac{exp[-Dn^2\pi^2t/R^2]}{n^2}$ $Cylinder$: $\frac{M_t}{M_\infty} = 1 - \frac{32}{\pi^2}\sum_{n=0}^{\infty}\frac{1}{q_n^2}\exp(-\frac{q_n^2}{n^2}Dt)\cdot\sum_{n=0}^{\infty}\frac{1}{(2p+1)^2}\exp(-\frac{(2p+1)^2\pi^2}{H^2}Dt)$
	Monolithic dispersions $c_{ini} > c_s$	$Slab$: $M_t = A\sqrt{Dc_s(2C_{ini} - C_s)t}$ $Sphere$: $\frac{M_t}{M_\infty} - \frac{3}{2}\left[1 - \left(1 - \frac{M_t}{M_\infty}\right)^{2/3}\right] = -\frac{3D}{R^2}\cdot\frac{C_s}{C_{ini}}\cdot t$ $Cylinder$: $\frac{M_t}{M_\infty} + \left(1 - \frac{M_t}{M_\infty}\right)ln\left[1 - \frac{M_t}{M_\infty}\right] = \frac{4D}{R^2}\cdot\frac{C_s}{C_{ini}}\cdot t$

Chapter 3 Rhodamine B *in vitro* release study of silica-alginate composite materials

Rhodamine B, a fluorescent dye, was used as a model drug to test the pH-responsive release ability of silica-alginate composite materials. Due to its easy detection method, rhodamine B has been widely used as a model drug for *in vitro* release studies of different materials.[147-151] In this chapter, the goal was to evaluate the potential of silica-alginate composite materials to modulate drug release profiles as a function of pH. Different types of silica-alginate composite materials were studied for the *in vitro* release of rhodamine B in different pH solutions. First alginate beads were used as rhodamine B delivery vehicles, and then silica nanoparticle incorporated alginate beads were also studied as a comparison for the release performance. Next, silica-alginate monolithic gels were used for the *in vitro* release of rhodamine B, and pure silica monolithic gels were used as a control.

3.1 Materials and methods

3.1.1 Materials

Rhodamine B, calcium chloride, sodium phosphate monobasic monohydrate, sodium phosphate dibasic heptahydrate and Triton X-100 were purchased from AMRESCO; sodium alginate and tetramethyl orthosilicate were purchased from Acros, isopropyl alcohol (70 %), cyclohexane, aqueous ammonia solution (29 wt%) and hydrochloric acid (37 %) were purchased from BDH Chemicals; tetraethyl orthosilicate was purchased from Sigma Aldrich; sodium alginate (very low viscosity) and n-hexanol were purchased from Alfa Aesar. All chemicals were used without further purification. Deionized water used throughout the experiments was purified with an ELGA PURELAB Flex water purification system.

3.1.2 Preparation of phosphate buffer

Phosphate buffer (pH 2.5, 10 mM) was prepared by dissolving 1.380 g sodium phosphate monobasic monohydrate to 1000 mL deionized water. Then adjusted the pH to 2.5 by hydrochloric acid (1 M).

Phosphate buffer (pH 7.5, 10 mM) was prepared by dissolving 0.227 g sodium phosphate monobasic monohydrate and 2.238 g sodium phosphate dibasic heptahydrate to 1000 mL deionized water.

3.1.3 Preparation of rhodamine B loaded alginate beads

Rhodamine B (0.1 %w/v) was dissolved in aqueous solutions of sodium alginate (very low viscosity, 5 %w/v). This solution was added dropwise to a calcium chloride solution (5

%w/v) under magnetic stirring for 15 min to form spherical beads. The wet rhodamine B loaded alginate beads were washed with deionized water to remove unreacted calcium chloride and dried at ambient condition overnight.

3.1.4 Rhodamine B *in vitro* release study from alginate beads

All groups of beads were placed into 1 mL phosphate buffer (pH 2.5, 10 mM) for the first 1 hour. During this period, 1 mL buffer was withdrawn every 10 min and replaced with 1 mL fresh phosphate buffer (pH 2.5, 10 mM). After 1 hour, half of the beads were exchanged into phosphate buffer (pH 7.5, 10 mM), whereas the other half were kept in phosphate buffer (pH 2.5, 10 mM), at predetermined time intervals, 1 mL buffer was withdrawn and replaced with 1 mL fresh phosphate buffer with the same pH. The concentrations of rhodamine B in all release mediums were detected by UV-Vis spectrophotometry at a wavelength of 553 nm (SpectraMax i3, Molecular Devices, Sunnyvale, CA). The cumulative released percentage of rhodamine B was calculated from the calibration curve. All samples were analyzed in triplicate.

3.1.5 Preparation of silica nanoparticles

Silica nanoparticles were prepared in water-in-oil microemulsion system. Initially, 12 mL n-hexanol was dissolved in 60 mL cyclohexane, followed by adding 4mL deionized water. After 5 min, 10 mL Triton X-100 was added dropwise until the mixed solution became optically transparent. After 10 min of vigorous stirring, 500 μL aqueous ammonia solution (29 wt%) was added, followed by adding 1 mL TEOS. The reaction was allowed to stir for 24 hours at room temperature. 100 mL acetone was added to break the stability of microemulsion and the nanoparticles were recovered by centrifuge (4500 rpm, 10 min). In the end, nanoparticles were

washed three times with isopropyl alcohol and deionized water to remove the excess surfactant and cosurfactant.

3.1.6 Preparation of silica nanoparticles incorporated alginate beads

Rhodamine B (0.1 %w/v) was dissolved in 2 mL aqueous solutions of sodium alginate (very low viscosity, 5% w/v), then 174 mg wet silica nanoparticles were added and sonicated to get a good nanoparticle dispersion. This solution was added dropwise to a calcium chloride solution (5% w/v) under magnetic stirring for 15 min to form spherical beads. The wet rhodamine B loaded beads were washed with deionized water to remove unreacted calcium chloride and dried at ambient condition overnight.

3.1.7 Rhodamine B *in vitro* release study from silica nanoparticles incorporated alginate beads

All groups of beads were placed into 1 mL phosphate buffer (pH 2.5, 10 mM) for the first 1 hour. During this period, 1 mL buffer was withdrawn every 10 min and replaced with 1 mL fresh phosphate buffer (pH 2.5, 10 mM). After 1 hour, half of the beads were exchanged into phosphate buffer (pH 7.5, 10 mM), whereas the other half were kept in phosphate buffer (pH 2.5, 10 mM), at predetermined time intervals, 1 mL buffer was withdrawn and replaced with 1 mL fresh phosphate buffer with the same pH. The concentrations of rhodamine B in all release mediums were detected by UV-Vis spectrophotometry at a wavelength of 553 nm (SpectraMax i3, Molecular Devices, Sunnyvale, CA). The cumulative released percentage of rhodamine B was calculated from the calibration curve. All samples were analyzed in triplicate.

3.1.8 Preparation of silica-based monolithic gels

Rhodamine B loaded silica-alginate monolithic gels were prepared as follows, mixed 200 µL phosphate buffer (pH 2.5, 10 mM) with 1 mL TMOS solution for 2 min to form hydrolyzed TMOS solution. Rhodamine B (0.05 %w/v) was dissolved in aqueous solutions of sodium alginate (very low viscosity, 2.5 %w/v). Added 200 µL hydrolyzed TMOS solution into 1 mL rhodamine B alginate solution. Placed on a vortex mixer for 10 s. Transferred 150 µL of this mixed solution into the wells of a 96 well plate. Allowed the gels to be aged and air dried under room temperature. Rhodamine B loaded silica monolithic gels were also prepared, as controls for the release study, by mixing rhodamine B (0.5 %w/v) in deionized water with hydrolyzed TMOS solution, and followed the same procedure.

3.1.9 Rhodamine B *in vitro* release study from silica-based monolithic gels

In vitro release study of rhodamine B for each silica-alginate monolithic gel or silica monolithic gel was performed in 1 mL phosphate buffer (10 mM) with different pH values (pH 2.5 or pH 7.5) under room temperature. At predetermined time intervals, 0.5 mL phosphate buffer was withdrawn and replaced with 0.5 mL fresh phosphate buffer with the same pH. The concentrations of rhodamine B in all release mediums were detected by UV-Vis spectrophotometry at a wavelength of 553 nm (SpectraMax i3, Molecular Devices, Sunnyvale, CA). The cumulative released percentage of rhodamine B was determined from the calibration curve. All samples were analyzed in triplicate.

3.2 Results and discussions

3.2.1 Rhodamine B *in vitro* release study from alginate beads

Rhodamine B was encapsulated into the alginate hydrogel beads once rhodamine B alginate solution was dropped into the calcium chloride solution as shown in Figure 3.1. The formation of alginate beads is mainly due to the cross-link between guluronate monomers in alginate molecules with divalent calcium cations.[152] These divalent calcium cations fit into electronegative cavities like eggs in a box to from this ‘‘Egg Box’’ structure as shown in Figure 3.1.

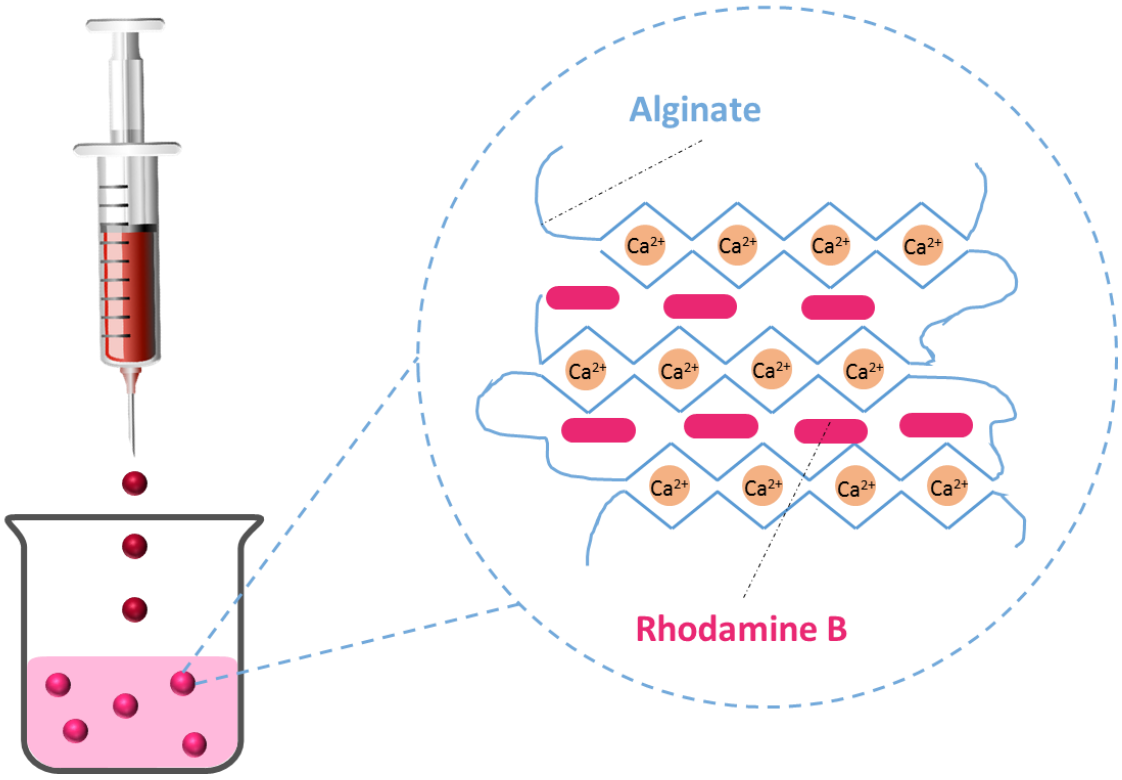

Figure 3.1 Illustration of the formation of rhodmine B loaded alginate beads in a calcium chloride solution and the ‘‘Egg Box’’ crosslinking structure of alginate beads.

Figure 3.2 shows the release profiles of rhodamine B from alginate beads. For the first 60 min, all beads were in pH 2.5 phosphate buffer to strength the structure, otherwise, alginate beads started to erosion if added directed into pH 7.5 phosphate buffer.[152] During this time, the release profiles were similar for both sets of beads with a range around 20 % cumulative released as shown in Figure 3.2 (A). Then, one set of beads was changed to pH 7.5 phosphate buffer; the other set of beads stayed in pH 2.5 phosphate buffer. As shown in Figure 3.2 (A), for the next hour, the beads in pH 7.5 phosphate buffer had a cumulative release percent increased to 41 %. However, the beads in pH 2.5 phosphate buffer only had a cumulative release percent increased to 33 %.

For the overall release profile for 48 hours as shown in Figure 3.2 (B), the beads in pH 7.5 phosphate buffer showed a rapid 90 % cumulative release in the first 8 hours and reached to 96 % at 48 hours. However, the beads in pH 2.5 phosphate buffer only had a 52 % cumulative release in the first 8 hours, and eventually reached to 76 % at 48 hours. This result showed the pH-responsive capability of alginate beads for rhodamine B. However, the cumulative release percent in pH 2.5 phosphate buffer got closer to the one in pH 7.5 phosphate buffer in the end. This is not the ideal situation for our target, which is limit the drug release at low pH. Therefore, the combination of silica and alginate might be a better solution.

The pH-dependent release could be due to the pH-responsive swelling ability of alginate beads or the pH-responsive interaction change between rhodamine B and alginate. Alginate hydrogel beads showed pH-responsive swelling capability as shown in Figure 3.3. The beads in pH 2.5 phosphate buffer showed almost no swelling from 3 hours-Figure 3.3 (B) to 8 hours-Figure 3.3 (D). However, the beads in pH 7.5 phosphate buffer showed significant swelling

during the same time. The pKa of alginate is about 3.2, this pH-responsive behavior is due to the $-COO^-$ groups of the hydrogel convert to -COOH groups in pH 2.5 phosphate buffer, which strengthens the hydrogen bonding interaction among hydrophilic groups and increases the physical crosslinking degree. Thus, the hydrogels show limited swelling capacity. However, in pH 7.5 phosphate buffer, the -COOH groups of the hydrogel become to $-COO^-$ groups, so the hydrogen bonding interaction among hydrophilic groups is broken, and the electrostatic repulsion among polymer chains is increased, which results in the hydrogels swell to enhance the diffusion of rhodamine B.[60, 62] In addition, rhodamine B also has COOH groups and with a pKa between 3.1-4.2.[153-155] Therefore, rhodamine B can also form hydrogen bonds with alginate molecules in pH 2.5 phosphate buffer, which would slow down the release. In contrast, the hydrogen bonds between rhodamine B and alginate would be broken in pH 7.5 phosphate buffer as they turn into ionic form. In the end, the release rate is faster than the one in pH 2.5 phosphate buffer.

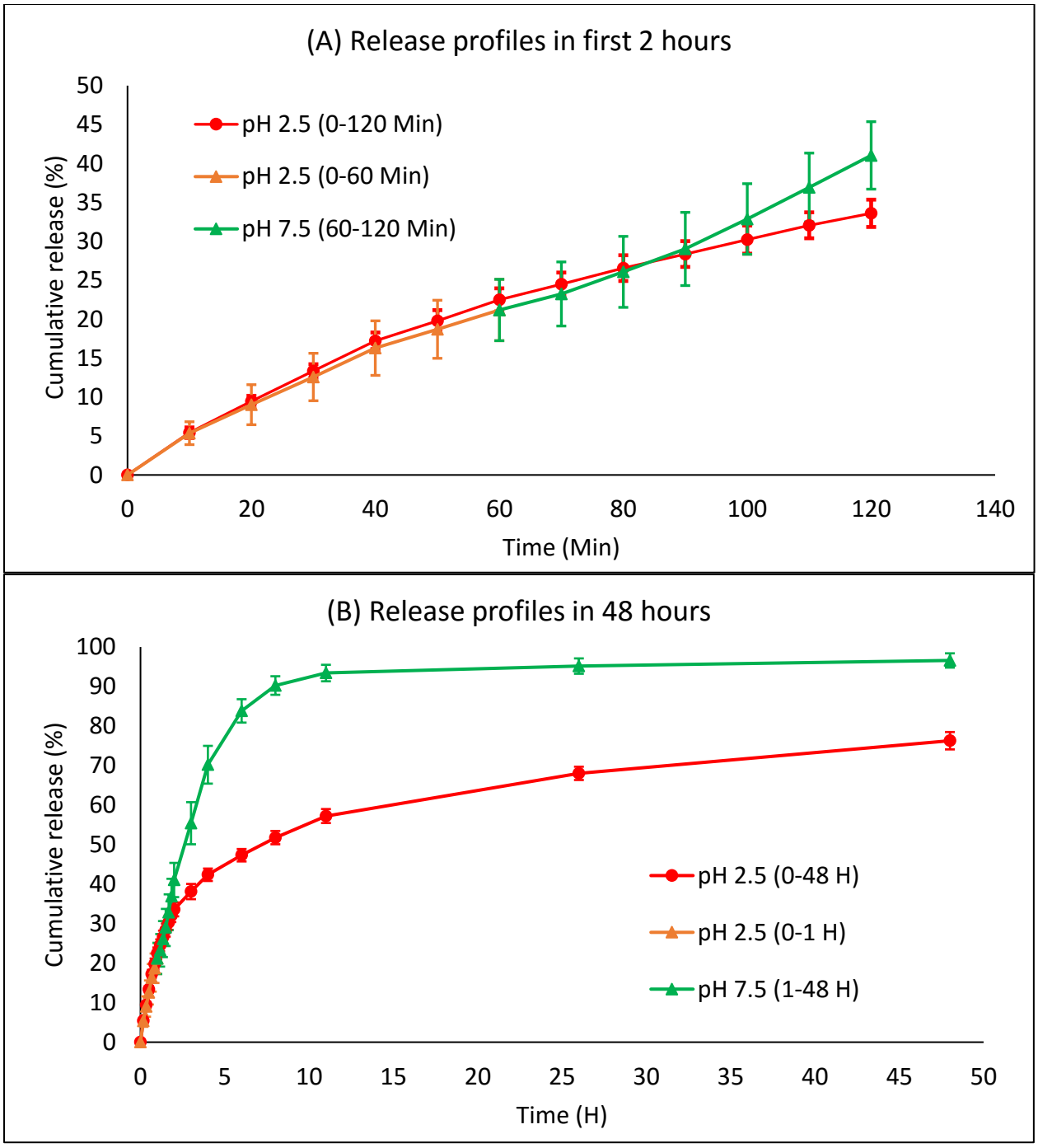

Figure 3.2 Rhodamine B *in vitro* release profiles from alginate (5 %w/v) beads in phosphate buffers with different pH values (pH 2.5 or pH 7.5). (A) Release profiles in first 2 hours. (B) Release profiles in 48 hours. The pH 7.5 sample was initially started in pH 2.5 buffer for 1 hour (no deviation observed from other pH 2.5 release profile) before change of buffer to pH 7.5 (at which point the release deviates from the other sample).

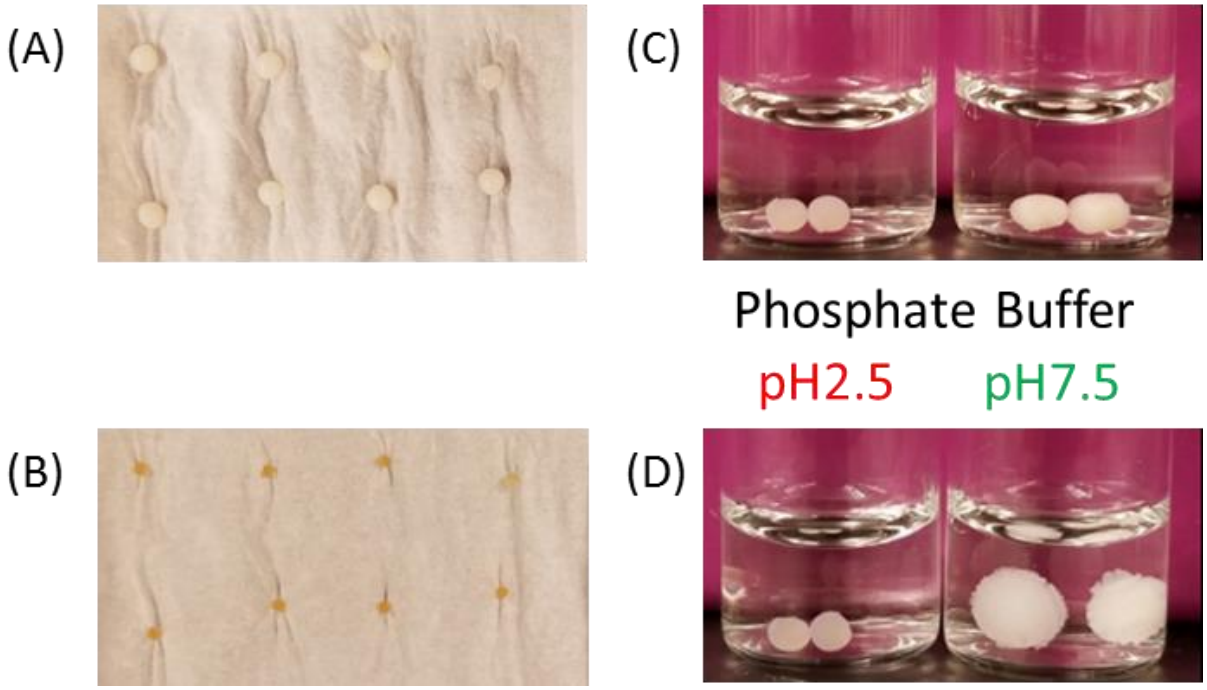

Figure 3.3 Alginate beads in different condition. (A) Wet beads after gelation. (B) Beads after air dried overnight. (C) Beads after swelling in phosphate buffers for 3 hours, left vial in pH 2.5 and right in pH 7.5. (D) Beads after swelling in phosphate buffers for 8 hours, left vial in pH 2.5 and right in pH 7.5.

3.2.2 Rhodamine B *in vitro* release study from silica nanoparticle incorporated alginate beads

Figure 3.4 shows the *in vitro* release profiles of rhodamine B from silica nanoparticles incorporated alginate beads. The release condition was same as the one used for the alginate beads. For the first 60 min, all beads were in pH 2.5 phosphate buffer, and the release profiles were also similar for both sets of beads with around 8 % released as shown in Figure 3.4 (A). Then, one set of beads was changed to pH 7.5 phosphate buffer, the other set of beads was stayed in pH 2.5 phosphate buffer. As shown in Figure 3.4 (A), for the next hour, the beads in pH 7.5 phosphate buffer had a cumulative release percent increased to 23%. However, the beads in pH 2.5 phosphate buffer only had a cumulative release percent increased to 16 %. For the overall release profile for 48 hours as shown in Figure 3.4 (B), the beads in pH 7.5 phosphate buffer showed a rapid 81% cumulative relate in the first 8 hours and reached to 93% at 48 hours. However, the beads in pH 2.5 phosphate buffer only had a 28 % cumulative release in the first 8 hours, and eventually reached to 50% at 48 hours.

This result also showed the pH-responsive capability of alginate beads even with silica nanoparticles inside. The addition of silica nanoparticles slowed down the release rate at both pH conditions as shown in Figure 3.5. This is probably due to the silica nanoparticles inside the alginate beads blocked parts of the pore of the beads, and served as diffusion barriers for rhodamine B diffusion process. This result showed that the addition of silica nanoparticles not only can improve the sustained release property of alginate hydrogel beads, but also keep the pH-responsive ability of the alginate beads.

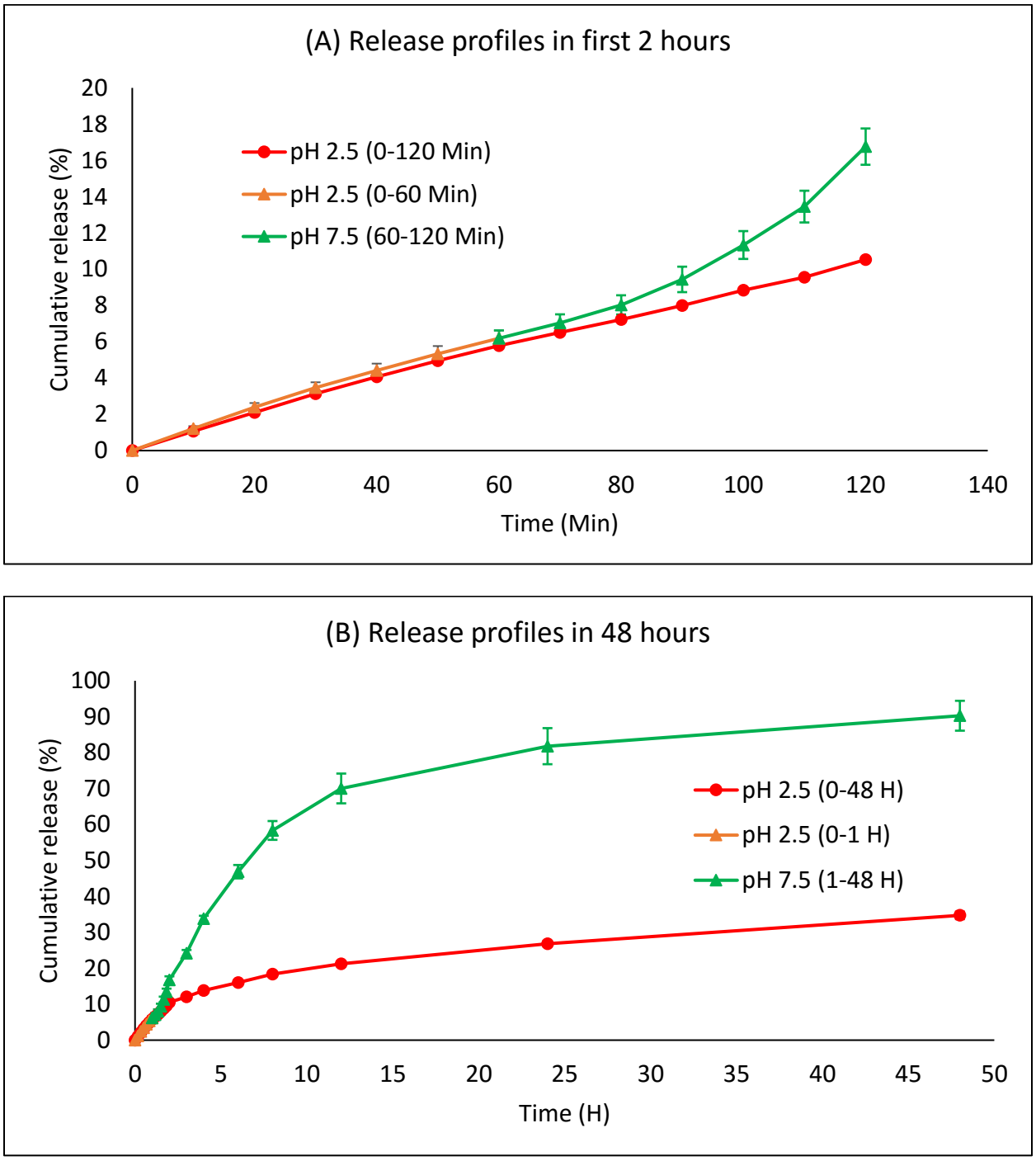

Figure 3.4 Rhodamine B *in vitro* release profiles from silica nanoparticle incorporated alginate beads in phosphate buffers with different pH values (pH 2.5 or pH 7.5). (A) Release profiles in first 2 hours. (B) Release profiles in 48 hours.

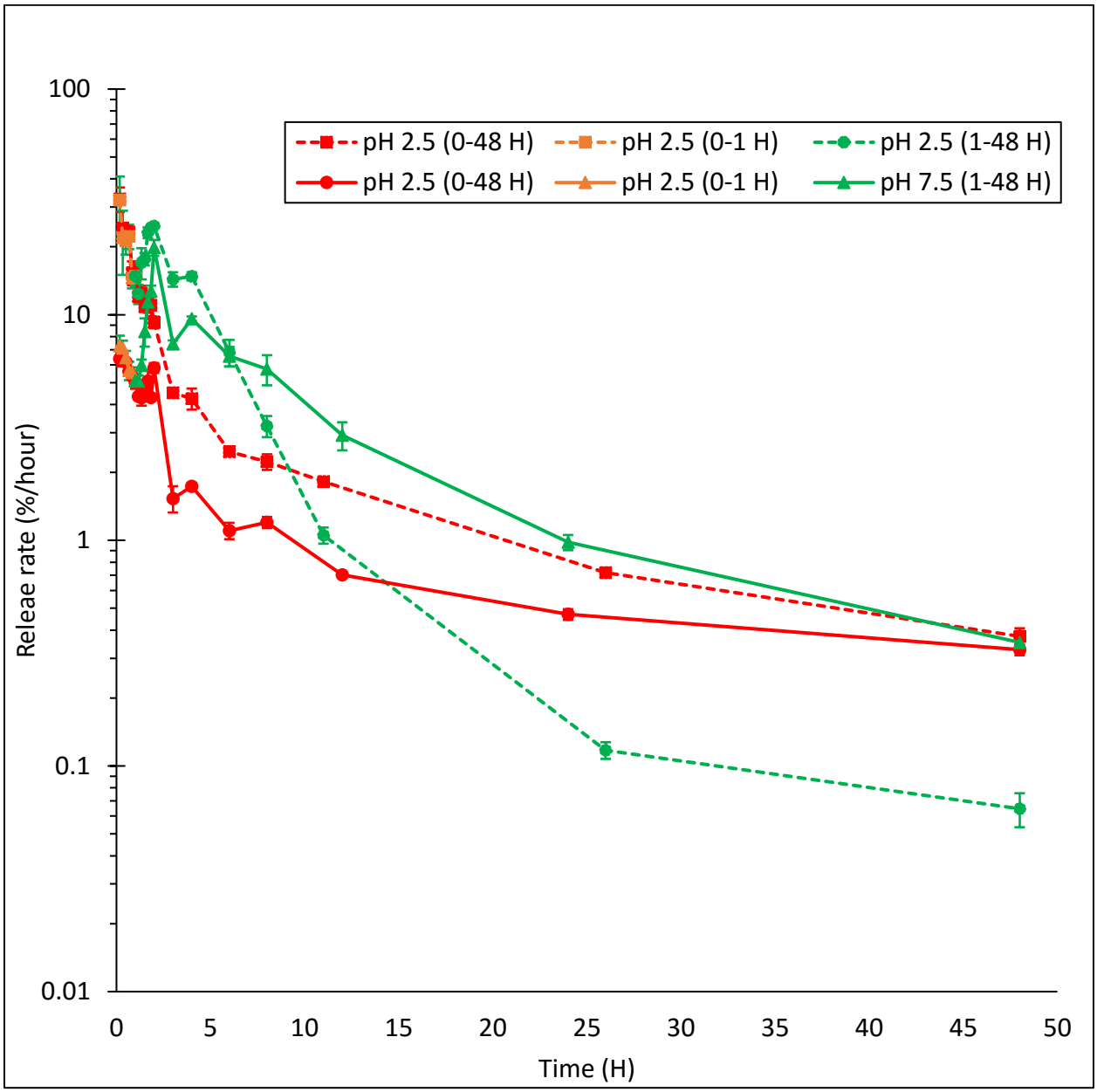

Figure 3.5 Comparison of release rate (%/hour) from alginate beads (dash line) and silica nanoparticle incorporated alginate beads (solid line) in phosphate buffers with different pH values (pH 2.5 or pH 7.5).

3.2.3 Rhodamine B *in vitro* release study from silica-based monolithic gels

This experiment was designed to evaluate the pH-responsive release ability of silica-alginate monolithic gels. To produce the drug loaded composite monolithic gels, rhodamine B was first dissolved in alginate solution, and then mixed with pre-hydrolyzed TMOS to form monolithic gels. *In vitro* release study was conducted in phosphate buffers (pH 2.5 and pH 7.5) at room temperature. As shown in Figure 3.6, the release profiles for silica monolithic gels (TMOS Gel) without alginate were similar at both pH buffers with around 18 % cumulative rhodamine B released over 25 days. The silica-alginate monolithic gels (TMOS/ALG Gel), however, displayed a significant difference in release rates with pH variation. In pH 2.5 phosphate buffer, only 2.6 % loaded rhodamine B was released over 25 days; however, 15.7 % loaded rhodamine B was released over the same period in pH 7.5 phosphate buffer. This difference in release profiles may be due to that at pH 2.5, hydrogen bonding among alginate and rhodamine B by protonation of the carboxylic acid groups slowed the release of rhodamine B, however, as pH increased to 7.5, the hydrogen bonding interaction between alginate and rhodamine B was broken, which resulted in a greater release of rhodamine B.

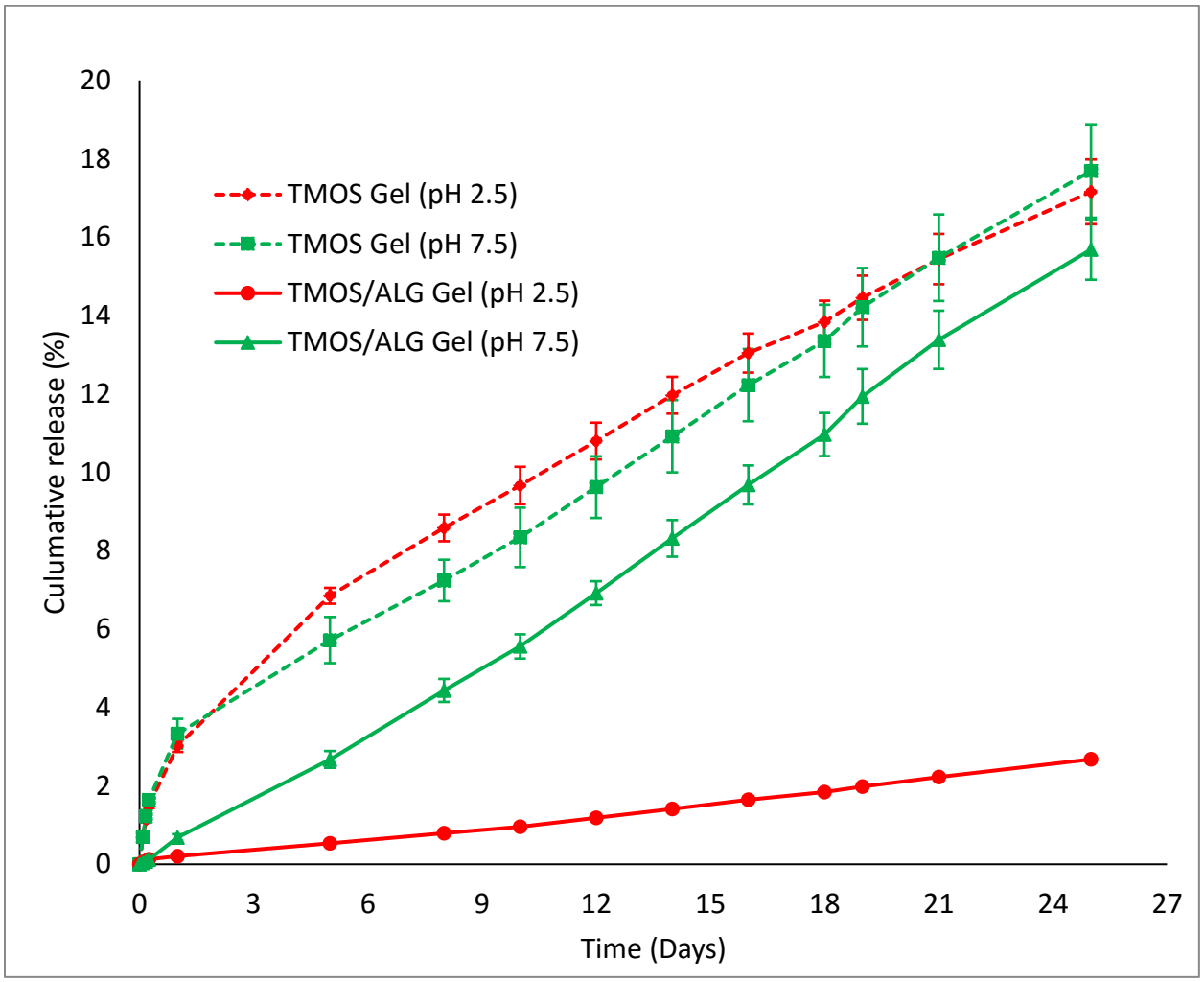

Figure 3.6 Rhodamine B *in vitro* release profiles from silica-based monolithic gels in phosphate buffers with different pH values (pH 2.5 or pH 7.5). Silica monolithic gel (dash line); silica-alginate monolithic gel (solid line)

3.3 Conclusions

Alginate beads showed pH-dependent release ability for rhodamine B. The release profile showed a significantly higher cumulative release percent in the first 8 hours in pH 7.5 phosphate buffer compared to the one in pH 2.5 phosphate buffer. However, after 48 hours, the gap of the release percent between two phosphate situations was reduced from 40 % (maximum) to 20 %. This showed us that although alginate beads had the pH-responsive control release ability, they cannot prevent most of the rhodamine B release at low pH solution, as still 76% released at 48 hours in pH 2.5 phosphate buffer. However, the addition of silica nanoparticles inside alginate beads can improve the sustained release of rhodamine B in both pH 2.5 and pH 7.5 phosphate buffers. In addition, the added silica nanoparticles caused no effect on the pH-responsive control release ability of alginate beads. Silica-alginate monolithic gels were also tested for the *in vitro* release study of rhodamine B. Encouraging result was observed with only 2.6 % loaded rhodamine B was released over 25 days; whereas, 15.7 % loaded rhodamine B was released over the same period in pH 7.5 phosphate buffer. This positive result with silica-alginate monolithic gels was promising for further studies with silica-alginate nanoparticles as pH-responsive drug carriers.

Chapter 4 Silica-alginate nanoparticles preparation by microemulsion

Silica sol-gel encapsulation via water-in-oil microemulsion has been widely studied for synthesis nano sized silica-based nanocomposites with different structures and compositions.[156] Silica sol-gel technique is under mild reaction condition for entrapping organic or biomolecules at ambient temperature through hydrolysis and polycondensation of the silica sol-gel precursor. In water-in-oil microemulsion system, water droplets, which are stabilized by surfactant, and sometimes cosurfactant, serve as nanoreactors for nanoparticle synthesis.[157] In this process, silica sol-gel precursor, typically TEOS, is first added into bulk oil phase, then diffuses into water droplets as hydrolyzed TEOS molecules. Components inside the water droplets prior to addition of TEOS can be effectively encapsulated inside the silica nanoparticles by polycondensation process.[158] The structure and size of the silica-based particles can be simply controlled by varying microemulsion parameters.[159] Most of the organic compositions encapsulated into silica nanoparticles via microemulsion method are fluorescent dye molecules, such as tetramethylrhodamine[108], rhodamine B[160], and fluorescein isothiocyanate.[161] To our knowledge, no silica-polysaccharide nanocomposites particles have been synthesis by this method.

4.1 Materials and methods

4.1.1 Materials

Sodium alginate was purchased from Acros; tetraethyl orthosilicate with 98 % purity was purchased from Sigma Aldrich; Triton X-100 and rhodamine B were purchased from AMRESCO; cyclohexane, ethanol, aqueous ammonia solution (29 wt% ammonia), isopropyl alcohol (70 %), hydrochloric acid (37 %), sulfuric acid was purchased from BDH Chemicals; n-hexanol, ammonium molybdate, 4-methylaminophenol sulfate, oxalic acid dehydrate were purchased from Alfa Aesar. All chemicals were used without further purification. Deionized water used throughout the experiments was purified with an ELGA PURELAB Flex water purification system.

4.1.2 Stability of alginate in silica sol-gel process

Alginate solution (2 %w/v) was prepared by dissolving 2 g sodium alginate in 100 mL deionized water. To test the stability of alginate with the presence of ethanol, different volumes of ethanol were mixed with fixed amount of alginate solutions. After mixing for 24 hours, the stability of all mixed solutions was checked by the presence of alginate precipitation. Pure alginate solution was used as a control group.

4.1.3 Synthesis of silica nanoparticles

Silica nanoparticles were prepared in water-in-oil microemulsion system. Typically, 12 mL n-hexanol was dissolved in 60 mL cyclohexane, followed by adding 4mL deionized water. After 5 min, 10 mL Triton X-100 was added dropwise until the mixed solution became optically

transparent. After 10 min of vigorous stirring, 500 μL aqueous ammonia solution (29 wt%) was added, followed by adding 1 mL TEOS. The reaction was allowed to stir for 24 hours at room temperature. 100 mL acetone was added to break the stability of microemulsion and the nanoparticles were recovered by centrifuge (4500 rpm, 10 min). In the end, nanoparticles were washed three times with isopropyl alcohol and deionized water to remove the excess surfactant and cosurfactant.

4.1.4 Synthesis of silica-alginate nanoparticles

Silica-alginate nanoparticles were prepared in water-in-oil microemulsion system. Typically, 12 mL n-hexanol was dissolved in 60 mL cyclohexane, followed by adding 4 mL alginate aqueous solution. After 5 min, 10 mL Triton X-100 was added dropwise until the mixed solution became optically transparent. After 10 min of vigorous stirring, 500 μL aqueous ammonia solution (29 wt%) was added, followed by adding 1 mL TEOS. The reaction was allowed to stir for 24 hours at room temperature. 100 mL acetone was added to break the stability of microemulsion and the nanoparticles were recovered by centrifuge (4500 rpm, 10 min). In the end, nanoparticles were washed three times with isopropyl alcohol and deionized water to remove the excess surfactant and cosurfactant.

4.1.5 Thermogravimetric analysis

Thermogravimetric analysis (TGA) was performed with a TA-500 thermogravimetric analyzer (TA). The experiments were carried out in an atmosphere of flowing air (40 mL/min) at a heating rate of 10 °C/min up to 900 °C with an isothermal condition at 120 °C for 20 mins. The

samples of silica nanoparticles and silica-alginate nanoparticles were prepared by freeze drying method for 24 hours.

4.1.6 Silicomolybdic acid assay of silica concentration in aqueous solution

Silica concentrations in composite particles were determined by silicomolybdic acid assay prepared by a modified literature procedure.[162] The reagents used for this method were prepared as follows: Acidified ammonium molybdate: dissolved 1 g ammonium molybdate with 100 mL pure water. Then added 3 mL concentrated hydrochloric acid. Metol-sulfite reagent: dissolved 0.6 g of anhydrous sodium sulfite with 40 mL pure water, and added 1 g 4-methylaminophenol sulfate. Then added pure water to 50 mL, and filtered through a 0.2 μm filter. Mixed reducing reagent: mixed 10 mL metol-sulfite reagent, 6 mL 10 % oxalic acid, 6 mL sulfuric acid and 8 mL pure water. In a typical experiment, 0.2 mL of acidified ammonium molybdate reagent was added into 0.5 mL sample. After 15 min, 0.3 mL of mixed reducing reagent was added. Developed the sample for 2.5 hours at room temperature before measuring the absorbance by UV-Vis spectrophotometry at a wavelength of 810 nm (SpectraMax i3, Molecular Devices, Sunnyvale, CA). Known amount of silica nanoparticle dissolved in sodium hydroxide (1 M) was used for standard curve. And known amount of silica-alginate nanoparticle dissolved in sodium hydroxide (1 M) was used sample testing.

4.1.7 Transmission electron microscopy

A Zeiss EM 10 Transmission electron microscopy (TEM) operating at a voltage of 60 kV was used to determine size of silica-alginate nanoparticles. TEM samples were prepared by placing a single drop of the silica-based nanoparticle suspension on a carbon type B, 300 mesh

grid. This grid was then placed in a petri dish and allowed to dry at ambient condition. Size distributions were obtained using ImageJ software.

4.2 Results and discussions

4.2.1 Stability of alginate in silica sol-gel process

Ethanol is the byproduct of TEOS hydrolysis during silica sol-gel process. And this byproduct could cause denaturation of enzymes or unfolding of biomacromolecules.[163] Therefore, it is important to find out how ethanol affects the stability of alginate in silica sol-gel process. In this study, four different alginate-ethanol mixed solutions were tested, which are presented in Figure 4.1. There was no alginate precipitation out of the solution for sample A, which had 10% v/v ethanol. Moreover, this mixing solution looked the same as control group E, which was pure alginate solution. All the other three samples (B, C, D) with higher ethanol volume ratios showed phase separation immediately after mixing. Therefore, this result showed that alginate had good stability with 10% v/v ethanol. For the all the silica-alginate nanoparticles synthesized by water-in-oil microemulsion in this study, ethanol produced by TEOS hydrolysis were smaller than 10% v/v, so there was no need to remove ethanol during the silica sol-gel encapsulation process.

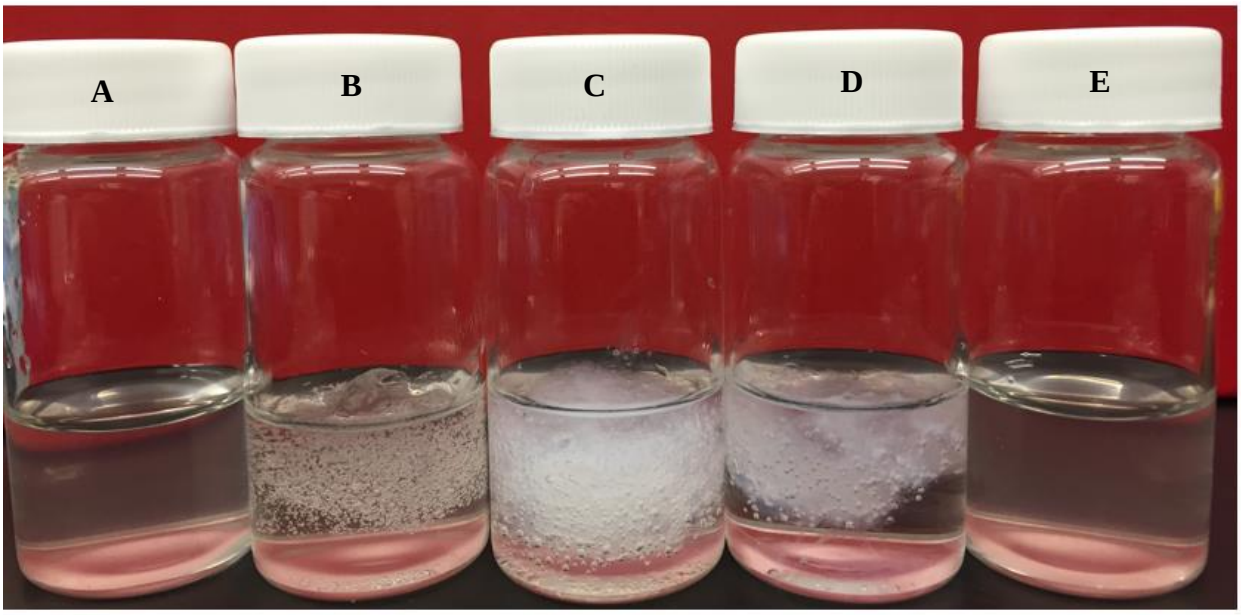

Figure 4.1 Photographs of alginate (2 %w/v) solutions mixed with ethanol. Phase separation is due to the insoluble alginate. (A)10 %v/v ethanol (9 mL alginate solution + 1 mL ethanol); (B) 20 %v/v ethanol (8 mL alginate solution + 2 mL ethanol); (C) 50 %v/v ethanol (5 mL alginate solution + 5 mL ethanol); (D) 80 %v/v ethanol (2 mL alginate solution + 8 mL ethanol); E (10 mL alginate solution)

4.2.2 Synthesis of silica-alginate nanoparticles

Figure 4.2 shows the schematic drawing of silica sol-gel encapsulation process in water-in-oil microemulsion. In this system, cyclohexane was the bulk oil phase, Triton X-100 was the surfactant, n-hexanol was the cosurfactant, and sodium alginate aqueous solution formed the water phase droplets, as shown in Figure 4.2 (A). There are three stages of silica-alginate nanoparticles formation within water-in-oil microemulsion:[164] (1) association of TEOS with water-in-oil microemulsion, at this stage, most of the TEOS molecules are outside the water droplets due to the hydrophobicity of TEOS molecules, as shown in Figure 4.2 (B); (2) hydrolysis of TEOS and formation of monomers, the addition of NH_4OH increases the hydrolysis of TEOS, then hydrolyzed TEOS species become more hydrophilic and penetrate into the water droplets, as shown in Figure 4.2(C); (3) after nucleation and particle growth process, alginate is encapsulated inside silica nanoparticles, as shown in Figure 4.2 (D).

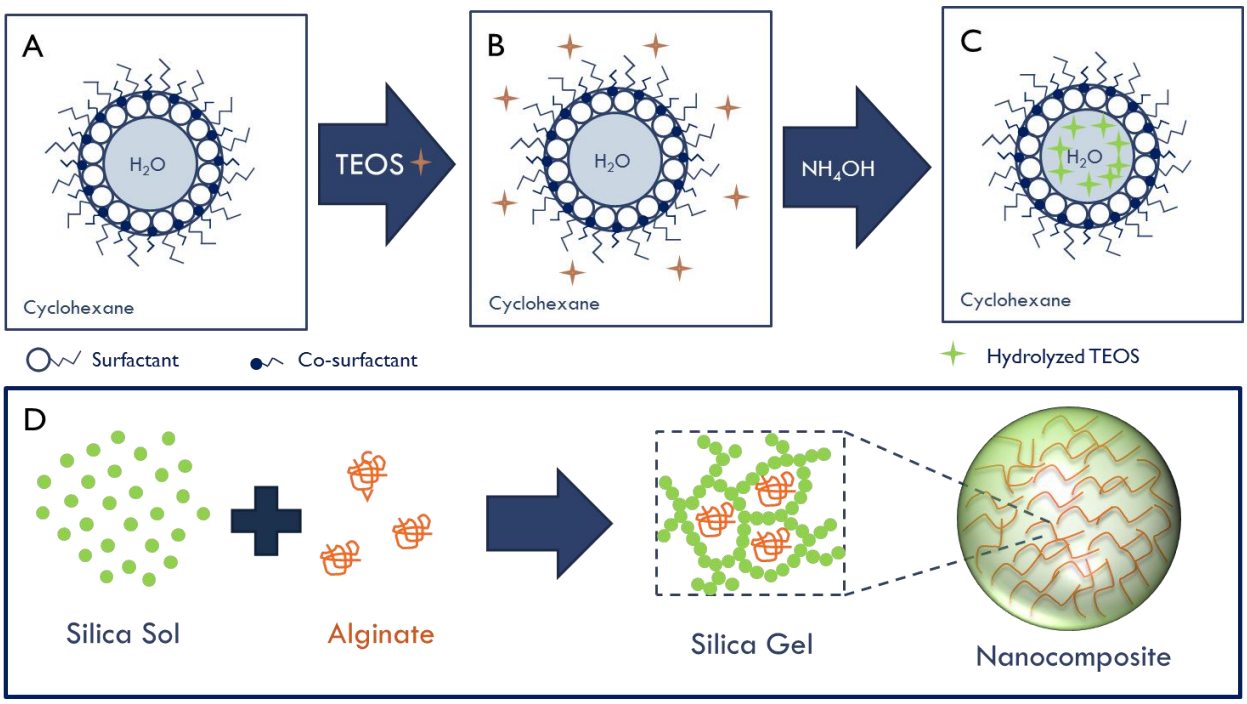

Figure 4.2 Schematic illustration of silica sol-gel encapsulation process in water-in-oil microemulsion. (A) Water phase droplet surrounded by surfactant and cosurfactant in water-in-oil microemulsion. (B) Association of TEOS with water-in-oil microemulsion, at this stage, most of the TEOS molecules are outside the water droplets due to the hydrophobicity of TEOS molecules. (C) Hydrolysis of TEOS and formation of monomers due to the addition of NH_4OH, hydrolyzed TEOS species become more hydrophilic and penetrate into the water droplets. (D) Encapsulation process of alginate into silica nanoparticles in water phase droplets.

In most literature, the synthesis time was 24 hours for silica nanoparticles by water-in-oil microemulsion.[165, 166] Although, 2 hour reaction time was chosen by García, et al.[167], they used methanol as cosurfactant instead of n-hexanol. In order to determine the relationship between reaction time and the formation of nanoparticles, 3.6 mL n-hexanol, 15 mL cyclohexane, 1 mL alginate aqueous solution (0.1 %w/v), 3.6 mL Triton X-100, 1200 µL aqueous ammonia solution (29 wt%), and 0.5 mL TEOS were used. Parts of the mIcroemulsion was taken at 24 hours, 48 hour, 72 hour, 96 hour and 120 hour. Time is a parameter that directly affects the size distribution of silica-based nanoparticles. An increase in time usually involves an

increase in particle size, because of nuclei formed in the nucleation stage stop growing and start to coalesce.

As shown in Figure 4.3, all particles were spherical in shape and monodispersed at different reaction times. In addition, only a 5 % size increase of nanoparticles was observed from 24 to 120 hours. The average size for nanoparticles obtained was 73.40 ± 2.33 nm at 24 hours; 75.98 ± 3.51 nm at 48 hours; 76.74 ± 2.81nm at 72 hours; 79.44 ± 2.10 nm at 96 hours; and 77.24 ± 1.80 nm at 120 hours. This indicated there were limited number of monomers for particle growth after 24 hours, and most of the silica sol-gel encapsulation process was finished during this time. Therefore, 24 hours was used for as reaction time of nanoparticles preparation for silica-based nanoparticle synthesis.

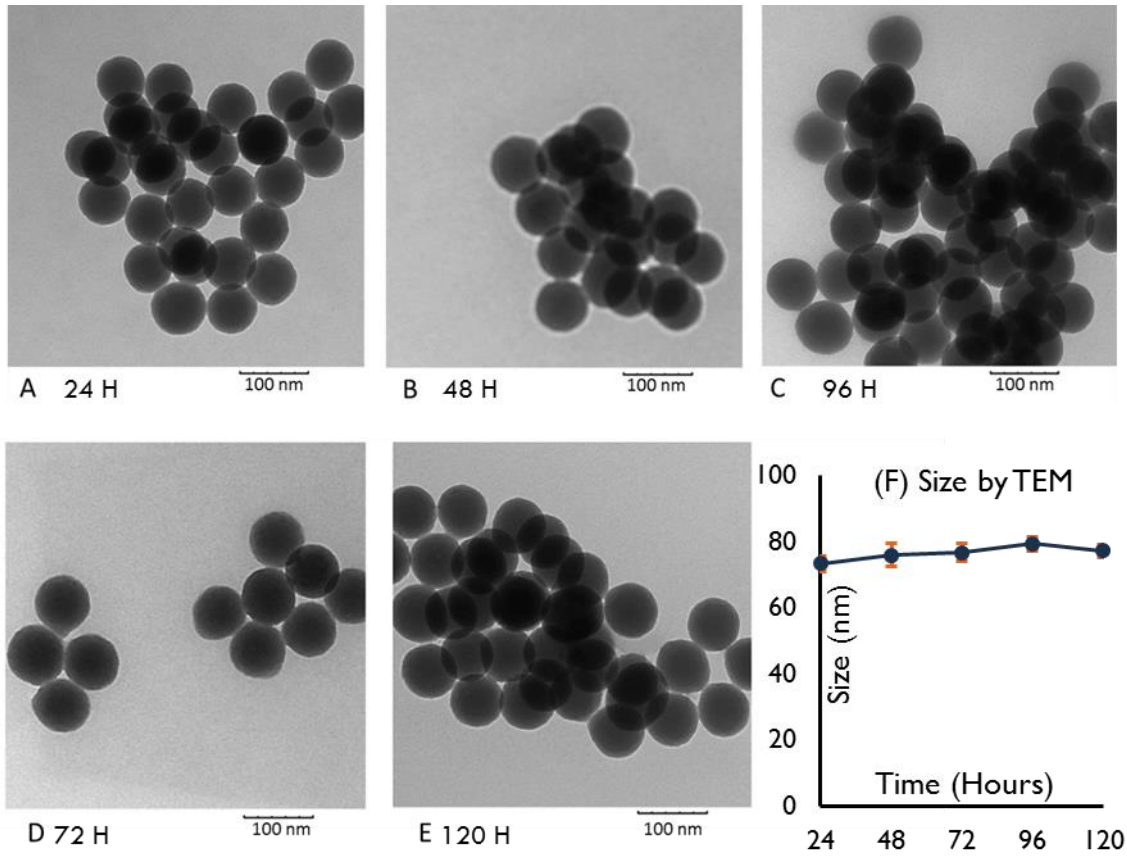

Figure 4.3 TEM images of silica-alginate nanocomposite nanoparticles obtained after different reaction times, (A) 24 hours, (B) 48 hours, (C) 72 hours, (D) 96 hours and (E) 120 hours. (F) Average size at different reaction time from TEM images.

4.2.3 Encapsulation of alginate inside silica nanoparticle

To confirm the encapsulation of alginate inside silica nanoparticles, TGA characterizations of sodium alginate, silica nanoparticles, and silica-alginate nanoparticles were carried out. In order to minimize the effect of surface bonded water, all experiments had an isothermal condition at 120 °C for 20 min. The TGA and DTGA (first derivative TGA) curves in Figure 4.4 (A) suggests that, under heating, sodium alginate showed an initial dehydration process followed by two decomposition steps, 200-300 °C and 500-600 °C, then formed sodium carbonate residue with 85 % weight loss.[168] As shown in Figure 4.4 (B), the weight of pure silica nanoparticles was 5 % in the process. After the initial dehydration step, the main weight loss occurred between 400-600 °C, which was due to further condensation of surface and internal hydroxyl groups.[169] Figure 4.4 (C) presents the TGA and DTGA curves of silica-alginate nanoparticles with three different initial concentrations (1% w/v; 0.5% w/v; 0.1% w/v) of alginate solutions used in water-in-oil microemulsion. All of them had the similar decomposition steps as sodium alginate. These results confirmed the encapsulation of alginate during the silica sol-gel process in water-in-oil microemulsion. In addition, the weight ratio of alginate inside the silica nanoparticle can also be controlled by changing the initial concentration of alginate solution used. As shown in Figure 4.4 (C), 0.1% w/v alginate solution used resulted in 9.5% weight loss, 0.5% w/v alginate solution used resulted in 12 % weight loss, 1% w/v alginate solution used resulted in 15 % weight loss.

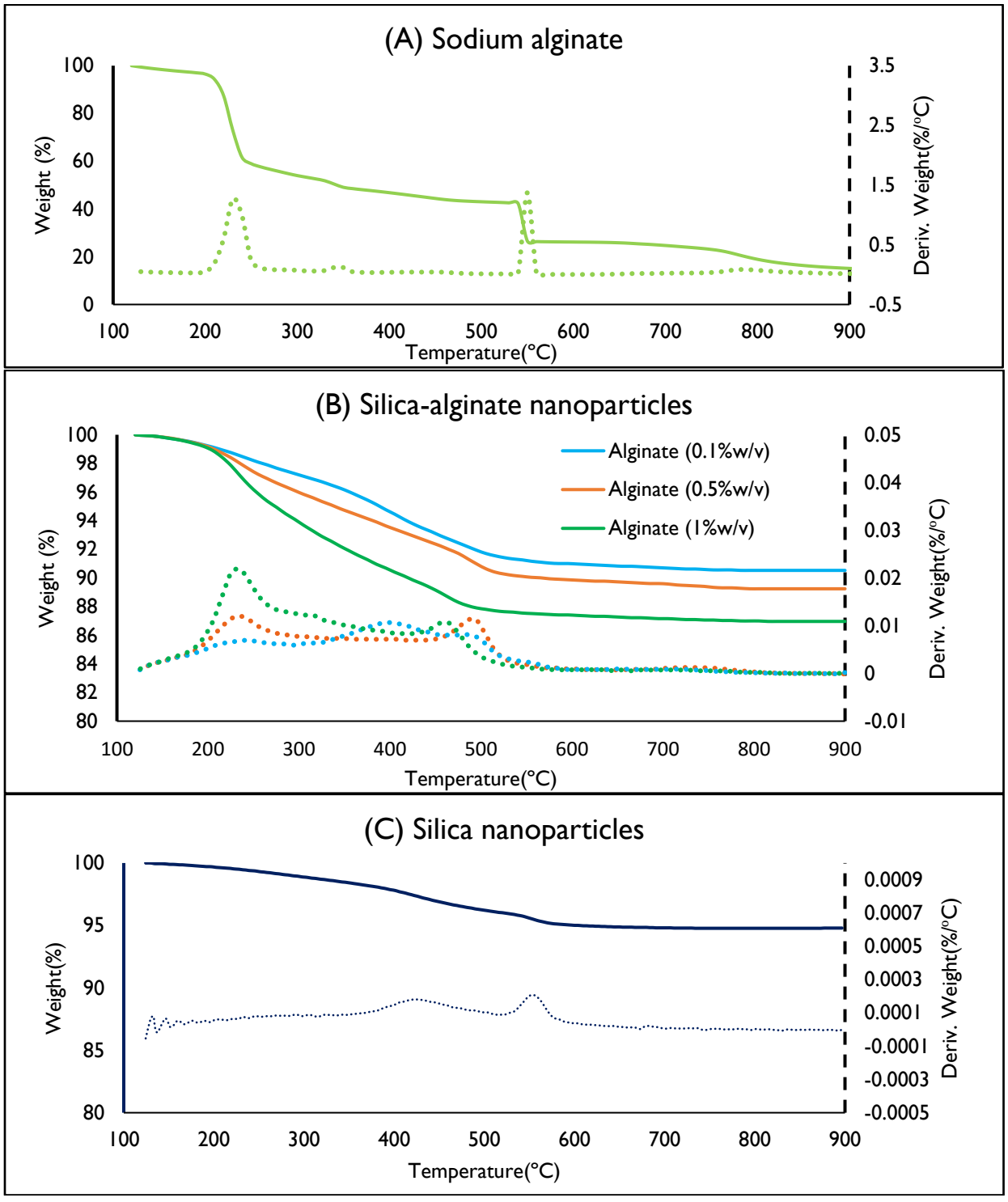

Figure 4.4 TGA (solid) and DTG (dash) curves for (A) sodium alginate, (B) silica-alginate nanoparticles, (C) silica nanoparticles.

Silicomolybdic acid assay is another way to calculate the weight ratio of alginate in silica-alginate composite materials. This analysis method detects dissolved silica concentration in aqueous solution. Silica reacts with acidified ammonium molybdate to form beta-molybdosilicic acid (silicomolybdate). A mixed reducing solution, containing metol (4-methylaminophenol sulfate) and oxalic acid, is then added to form a molybdenum blue complex, which shows a maximum absorbance at 810 nm.[162] TEOS silica nanoparticles, via the same water-in-oil microemulsion method, dissolved in NaOH (1 M) was used as the standard solution. Figure 4.5 (A) shows the standard curve of dissolved silica nanoparticles with a linear relationship of silica concentration and absorbance. Silica-alginate nanoparticles were also dissolved in NaOH (1 M) with a concentration of 5 μg/mL, and then the concentration of silica in nanocomposite solution was obtained by this assay. In the end, the alginate weight ratio can be calculated according to the standard curve. As shown in Figure 4.5 (B), for 0.1 %w/v initial alginate solution used, alginate weight ratio was 10.70 % from silica assay (9.47 % from TGA); for 1 %w/v initial alginate solution used, alginate weight ratio was 14.97 % from silica assay (13.04 % from TGA). Although more alginate weight ratios were obtained compared to TGA weight loss, the weight ratio trend was the same as TGA. The nanoparticles made from 0.1 %w/v alginate showed less alginate weight ratio compared to the nanoparticles made from 1 %w/v alginate. This variation may be due to the experimental error by different methods. Therefore, silica assay provides another way to confirm the encapsulation of alginate inside silica-based nanoparticles.

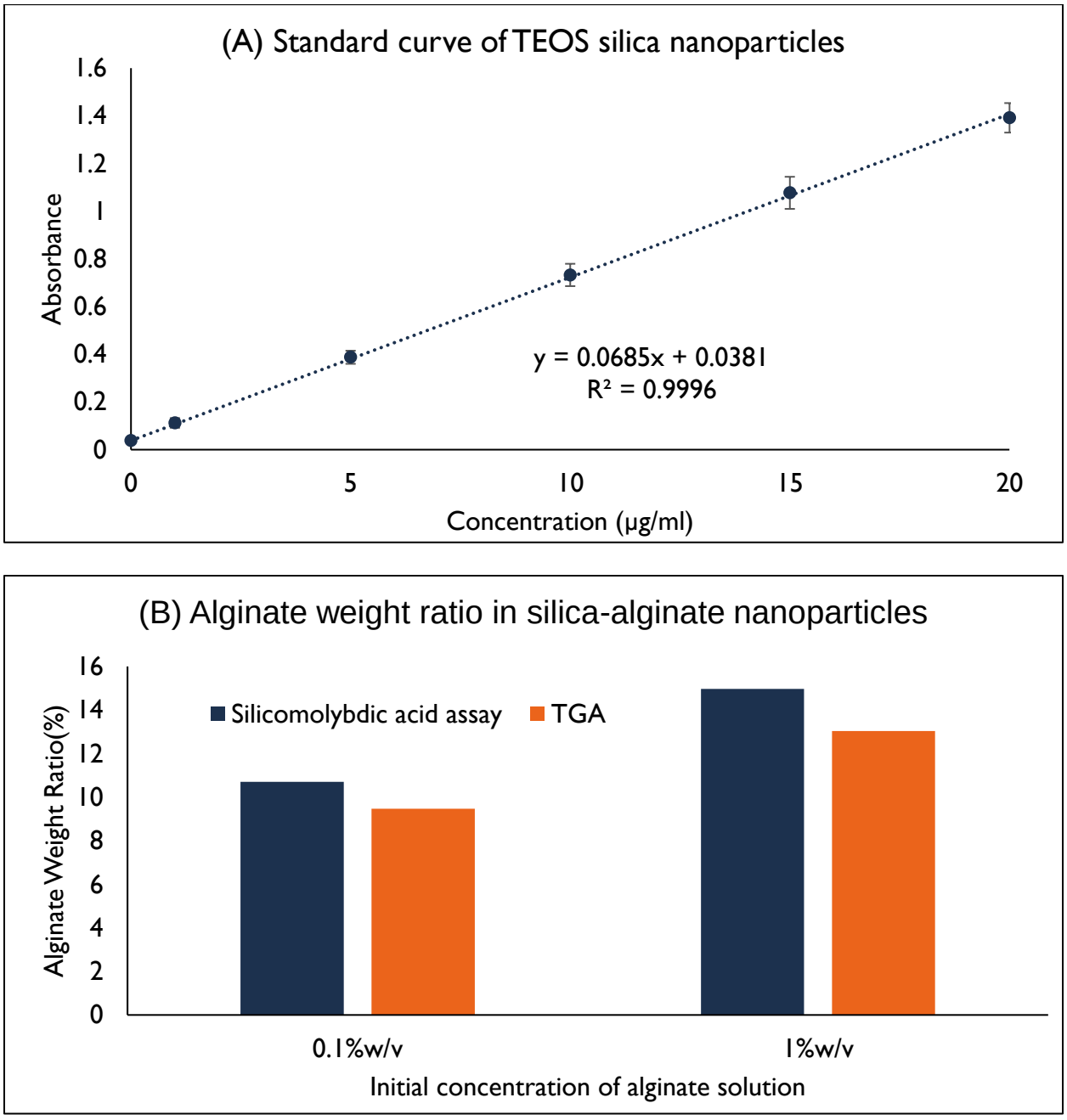

Figure 4.5 (A) Standard curve of TEOS silica nanoparticles by silicomolybdic acid assay, (B) Alginate weight ratio in silica-alginate nanoparticles measured by TGA and silicomolybdic acid assay.

4.2.4 Size control of silica-based nanoparticles

The size of silica-based nanoparticles can be controlled by different parameters in water-in-oil microemulsion, such as water to surfactant molar ratio (R), cosurfactant to surfactant molar ratio (ρ), catalyst concentration and even types of silica sol-gel precursors. Here we studied how water to surfactant molar ratio (R) and different silica sol-gel precursors affect the particle size. At first, TEOS silica nanoparticles with different R values were tested, the experimental detail is listed in Table 4.1 (A&B) and the TEM images of nanoparticles are shown in Figure 4.6 (A&B). At R = 6.40, the average size was 81.6 nm, however, at R = 11.20, average size was 52.6 nm. Next, TEOS silica nanoparticles and TMOS silica nanoparticles were produced, as listed in Table 4.1 (C&D), with same R value. As shown in Figure 4.6 (C&D), for TEOS silica nanoparticles, the average size was 79.6 nm; however, for TMOS silica nanoparticles, the average size was 26.6 nm.

Table 4.1 Experimental details for silica nanoparticles

	Cyclohexane (mL)	n-hexanol (mL)	Water (mL)	Triton X-100 (mL)	NH_4OH (mL)	Silica source (mL)	R
A	60	14	4	21	0.2	TEOS 1 mL	6.40
B	60	8	4	12	0.2	TEOS 1 mL	11.20
C	60	20	6	25	0.5	TEOS 1.5 mL	8.06
D	60	20	6	25	0.5	TMOS 1.5 mL	8.06

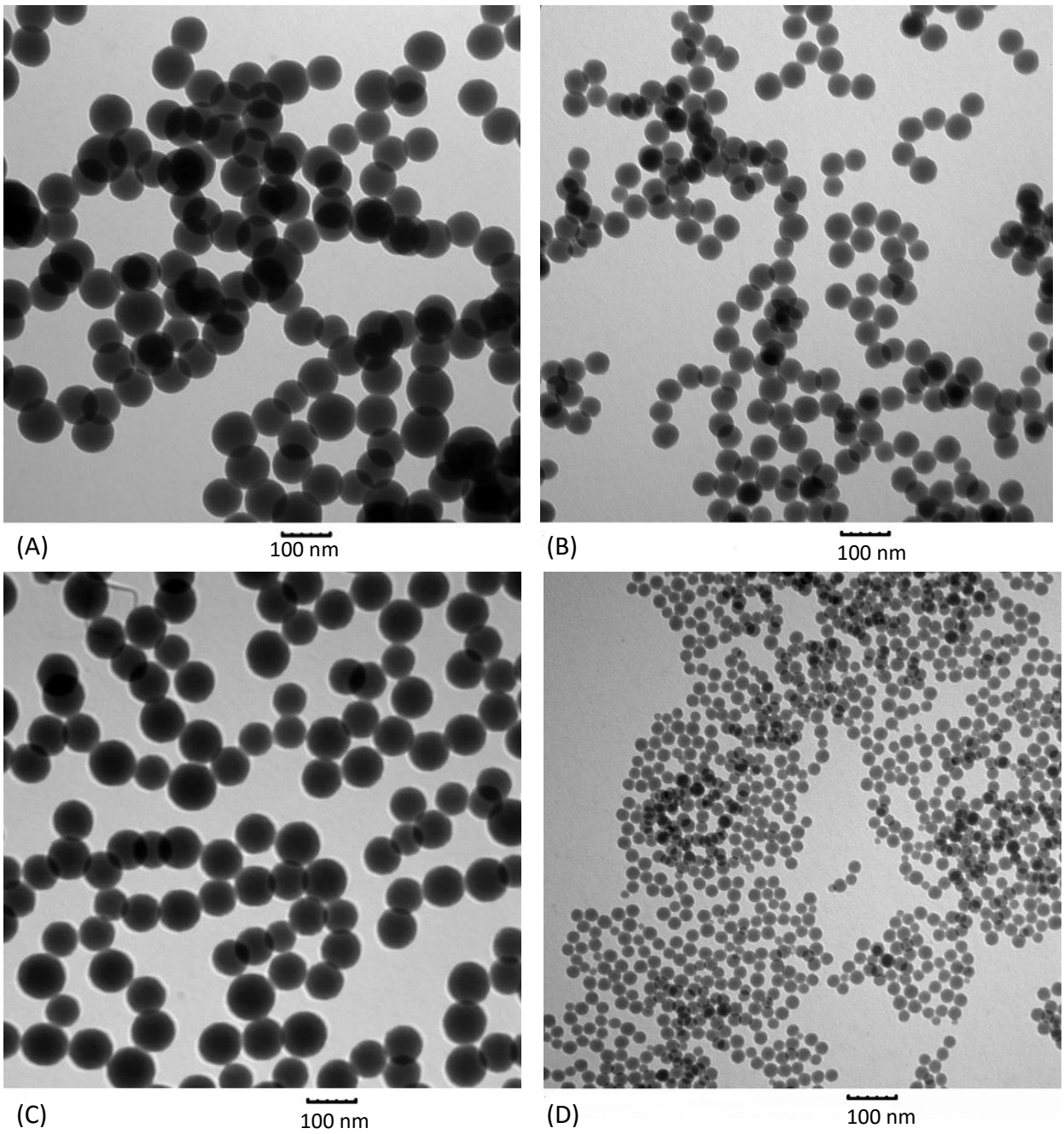

Figure 4.6 TEM images of silica nanoparticles. (A) TEOS silica nanoparticles, R = 6.40, particle size: 81.6 ± 7.2 nm; (B) TEOS silica nanoparticles, R = 11.20, particle size: 52.62± 4.5 nm; (C) TEOS silica nanoparticles, R = 8.06, particle size: 79.6 ± 8.3 nm; (D) TMOS silica nanoparticles, R = 8.06, particle size: 26.6 ± 3.7 nm.

Water to surfactant molar ratio (R) affects several parameters in water-in-oil microemulsion. Such as, the size of water droplets, the ratio of bulk water molecules to bound water molecules, the number of monomers per water droplet, the rigidity of the surfactant-water interface and the dynamics of intermicellar interaction.[170] For the synthesis of silica-based nanoparticles. The smaller the R value the smaller water droplets, which leads to less TEOS molecules at the surfactant-water interface. Consequently, there is a smaller number of monomers and less nuclei formation. In addition, the intermicellar exchange decreases due to the increased rigidity of surfactant-water interface, which makes less mobility of monomers. However, there are more monomers and oligomers available for particle growth, therefore particle size is larger in the end.[103, 167, 171]

For the different type of silica sol-gel precursors, TMOS has higher hydrolysis rates compared to TEOS due to the retarding effect of the bulkier ethoxide group.[164] Therefore, in the case of TMOS nanoparticles, faster hydrolysis rate results in a large number of monomers, which turns into a larger number of nuclei. Faster hydrolysis rate also produces more methanol, which can be used as a cosurfactant to increase the fluidity of the interface, therefore increasing the intermicellar exchange. These conditions lead to smaller particle size.[103]

The impact of water to surfactant molar ratio (R) on the size of silica-alginate nanoparticles was also studied. The experimental design is listed in Table 4.2. As shown Figure 4.7, all particles showed spherical shape particles, and the particle size increased with decreased R value. At R=22.39, the average particle size was 24.3 nm and increased to 39.0 nm when R=16.79, further increased to 49.3 nm with R=9.59. Therefore, the size changing by water to

surfactant molar ratio (R) of silica-alginate nanoparticles followed the same trend of silica nanoparticles.

Table 4.2 Experimental details for silica-alginate nanoparticles with different R values

	Cyclohexane (mL)	n-hexanol (mL)	Alginate(0.05%w/v) (mL)	Triton X-100 (mL)	NH_4OH (mL)	TEOS (mL)	R
A	60	7.2	4	6	0.5	1	22.39
B	60	9.6	4	8	0.5	1	16.79
D	60	16.8	4	14	0.5	1	9.59

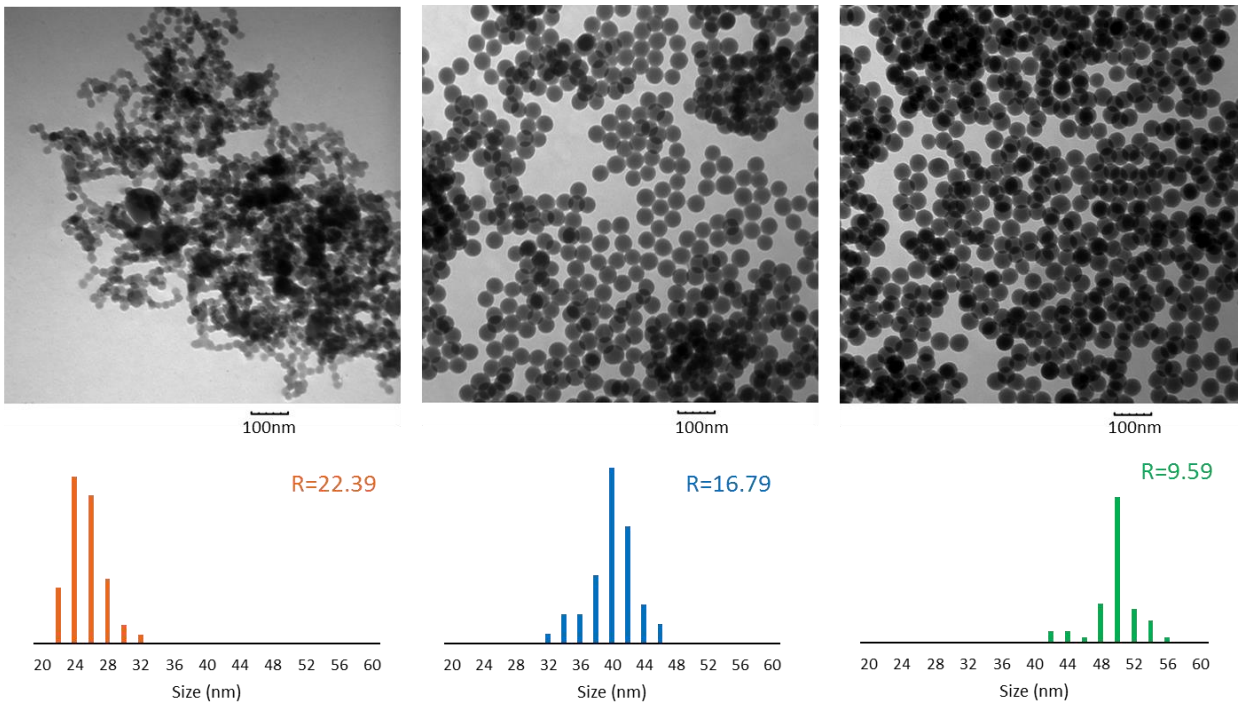

Figure 4.7 TEM images of silica-alginate nanoparticles with different R values (Particle size 24.3 ± 2.4 nm at R=22.39, particle size 39.0 ± 3.1 nm at R=16.79, particle size 49.3 ± 3.3 nm at R=9.59.)

Alginate concentration is another factor to control the size of silica-alginate nanoparticles. As the TEM images shown in Figure 4.8 and the experimental design is listed in Table 4.3. The higher the alginate concentration used the smaller the particles size. The average particles size was 37.3 nm when 1 %w/v alginate was used, while the average size increased to 57.2 nm when 0.05 %w/v alginate was used. Although, alginate can form hydrogen bonding with silica source during the sol-gel process,[172] the interaction of alginate solution with flexible surfactant layers should be the control factor. This interaction may change droplet elasticity parameters, shape, fluctuations, mutual interactions and affect deeply the system phase behavior and rheological properties.[173] In our system, alginate inside the water droplet may increases the fluctuations of these dispersed droplets, which destabilizes larger domains and results in smaller domains with a larger surface to volume ratio.[174] As a result, more TEOS associates with water droplets, which results in the increasing of hydrolysis rate of TEOS for a higher number of nuclei, and eventually smaller particle size.

Table 4.3 Experimental details for silica-alginate nanoparticles with different initial alginate concentrations used in microemulsion.

	Cyclohexane (mL)	n-hexanol (mL)	Alginate (7.5 mL)	Triton X-100 (mL)	NH_4OH (mL)	TEOS (mL)	R
A	80	30	1 %w/v	45	0.9	1.5	5.60
B	80	30	0.5 %w/v	45	0.9	1.5	5.60
D	80	30	0.05 %w/v	45	0.9	1.5	5.60

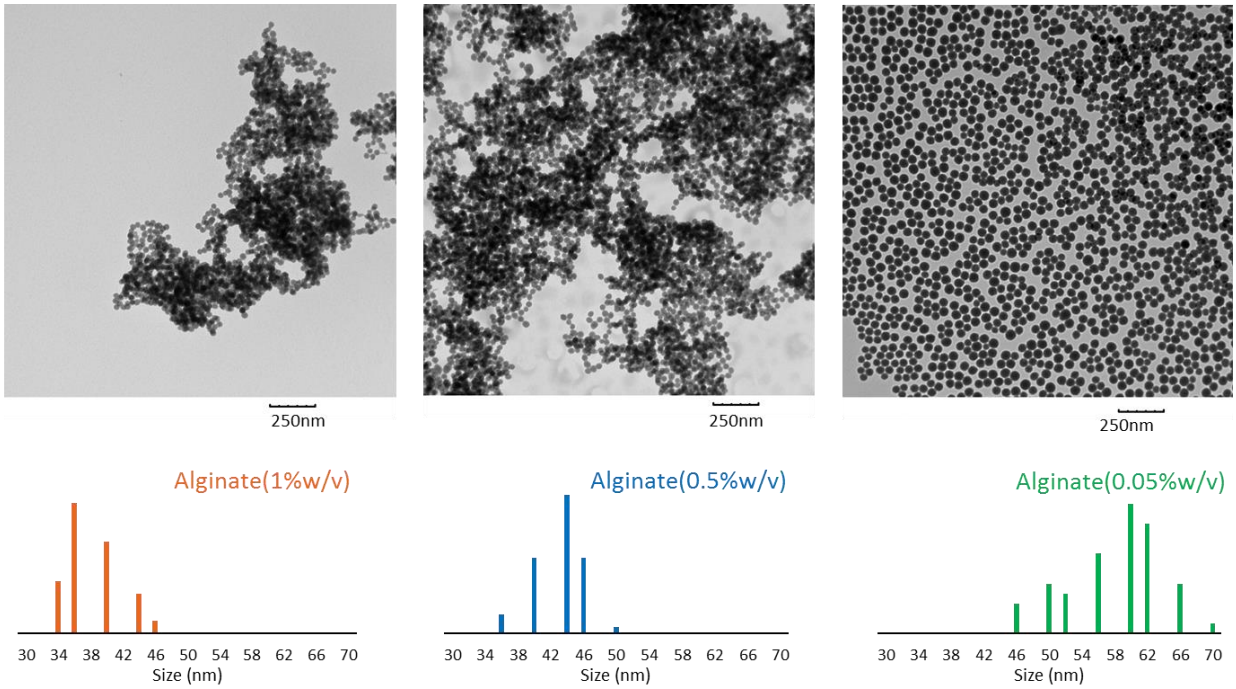

Figure 4.8 TEM images of silica-alginate nanoparticles with different initial alginate concentrations used in microemulsion. (Particle size 37.3 ± 3.4 nm with alginate (1 %w/v), particle size 42.0 ± 2.9 nm with alginate (0.5 %w/v), particle 27.2 ± 5.7 nm with alginate (0.05 %w/v).)

4.3 Conclusions

Silica-alginate nanoparticles with pH-responsive release ability of rhodamine B were synthesized in water-in-oil microemulsion system. The experimental design allowed compatibility of alginate solution in silica sol-gel process. Encapsulated alginate in silica-alginate nanoparticles was confirmed by TGA and silicomolybdic acid assay. Furthermore, the size of silica-alginate nanoparticles can be controlled by changing the water to surfactant molar ratio or initial alginate solution concentration.

Chapter 5 *In vitro* release study of silica-alginate nanoparticles

Nanocomposites have drawn significant interest for their enhanced properties compared to that of their neat, individual components. Much of the nanocomposite work, however, has been focused on relatively large systems (i.e. micrometer or larger)[175, 176] or with nanoparticles coated with a second substance (i.e. a core-shell morphology).[177, 178] In chapter 4, we provided a system that wass comprised of interpenetrating networks of silica, which provided mechanical integrity, and a biopolymer, alginate, that provided pH-responsive functionality. In chapter 3, we confirmed that nanocomposite materials comprised of silica and alginate showed pH-dependent control release of rhodamine B, a hydrophilic small molecular drug model. In this chapter, the *in vitro* release performance of silica-alginate nanoparticles was tested.

5.1 Materials and methods

5.1.1 Materials

Rhodamine B, calcium chloride, sodium phosphate monobasic monohydrate, sodium phosphate dibasic heptahydrate and Triton X-100 were purchased from AMRESCO; tetraethyl orthosilicate with 98 % purity and timolol maleate were purchased from Sigma Aldrich; sodium alginate and tetramethyl orthosilicat were purchased from Acros, isopropyl alcohol (70 %), cyclohexane, aqueous ammonia solution (29 wt%) and hydrochloric acid (37 %) were purchased from BDH Chemicals; sodium alginate (very low viscosity) and n-hexanol were purchased from Alfa Aesar. All chemicals were used without further purification. Deionized water used throughout the experiments was purified with an ELGA PURELAB Flex water purification system.

5.1.2 Preparation of phosphate buffer

Phosphate buffer (pH 2.5, 10 mM) was prepared by dissolving 1.380 g sodium phosphate monobasic monohydrate to 1000 mL deionized water. Then adjusted the pH to 2.5 by hydrochloric acid (1 M).

Phosphate buffer (pH 7.5, 10 mM) was prepared by dissolving 0.227 g sodium phosphate monobasic monohydrate and 2.238 g sodium phosphate dibasic heptahydrate to 1000 mL deionized water.

5.1.3 Preparation of rhodamine B loaded silica-alginate nanoparticles in microemulsion

Rhodamine B (0.1 %w/v) was dissolved in aqueous solutions of sodium alginate (very low viscosity, 5 %w/v). Rhodamine B loaded silica-alginate nanoparticles were prepared in water-in-oil microemulsion system. Initially, 20 mL n-hexanol was dissolved in 60 mL cyclohexane, followed by adding 6 mL rhodamine B alginate solution. After 5 min, 25 mL Triton X-100 was added dropwise until the mixed solution became optically transparent. After 10 min of vigorous stirring, 500 μL aqueous ammonia solution (29 wt%) was added, followed by adding 1 mL TEOS. The reaction was allowed to stir for 24 hours at room temperature. 100 mL acetone was added to break the stability of microemulsion and recovered the particles by centrifuge (4500 rpm, 10 min). The particles were washed three times with isopropyl alcohol and deionized water to remove the excess surfactant and cosurfactant.

5.1.4 Rhodamine B *in vitro* release study from *in situ* loading silica-alginate nanoparticles

Rhodamine B loaded silica-alginate nanoparticles were suspended in 1 mL phosphate buffer (10 mM) with different pH values (pH 2.5 or pH 7.5) under room temperature. At predetermined time intervals, all release samples were centrifuged (14800 rpm) for 10 min, and 0.5 mL supernatant was withdrawn and replaced with 0.5 mL fresh phosphate buffer. After 27 days, nanoparticles were dissolved in 1 mL NaOH (1 M) to detect rhodamine B left inside the nanoparticles. The concentrations of rhodamine B in all release mediums were detected by fluorescence spectroscopy (SpectraMax i3, Molecular Devices, Sunnyvale, CA) with excitation at 542 nm and emission at 583 nm. The percentage of cumulative released rhodamine B was determined from calibration curve. All samples were analyzed in triplicate.

5.1.5 Preparation of timolol maleate loaded silica-alginate nanoparticles in microemulsion

Timolol maleate (0.1 %w/v) was dissolved in aqueous solutions of sodium alginate (very low viscosity, 4 %w/v). Timolol maleate loaded silica-alginate nanoparticles were prepared in water-in-oil microemulsion system. Initially, 20 mL n-hexanol was dissolved in 60 mL cyclohexane, followed by adding 6 mL timolol maleate B alginate solution. After 5 min, 25 mL Triton X-100 was added dropwise until the mixed solution became optically transparent. After 10 min of vigorous stirring, 500 μL aqueous ammonia solution (29 wt%) was added, followed by adding 1.5 mL TEOS. The reaction was allowed to stir for 24 hours at room temperature. 100 mL acetone was added to break the stability of microemulsion and recovered the particles by centrifuge (4500 rpm, 10 min). The particles were washed three times with isopropyl alcohol and deionized water to remove the excess surfactant and cosurfactant.

5.1.6 Timolol maleate *in vitro* release study from *in situ* loading silica-alginate nanoparticles

Timolol maleate loaded silica-alginate nanoparticles were suspended in 1 mL phosphate buffer (10 mM) with different pH values (pH 2.5 or pH 7.5) under room temperature. At predetermined time intervals, all release samples were centrifuged (14800 rpm) for 10 min, and 0.5 mL supernatant was withdrawn and replaced with 0.5 mL fresh phosphate buffer. After 24 hours, nanoparticles were dissolved in 1 mL NaOH (1 M) to detect timolol maleate left inside the nanoparticles. The concentrations of timolol maleate in all release mediums were detected by UV-Vis spectrophotometry at a wavelength of 294 nm (SpectraMax i3, Molecular Devices, Sunnyvale, CA). The percentage of cumulative released timolol maleate was determined from calibration curve. All samples were analyzed in triplicate.

5.1.7 Synthesis of silica-alginate nanoparticles

Silica-alginate nanoparticles were prepared in water-in-oil microemulsion system. Typically, 12 mL n-hexanol was dissolved in 60 mL cyclohexane, followed by adding 4 mL alginate aqueous solution. After 5 min, 10 mL Triton X-100 was added dropwise until the mixed solution became optically transparent. After 10 min of vigorous stirring, 500 μL aqueous ammonia solution (29 wt%) was added, followed by adding 1 mL TEOS. The reaction was allowed to stir for 24 hours at room temperature. 100 mL acetone was added to break the stability of microemulsion and the nanoparticles were recovered by centrifuge (4500 rpm, 10 min). In the end, nanoparticles were washed three times with isopropyl alcohol and deionized water to remove the excess surfactant and cosurfactant.

5.1.8 Timolol maleate freeze dry post loading for silica-alginate nanoparticles

Silica-alginate nanoparticles (400 mg) were mixed with 1 mL deionized water containing 2 mg timolol maleate at room temperature for 10 hours, and froze this loading solution at -80 °C for overnight, then lyophilized for 24 hours (Labconco freeze dryer at a pressure of 0.040 mbar and a temperature of -52 °C). Drug loaded silica-alginate nanoparticles were washed twice with phosphate buffer solution (10 mM, pH 2.5) to remove timolol maleate that was adsorbed on the surface. Timolol maleate concentration in washing solution was determined via UV-spectrophotometry at a wavelength of 294 nm (SpectraMax i3, Molecular Devices, Sunnyvale, CA). All samples were analyzed in triplicate.

5.1.9 Timolol maleate *in vitro* release study from freeze dry post loading nanoparticles

Timolol maleate loaded silica-alginate nanoparticles were divided into six groups and each group was suspended in 5 mL phosphate buffer (10 mM) with different pH values (pH 2.5 or pH 7.5) under room temperature. At predetermined time intervals, all release samples were centrifuged (4500 rpm) for 10 min, and 1 mL supernatant was withdrawn and replaced with 1 mL fresh phosphate buffer with the same pH. The concentrations of timolol maleate in all release mediums were detected by UV-spectrophotometry spectroscopy (SpectraMax i3, Molecular Devices, Sunnyvale, CA) at a wavelength of 294 nm. The percentage of cumulative released timolol maleate was determined from the calibration curve. All samples were analyzed in triplicate.

5.1.10 Timolol maleate oven drying loading into silica-alginate nanoparticles

For a typical loading process, silica-alginate nanoparticles were first divided for six groups, and each group of nanoparticles was mixed with 0.1 mL deionized water containing 1 mg timolol maleate at room temperature for 5 hours, then timolol maleate nanoparticle mixtures were transferred to the oven at 80 ºC overnight. The drug loaded silica-alginate nanoparticles were washed twice with phosphate buffer solution (10 mM, pH 2.5) to remove timolol maleate that was adsorbed on the surface. The timolol maleate concentration in washing solution was determined via UV-spectrophotometry at a wavelength of 294 nm (SpectraMax i3, Molecular Devices, Sunnyvale, CA).

5.1.11 Timolol maleate *in vitro* release study from oven drying post loading nanoparticles

Timolol maleate loaded silica-alginate nanoparticles were suspended in 1 mL phosphate buffer (10 mM) with different pH values (pH 2.5 or pH 7.5) under room temperature. At predetermined time intervals, all release samples were centrifuged (14800 rpm) for 10 min, and 0.5 mL supernatant was withdrawn and replaced with 0.5 mL fresh phosphate buffer with the same pH. In the end of release study, nanoparticles were dissolved in 1 mL NaOH (1 M) to detect timolol maleate left inside the nanoparticles. The concentrations of timolol maleate in all release mediums were detected by UV-spectrophotometry spectroscopy (SpectraMax i3, Molecular Devices, Sunnyvale, CA) at a wavelength of 294 nm. The percentage of cumulative released timolol maleate was determined from the calibration curve. All samples were analyzed in triplicate.

5.1.12 Preparation of timolol maleate loaded alginate beads

Timolol maleate (0.1 %w/v) was dissolved in aqueous solutions of sodium alginate (very low viscosity) (5 %w/v). This solution was added dropwise to a calcium chloride solution (5 %w/v) under magnetic stirring for 15 min to form spherical beads. The wet rhodamine B loaded alginate beads were washed with deionized water to remove unreacted calcium chloride and dried at ambient condition overnight.

5.1.13 Timolol maleate *in vitro* release study from alginate beads

Each bead was placed into 1 mL phosphate buffer (10 mM) with different pH values (pH 2.5 or pH 7.5) under room temperature. Every 10 min, 0.5 ml buffer was withdrawn and replaced with 0.5 mL fresh phosphate buffer with the same pH. The concentrations of timolol maleate in

all release mediums were detected by UV-Vis spectrophotometry at a wavelength of 294 nm (SpectraMax i3, Molecular Devices, Sunnyvale, CA). The percentage of cumulative released timolol maleate was determined from the calibration curve. All samples were analyzed in triplicate.

5.1.14 Preparation of silica-alginate monolithic gels

Timolol maleate loaded silica-alginate monolithic gels were prepared as follows, mixed 200 µL phosphate buffer (pH 2.5, 10 mM) with 1 mL TMOS solution for 2 min to form hydrolyzed TMOS solution. Timolol maleate (0.05 %w/v) was dissolved in aqueous solutions of sodium alginate (very low viscosity, 2.5 %w/v). Added 200 µL hydrolyzed TMOS solution into 1 mL rhodamine B alginate solution. Placed on a vortex mixer for 10 s. Transferred 150 µL of this mixed solution into the wells of a 96 well plate. Allowed the gels to be aged and air dried under room temperature. Timolol maleate loaded silica monolithic gels were also prepared, as controls for the release study, by mixing timolol maleate (0.5 %w/v) in deionized water with hydrolyzed TMOS solution, and followed the same procedure.

5.1.15 Timolol maleate *in vitro* release study from silica-alginate monolithic gel

In vitro release study of timolol maleate from silica-alginate monolithic gel and silica monolithic gel was performed in 1 mL phosphate buffer (10 mM) with different pH values (pH 2.5 or pH 7.5) under room temperature. At predetermined time intervals, 0.5 mL phosphate buffer was withdrawn and replaced with 0.5 mL fresh phosphate buffer with the same pH. The concentrations of timolol maleate in all release mediums were detected by UV-Vis spectrophotometry at a wavelength of 294 nm (SpectraMax i3, Molecular Devices, Sunnyvale,

CA). The percentage of cumulative released timolol maleate was determined from the calibration curve. All samples were analyzed in triplicate.

5.2 Results and discussions

5.2.1 Rhodamine B *in vitro* release study from *in situ* loading silica-alginate nanoparticles

Rhodamine B was loaded into silica-alginate nanoparticles during the silica sol-gel encapsulation process in water-in-oil microemulsion system. This method has been used to make rhodamine B doped silica nanoparticles.[179-182] The loading efficiency was low for this method. Due to rhodamine B diffused out of water phase during reaction and washed away during multiple washing steps, the overall loading efficiency was 0.31 %. Therefore, the detection of rhodamine B in release samples was used by fluorescence spectroscopy as its high sensitivity.

Figure 5.1 shows the cumulative release percent of rhodamine B from silica-alginate nanoparticles in phosphate buffers at different pH values (pH 2.5 or pH 7.5). Rhodamine B released with a faster rate at pH 7.5 compared to pH 2.5. There was a very limited amount of rhodamine B released over 27 days in phosphate buffer (pH 2.5) with only 7 % cumulative released from silica-alginate nanoparticles. However, 42 % rhodamine B was released in phosphate buffer (pH 7.5) during the same time. This result confirmed the concept of using silica-alginate nanoparticles for pH-responsive drug release. As mentioned in Chapter 3, this pH-responsive behavior may be due to increased hydrogen bonding interactions of protonated carboxylic acid groups between alginate and rhodamine B in pH 2.5 phosphate buffer. At pH 7.5, the hydrogen bonding interaction is broken, which results in enhanced release of rhodamine B.

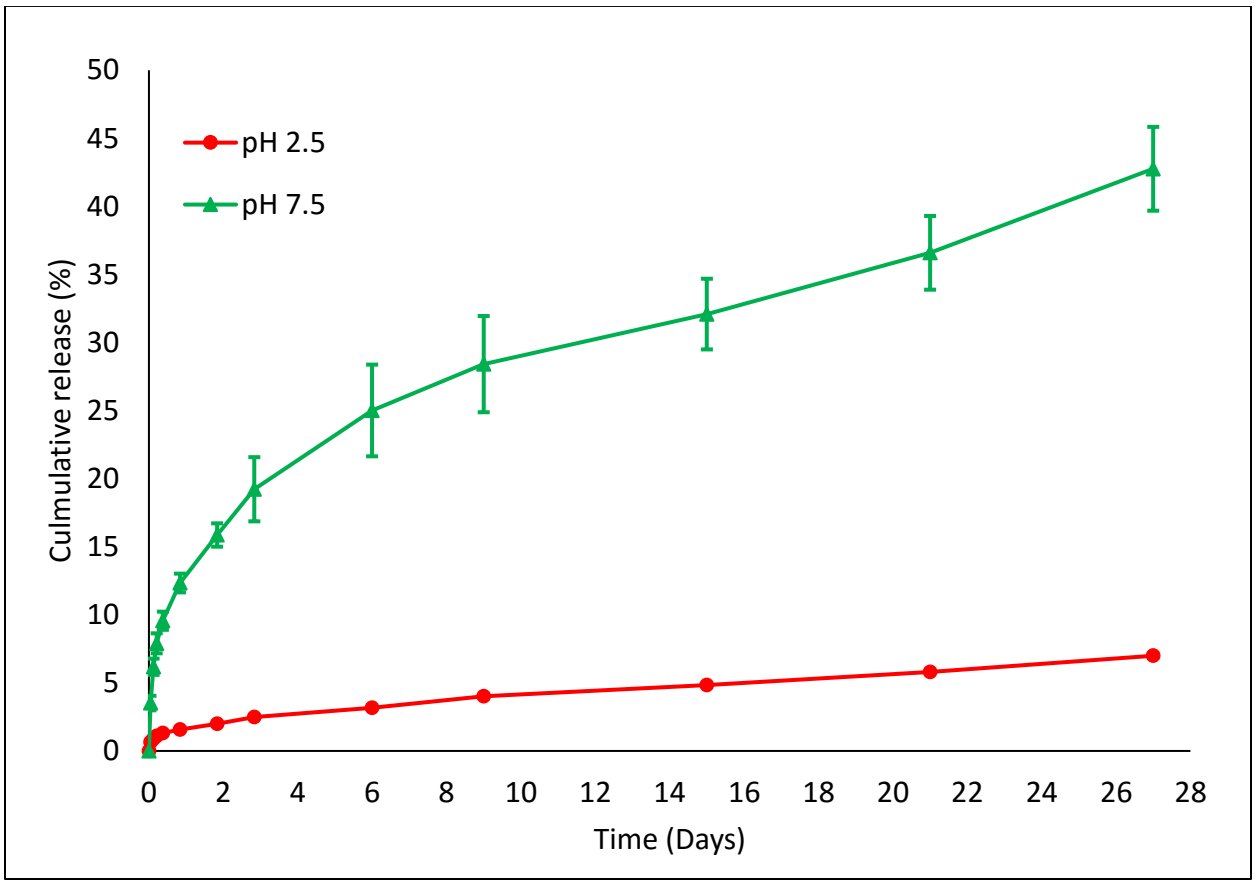

Figure 5.1 *In suit* loaded rhodamine B release study from silica-alginate nanoparticles in phosphate buffer with different pH values (pH 2.5 and pH 7.5).

Mathematical modeling of kinetics drug release provides insights for the understanding of mass transport processes. These processes might include the diffusion of water into the system, polymer swelling, matrix erosion, drug diffusion or dissolution.[140-142] Figure 5.2 shows the mathematical modeling for *in situ* loaded rhodamine B release from silica-alginate nanoparticles. Two models were used in this study, Peppas equation and sphere monolithic solution model, as listed in Table 5.1. They both showed good fit with the experimental release

data. For the Peppas equation of sphere, the release exponent n = 0.43 corresponds to a Fickian diffusion mechanism, 0.43 < n < 0.85 to non-Fickian transport, n = 0.85 to Case-II transport.[140] Several litterateurs also mentioned that n < 0.43 also represented for Fickian diffusion. [92, 183-185] In addition, n id also depended on the width of the particle distribution.[145] In this study, n values were obtained from Matlab fitting, in pH 2.5 phosphate buffer n = 0.42, and in pH 7.5 phosphate buffer n = 0.35. Therefore, the release mechanism should be Fickian diffusion in both phosphate buffer. Monolithic solution model represents a system with homogeneously distributed drug inside. Good fist were also observed for both phosphate buffer solutions by early time monolithic solution modeling. This confirmed the homogeneously encapsulation of rhodamine B during the silica sol-gel process in microemulsion system. From this modeling, the diffusion coefficient in pH 7.5 phosphate buffer was 45 times higher than the one in pH 2.5 phosphate buffer.

Table 5.1 Mathematical models used for kinetics drug release

Model	Expression
Peppas equation	$\frac{M_t}{M_\infty} = k_1 t^n$
Monolithic solution(Sphere)	$\frac{M_t}{M_\infty} = 6(\frac{Dt}{\pi R^2})^{1/2} - \frac{3Dt}{R^2}$ (Early time $\frac{M_t}{M_\infty} < 0.4$) $\frac{M_t}{M_\infty} = 1 - \frac{6}{\pi^2} exp(-\frac{\pi^2 Dt}{\pi R^2})$ (Late time $\frac{M_t}{M_\infty} > 0.6$)

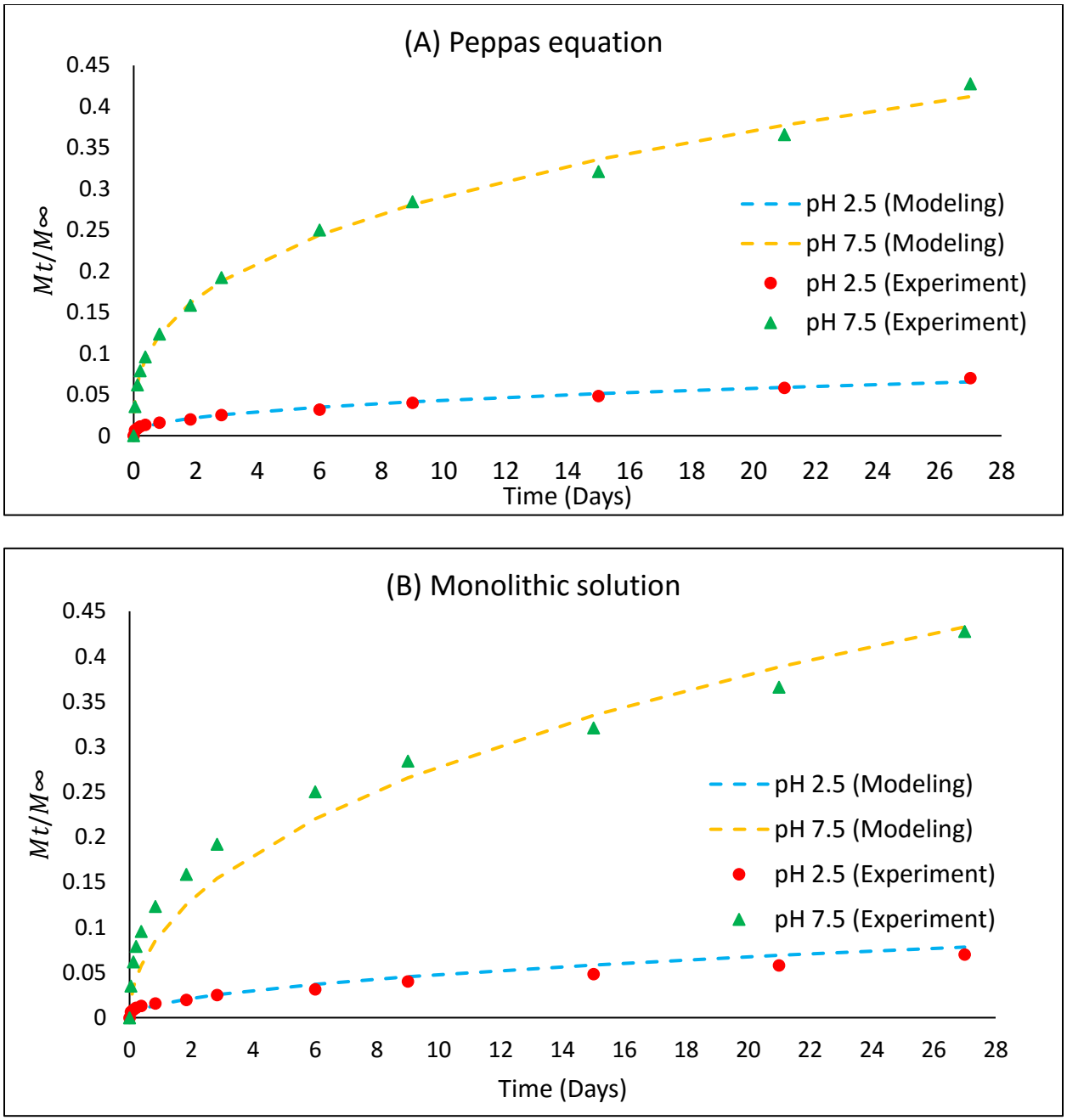

Figure 5.2 Mathematical models used for kinetics drug release of *in situ* loaded rhodamine B from silica-alginate nanoparticles. (A) Peppas equation modeling: pH 2.5 modeling (R^2= 0.9868); pH 7.5 modeling (R^2= 0.9954). (B) Monolithic solution modeling: pH 2.5 modeling (R^2= 0.9786); pH 7.5 modeling (R^2= 0.9470)

5.2.2 Timolol maleate *in vitro* release study from *in situ* loading silica-alginate nanoparticles

Timolol maleate is the most used β blocker in eye drop formulations for glaucoma treatment.[186] In this study, timolol maleate was loaded into silica-alginate nanoparticles during the silica sol-gel encapsulation process in water-in-oil microemulsion system with the same way as rhodamine B. However, no timolol maleate was detected by UV-Vis spectrophotometry at a wavelength of 294 nm during the *in vitro* release study from phosphate buffers at neither pH 2.5 nor pH 7.5 for 24 hours. Moreover, there was also no timolol maleate detected even after dissolving the silica-alginate nanoparticles. As discussed in Chapter 5.2.1, the loading efficiency for rhodamine B in water-in-oil microemulsion method was 0.31 %. In addition, the total amount in nanoparticles for release study was averaged 135 ng. The release study of rhodamine B was detected by fluorescence spectroscopy, which has much lower detection limit compared to UV-Vis spectrophotometry. However, timolol maleate cannot be detected by fluorescence spectroscopy. In summary, *in situ* loading method through water-in-oil microemulsion method showed low loading efficiency. This could be due to the small molecular weight of timolol maleate, which is 432.49 g/mol, and timolol maleate diffused out of water phase during the reaction as well as washed away during multiple washing steps as the high solubility of timolol maleate in both isopropyl alcohol and deionized water. Therefore, we studied post loading method of timolol maleate for silica-alginate nanoparticles.

5.2.3 Timolol maleate post loading and release study for silica-alginate nanoparticles

Two post loading methods were used in this study. Both of them involved mixing timolol maleate aqueous solution with silica-alginate nanoparticles. In the freeze drying loading method, the solvent of the mixed solution was removed by sublimation. For the oven drying loading method, the solvent was removed by evaporation.

Freeze drying loading method

Two types of silica-alginate nanoparticles were used in this study. ALG-1: silica-algiante nanoparticles made by 1 %w/v alginate solution for the water-in-oil microemulsion, and ALG-0.05: silica-alginate nanoparticles made by 0.05 %w/v alginate solution for the water-in-oil microemulsion. Table 5.2 lists the freeze drying loading efficiency. ALG-1 showed a higher loading ability than ALG-0.05, so higher ratio of alginate in the composite nanoparicles could increase the loading amount of timolol maleate.

Table 5.2 Loading efficiency by freeze drying method

Nanoparticles	Nanoparticles wet weight(mg)	Initial TM* (μg)	Loaded TM (μg)	Loaded TM per NPs (μg)/(mg)
ALG-1	463.8	2000	464.33	1.001
ALG-0.05	344.4	2000	268.39	0.779

* TM: timolol maleate

Figure 5.3 shows the cumulative release percent of timolol maleate from silica-alginate nanoparticles in phosphate buffer solutions at pH 2.5 and pH 7.5. The release profiles looked similar for both types of silica-alginate nanoparticles. For ALG-1, burst release was observed in both pH conditions at early times. Especially at pH 2.5, 67 % timolol maleate was released in the first 0.5 hours. After this, the release slowed down significantly. The overall release percent reached to 78 % at 24 hours. However, at pH 7.5, in the beginning, the release was less compared to the one at pH 2.5, 49 % timolol maleate was released in the first 0.5 hours. Whereas, after 24 hours, the release percent was increased to 83 %. For ALG-0.05, higher burst release rate was observed in both pH conditions at early times compared to ALG-1. Especially at pH 2.5, 79 % timolol maleate was released in the first 0.5 hours. After this, the release also slowed down significantly. The overall release percent reached to 92 % at 24 hours. However, at pH 7.5, the release was less compared to the one at pH 2.5 in the beginning, and 54 % timolol maleate was released in the first 0.5 hours. Whereas, after 24 hours, the release percent was increased to 93 %. Although the release profiles at pH 2.5 and pH 7.5 were different, there was no strong pH-dependent release ability exhibited by the silica-alginate nanoparticles. The burst release profiles may be due to the that most of the timolol maleate loaded into the silica-alginate nanoparticles was on the surface. However, silica-alginate nanoparticles made by higher concentration alginate solution showed less burst release performance. Therefore, higher alginate ratio inside the composite nanoparticles could improve the sustained release ability.

Figure 5.4 shows the mathematical modeling for freeze drying loaded timolol maleate release from silica-alginate nanoparticles. Two models were used, Peppas equation and sphere monolithic solution model, as listed in Table 5.1. Although Peppas equation showed good fit for both types of silica-alginate nanoparticles, Peppas equation is usually valid for $\frac{M_t}{M_\infty} < 0.6$.[145] In

this study, rapid burst release ($\frac{M_t}{M_\infty} > 0.6$) was observed after 0.5 hours, so the release mechanism could not be obtained due to the rapid burst release. Therefore, oven drying method was test for limiting the rapid burst release.

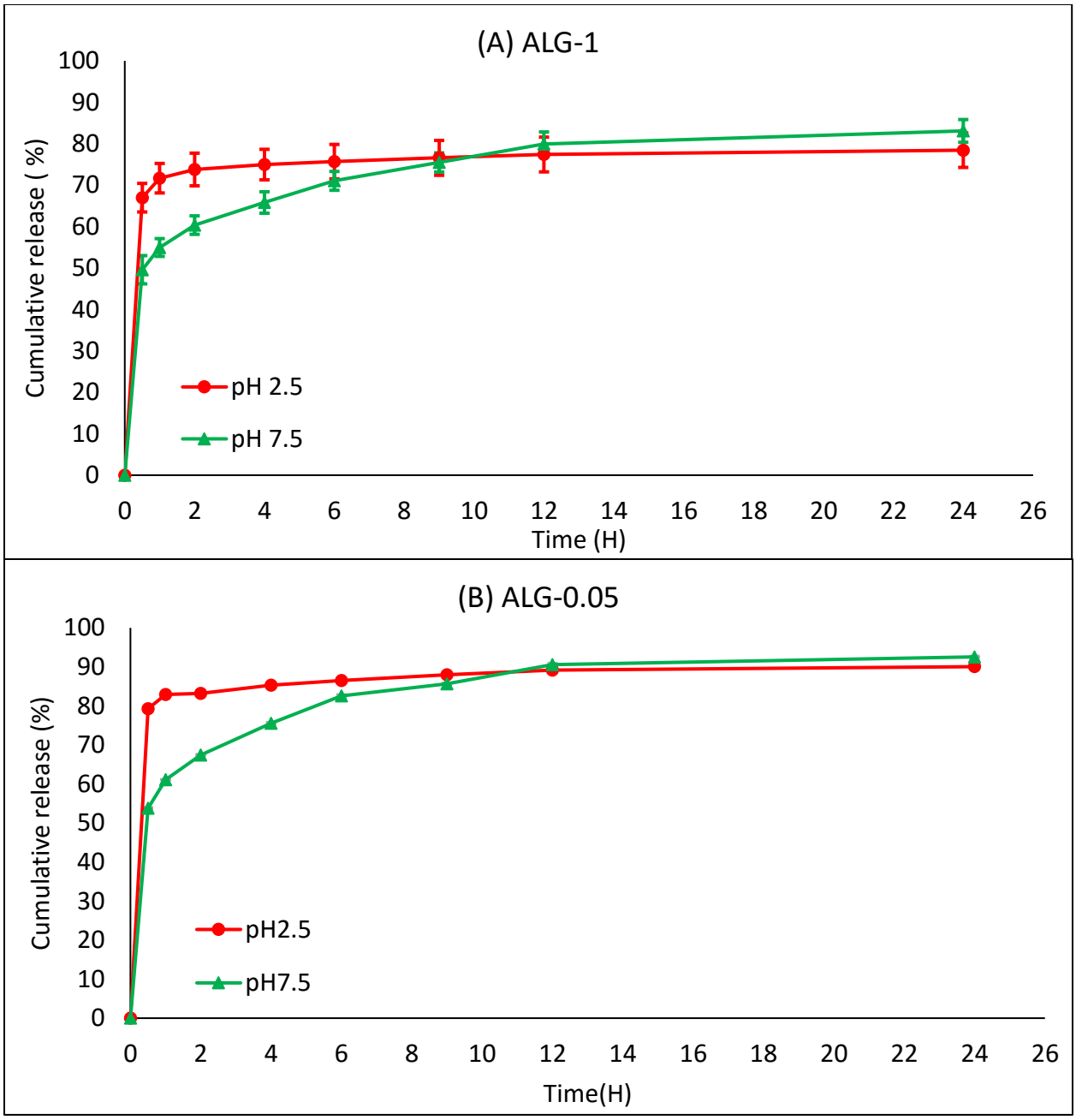

Figure 5.3 Timolol maleate *in vitro* release profiles from silica-alginate nanoparticles (A: ALG-1; B: ALG-0.05) in phosphate buffer at pH 2.5 and pH 7.5. (Timolol maleate was loaded into nanoparticles by freeze drying post loading method)

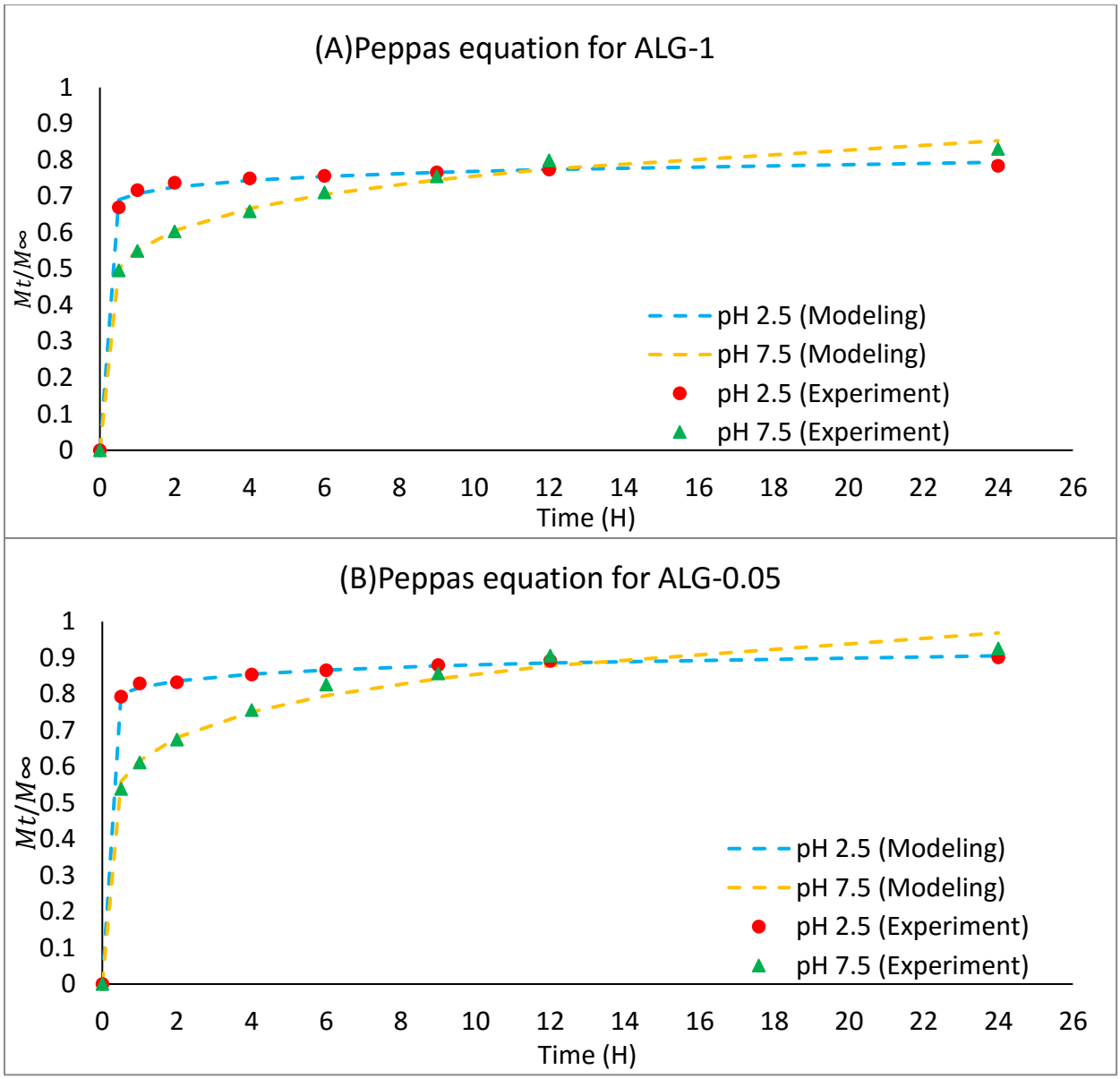

Figure 5.4 Mathematical models used for drug release. (A) Peppas equation modeling for ALG-1: pH 2.5 modeling (R^2= 0.9189); pH 7.5 modeling (R^2= 0.9872). (B) Peppas equation modeling for ALG-0.05: pH 2.5 modeling (R^2= 0.9714); pH 7.5 modeling (R^2= 0.9697).

Oven drying loading method

As from the freeze drying study, higher alginate weight ratio in composite materials could improve the loading ability of timolol maleate. Therefore, two types of silica-alginate nanoparticles were used in this study made by higher concentration (8 %w/v) of alginate solution, and TMOS also used as another silica sol-gel precursor in this study. TEOS-ALG-8: silica-alginate nanoparticles made by 8 %w/v alginate solution and TEOS for the water-in-oil microemulsion, and TMOS-ALG-8: silica-alginate nanoparticles made by 8 %w/v alginate solution and TMOS for the water-in-oil microemulsion. Table 5.3 lists the oven drying loading efficiency. TEOS-ALG-8 showed a higher loading ability than TMOS-ALG-8, but TEOS-ALG-8 also showed a higher variation in loading.

Table 5.3 Loading efficiency by oven drying method

Nanoparticles	Nanoparticles dry weight(mg)	Initial TM* (μg)	Loaded TM (μg)	Loaded TM per NPs (μg)/(mg)
TEOS-ALG-8	6.68 ± 0.38	1000	375.95 ± 52.76	56.63 ± 10.11
TMOS-ALG-8	12.47 ± 0.32	1000	553.45 ± 28.83	44.41 ± 2.35

* TM: timolol maleate

Figure 5.5 shows the cumulative release percent of timolol maleate from both types of silica-alginate nanoparticles in phosphate buffer solution at pH 2.5 and pH 7.5. TMOS-ALG-8 showed a more sustained release profile than TEOS-ALG-8, but they both had the similar release

trend for different pH buffers. For TEOS-ALG-8, as shown in Figure 5.5 (A), at pH 2.5, an averaged 78 % cumulative release of timolol maleate was observed in the first 8 hours. Then the release percent reached to 81 % at 24 hours. However, at pH 7.5, the release rate was slightly slower with a 69 % timolol maleate released in the first 8 hour. And at 24 hours, the cumulative release percent was 75 %. However, for TEOS-ALG-8, as shown in Figure 5.5 (B), at pH 2.5, an averaged 62 % cumulative release of timolol maleate was observed in the first 8 hours. The release percent reached to 66 % at 24 hours. However, at pH 7.5, the release rate was also slightly slower with 50 % timolol maleate released in the first 8 hours. And at 24 hours, the cumulative release percent was increased to 58 %. For both types of silica-alginate nanoparticles, the burst release was reduced compared to freeze drying loading method. However, no strong pH-dependent release profile was observed even with nanoparticles with 8 %w/v alginate concentration. Therefore, neither changing the concentration of alginate solution used in mocroemulsion nor loading method improved the pH-responsive release of timolol maleate.

Figure 5.6 shows the mathematical modeling for oven drying loaded timolol maleate release from silica-alginate nanoparticles. Two models were used, Peppas equation and sphere monolithic solutions model, as listed in Table 5.1. For TEOS-ALG-8, rapid burst release ($\frac{M_t}{M_\infty} > 0.6$) was observed after 2 hours, and neither Peppas equation nor monolithic solution model showed good fit with experimental release data. For Peppas equation modeling, it showed lower release profile compared to experimental data, which may be due to the surface adsorbed timolol maleate release faster by dissolution than diffusion. In addition, monolithic solution modeling was not fit with the experimental data (negative R^2 means that the modeling was worse than a horizontal line), which showed that timolol maleate was not homogeneously distributed inside

the nanoparticles. For TMOS-ALG-8, burst release ($\frac{M_t}{M_\infty} > 0.6$) was observed after 8 hours, but Peppas equation did not show good fit with experimental release data for neither pH 2.5 nor pH 7.5 condition. The surface adsorbed timolol maleate may be the reason why the experimental data showed faster release. However, a better fit of the experimental release profile was obtained by monolithic solution modeling at early time, which showed that TMOS-ALG-8 may have a better homogeneously distribution of timolol maleate than TEOS-ALG-8.

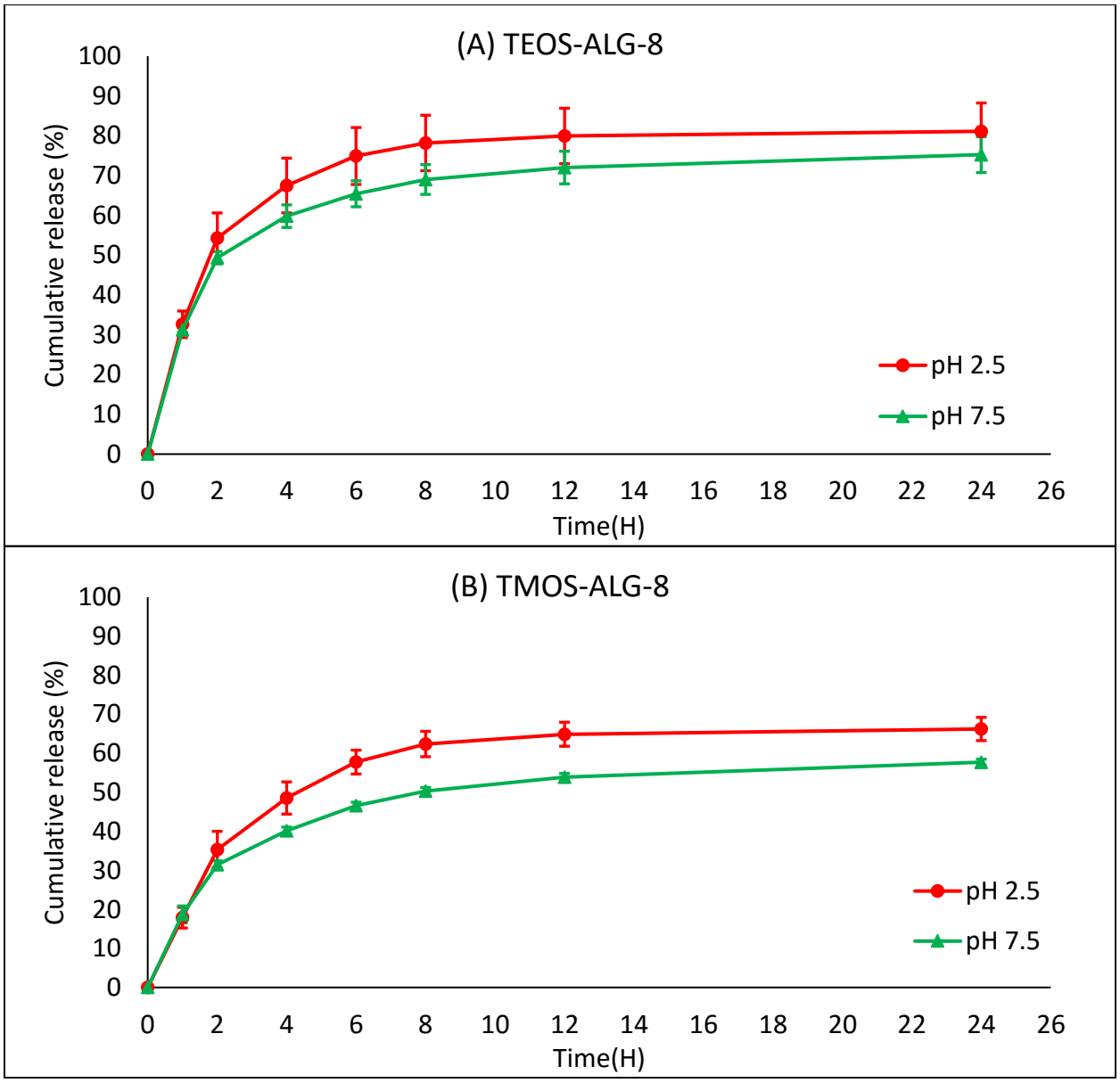

Figure 5.5 Timolol maleate *in vitro* release profiles from silica-alginate nanoparticles (A: TEOS-ALG-8, B: TMOS-ALG-8) in phosphate buffer at pH 2.5 and pH 7.5. (Timolol maleate was loaded into nanoparticles by oven drying post loading method)

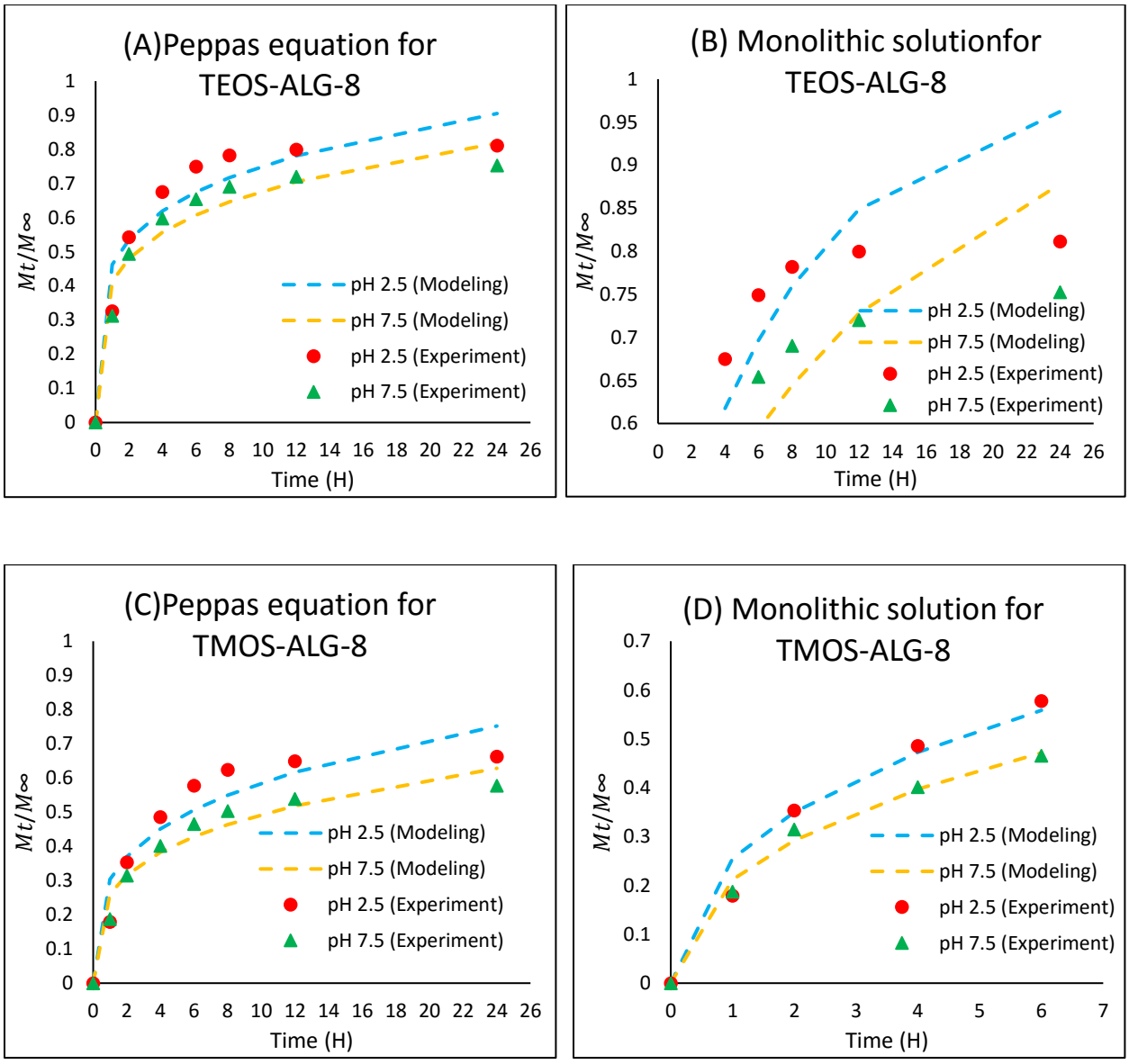

Figure 5.6 Mathematical models used for drug release kinetics. (A) Peppas equation modeling for TEOS-ALG-8: pH 2.5 modeling (R^2= 0.7874); pH 7.5 modeling (R^2= 0.8546). (B) Monolithic solution modeling for TEOS-ALG-8: pH 2.5 modeling (R^2= -1.662); pH 7.5 modeling (R^2= -0.7890). (C) Peppas equation modeling for TMOS-ALG-8: pH 2.5 modeling (R^2= 0.8116); pH 7.5 modeling (R^2= 0.8960). (D) Monolithic solution modeling for TMOS-ALG-8: pH 2.5 modeling (R^2= 0.9214); pH 7.5 modeling (R^2= 0.9731)

5.2.4 Timolol maleate *in vitro* release study from alginate beads

In order to understand whether alginate can control the release of timolol maleate at different pH, timolol maleate was loaded into alginate beads. These beads were made by dissolving timolol maleate in alginate solution prior to add into $CaCl_2$ solution. As shown in Figure 5.7, there was also no strong difference in drug release profiles between phosphate buffers with different pH values (pH 2.5 and pH 7.5), even though the alginate beads showed erosion and significant swelling at pH 7.5. This was the similar release performance as silica-alginate nanoparticles. In addition, burst release profiles with almost 100% timolol maleate released in 120 minutes were observed in both pH 2.5 and pH 7.5 conditions.

The large burst release and a lack of pH-dependence ability were consistent with the results from silica-alginate nanoparticle. This indicates that pH-dependent swelling of alginate was not the control factor for the delivery of timolol maleate. This may have occurred because of the high aqueous solubility of timolol maleate and its preferential partition into the aqueous phase, rather than the nanoparticles, were the driver for this result.

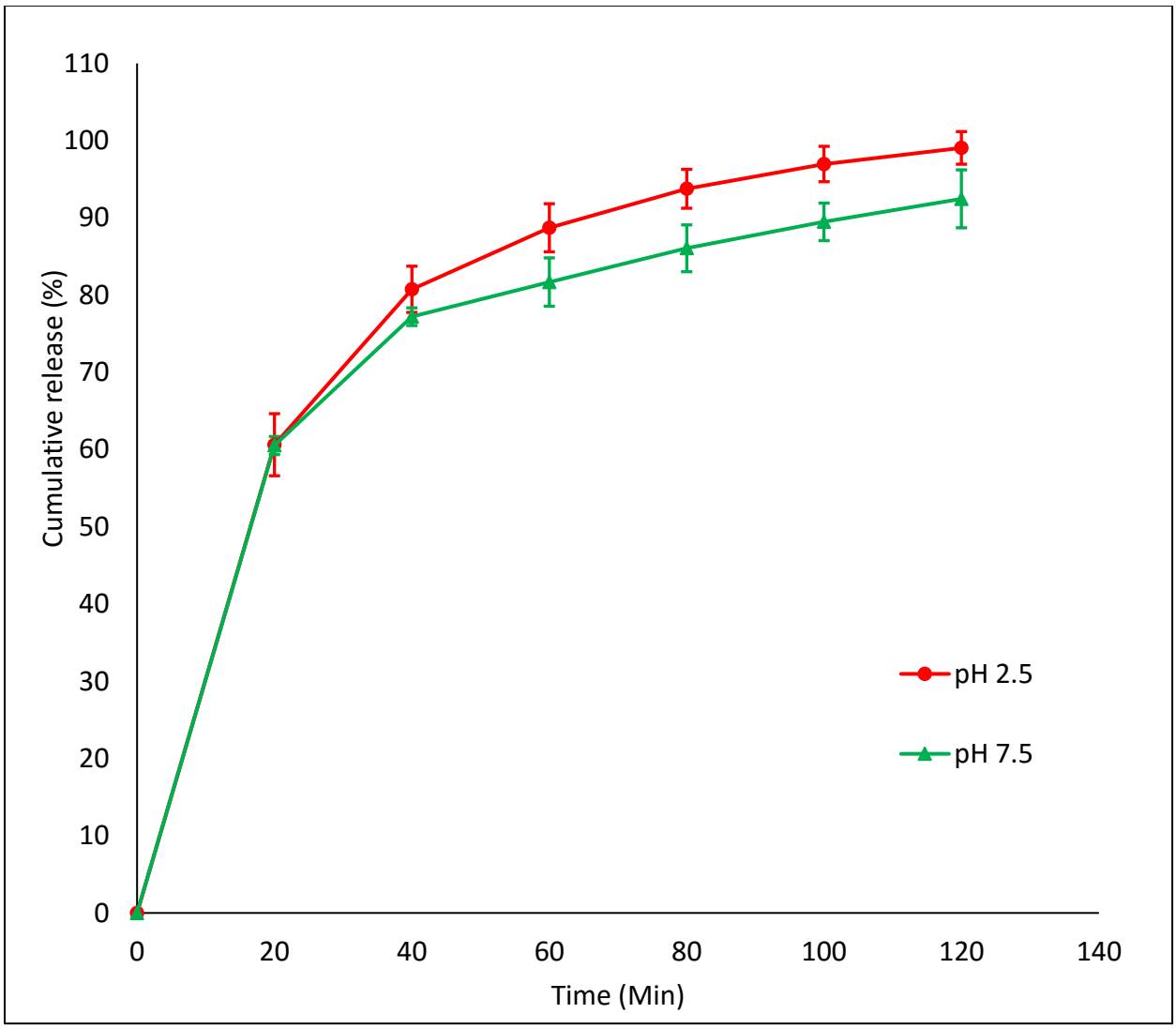

Figure 5.7 Timolol maleate *in vitro* release profiles from alginate beads in phosphate buffer with different pH values (pH 2.5 and pH 7.5).

5.2.5 Timolol maleate *in vitro* release study from monolithic gels

In chapter 3, silica-alginate composite monolithic gel showed pH-responsive release performance for rhodamine B. In pH 2.5 phosphate buffer, only 2.6 % loaded rhodamine B was released over 25 days; whereas 15.7 % loaded rhodamine B was released over the same period in pH 7.5 phosphate buffer. In this study, we made the same monolithic gels to study the timolol maleate release performance under different pH phosphate buffers.

As shown in Figure 5.8, the release profiles for silica gels, without alginate, were significantly different between pH 2.5 and pH 7.5. Burst release profile was observed in pH 2.5 phosphate buffer with a 66 % cumulative release of timolol maleate in the first day. Then the release slowed down, and reached to a 97 % cumulative timolol maleate release after 15 days. However, the release of timolol maleate was much slower in pH 7.5 phosphate buffer with only a 33 % cumulative timolol maleate release after 15 days. On the other hand, for silica-alginate composite gels, the release profile in pH 7.5 phosphate buffer (41 % cumulative in 15 days) was similar to the one from silica monolith gel. However, the release in pH 2.5 phosphate buffer (57 % cumulative in 15 days) was much slower than one from silica monolith gel.

This release performance of timolol maleate from silica-based monolithic gels was different compared to the one of rhodamine B. Especially in pH 2.5 phosphate buffer from silica gels, the rapid release profile may be due to the electrostatic interaction change between timolol maleate and silica gel. Timolol maleate has a pKa of 9.21.[187] Positively charged timolol maleate molecules are present in phosphate buffers at both pH 2.5 and pH 7.5. However, silica gel surface is negatively charged under pH 7.5 and near neutral at pH 2.5 condition. Therefore for this study, in pH 7.5 phosphate buffer, the relatively strong binding interaction of negatively

charged silica gel and positively charged timolol maleate molecules leaded to slower release profile. Whereas in pH 2.5 phosphate buffer, the decreased attraction between timolol maleate and silica resulted in the faster release. In addition, the addition of alginate showed stronger interaction with timolol maleate in pH 2.5 phosphate buffer as the slower release compared to silica gel. However, silica source was the control factor for the release of timolol maleate. This indicated that silica-alginate nanoparticles might not be suitable for pH-responsive delivery of timolol maleate.

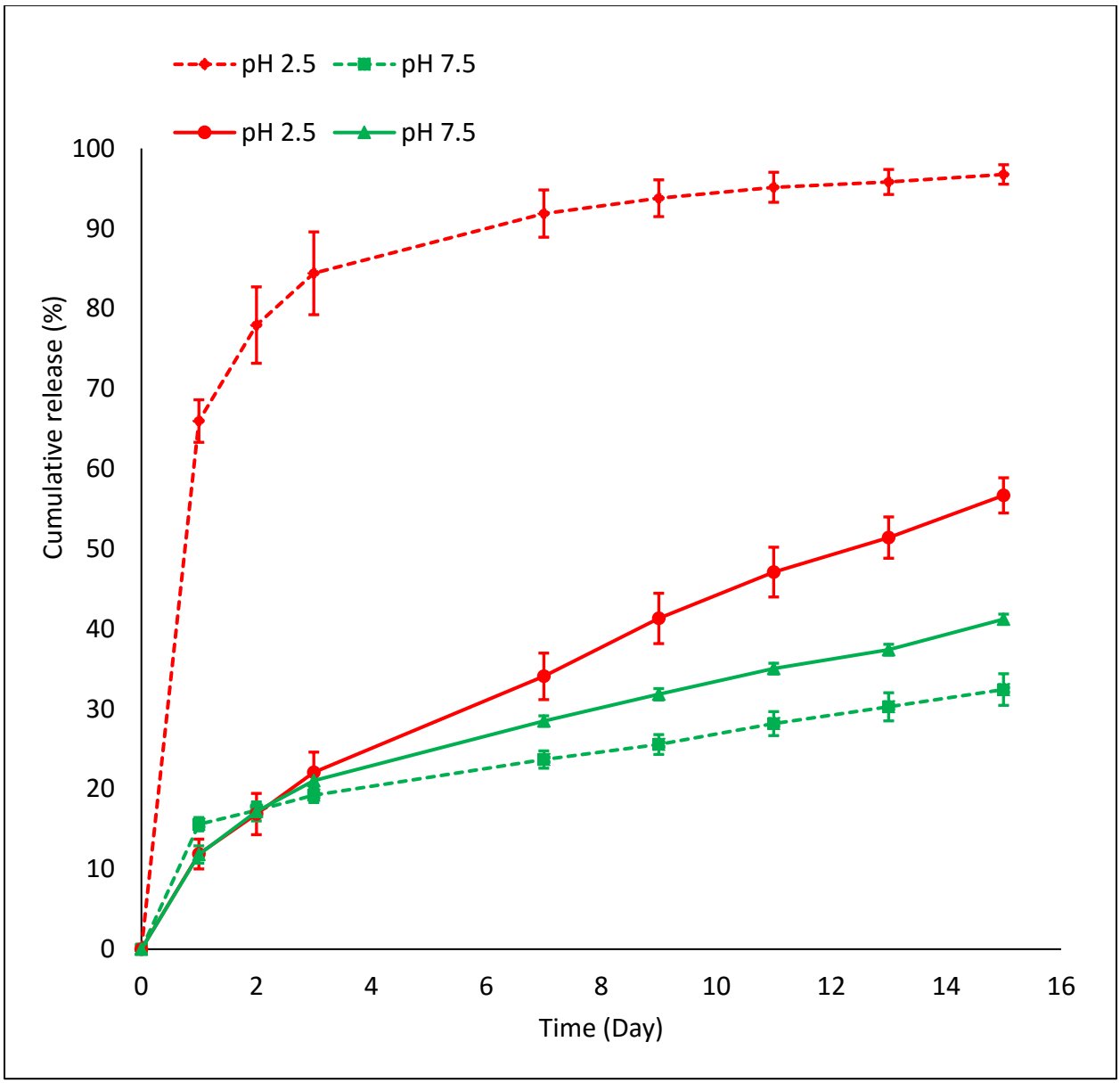

Figure 5.8 Timolol maleate *in vitro* release profiles from silica monolithic gels (dash lines) and silica-alginate monolithic gels (solid lines) in phosphate buffers with different pH values (pH 2.5 or pH 7.5).

5.3 Conclusions

In vitro release studies with silica-alginate nanoparticles were tested by rhodamine B and timolol maleate. Silica-alginate nanoparticles showed encouraged pH-responsive release performance for rhodamine B by *in situ* loading method. However, one limitation of this loading method was the low loading efficiency of 0.31 %. Moreover, this *in situ* loading method was not working for timolol maleate. Therefore, post loading method was studied for timolol maleate. However, no strong pH-dependent release was observed neither from freeze drying loading nanoparticles nor from oven drying loading nanoparticles. In order to understand whether alginate can control the release of timolol maleate at different pH, timolol maleate *in vitro* release studies were evaluated from both alginate beads and silica-based monolithic gels. The results showed that the electrostatic interaction between timolol maleate and silica surface was the control factor for the release. This indicated that silica-alginate nanoparticles might not be suitable for pH-responsive delivery of timolol maleate.

Chapter 6 *In vitro* release studies of Silica-PMAA nanoparticles

Since silica-alginate nanoparticles may be not suitable for pH-responsive delivery of timolol maleate. Poly (methacrylic acid) (PMAA) was used as another pH-responsive polymer to study the *in vitro* release ability of silica-PMAA nanoparticles. PMAA has a higher density of carboxyl group than alginate, which may help to improve the pH-responsive ability of silica-based composite nanoparticles. PMAA has shown promising applications in cosmetics,[74] pharmaceutics,[75] drug testing,[76] and biomedical technology,[77] due to its pH-induced conformational transition. In addition, a number of pH-responsive drug delivery systems have been studied using PMAA.[90-92] In this chapter, TMOS was used as silica sol-gel precursor instead of TEOS, as TMOS could provide more condense structure.[188] *In vitro* release of timolol maleate was studied to test the release performance of TMOS-PMAA nanoparticles.

6.1 Materials and methods

6.1.1 Materials

Sodium phosphate monobasic monohydrate, sodium phosphate dibasic heptahydrate and Triton X-100 were purchased from AMRESCO; tetramethyl orthosilicate was purchased from Acros, poly (methacrylic acid, sodium salt) solution (30 wt%) and timolol maleate were purchased from Sigma Aldrich; isopropyl alcohol (70 %), cyclohexane, aqueous ammonia solution (29 wt%) and hydrochloric acid (37 %) were purchased from BDH Chemicals; and n-hexanol were purchased from Alfa Aesar. All chemicals were used without further purification. Deionized water used throughout the experiments was purified with an ELGA PURELAB Flex water purification system.

6.1.2 Preparation of buffers

Phosphate buffer (pH 2.5, 10 mM) was prepared by dissolving 1.380 g sodium phosphate monobasic monohydrate to 1000 mL deionized water. Then adjusted the pH to 2.5 by hydrochloric acid (1 M).

Simulated tear fluid (pH 7.5) was prepared by dissolving 6.78 g sodium chloride, 1.38 g potassium chloride, 2.18 g sodium bicarbonate, 0.084 g calcium chloride dehydrate to 1000 mL deionized water. Then adjusted the pH to 7.5 by hydrochloric acid (1 M).

6.1.3 Preparation of timolol maleate loaded silica-PMAA nanoparticles in microemulsion

Timolol maleate (0.1 %w/v) was dissolved in aqueous solution of PMAA (4 %w/v). Timolol maleate loaded silica-PMAA nanoparticles were prepared in water-in-oil microemulsion

system. Initially, 20 mL n-hexanol was dissolved in 60 mL cyclohexane, followed by adding 6 mL timolol maleate-PMAA solution. After 5 min, 25 mL Triton X-100 was added dropwise until the mixed solution became optically transparent. After 10 min of vigorous stirring, 500 μL aqueous ammonia solution (29 wt%) was added, followed by adding 1.5 mL TEOS. The reaction was allowed to stir for 24 hours at room temperature. 100 mL acetone was added to break the stability of microemulsion and recovered the particles by centrifuge (4500 rpm, 10 min). The nanoparticles were washed three times with isopropyl alcohol and deionized water to remove the excess surfactant and cosurfactant.

6.1.4 Timolol maleate *in vitro* release study from *in situ* loading silica-alginate nanoparticles

Timolol maleate loaded silica-PMAA nanoparticles were suspended in 1 mL phosphate buffer (10 mM) with different pH values (pH 2.5 or pH 7.5) under room temperature. At predetermined time intervals, all release samples were centrifuged (14800 rpm) for 10 min, and 0.5 mL supernatant was withdrawn and replaced with 0.5 mL fresh phosphate buffer. After 24 hours, nanoparticles were dissolved in 1 mL NaOH (1 M) to detect timolol maleate left inside the nanoparticles. The concentrations of timolol maleate in all release mediums were detected by UV-Vis spectrophotometry at a wavelength of 294 nm (SpectraMax i3, Molecular Devices, Sunnyvale, CA). The percentage of cumulative released timolol maleate was determined from the calibration curve. All samples were analyzed in triplicate.

6.1.5 Synthesis of silica-PMAA nanoparticles

Silica-PMAA nanoparticles were prepared in water-in-oil microemulsion system. Typically, 20 mL n-hexanol was dissolved in 60 mL cyclohexane, followed by addition of 6 mL

PMAA solution with vigorously stirring at room temperature. After 5 min, 25 mL Triton X-100 was added dropwise until the mixed solution became optically transparent. After 10 min of vigorous stirring, 500 μL aqueous ammonia solution (29 wt%) was added, followed by adding 1.5 mL TMOS. The reaction was allowed to stir for 24 hours at room temperature. 100 mL acetone was added to break the stability of microemulsion and recovered the particles by centrifuge (4500 rpm, 10 min). The nanoparticles were washed three times with isopropyl alcohol and deionized water to remove the excess surfactant and cosurfactant.

6.1.6 Timolol maleate oven drying loading into silica-PMAA nanoparticles

For a typical loading process, silica-PMAA nanoparticles were first divided for six groups, and each group of nanoparticles was mixed with 0.1 mL deionized water containing 100 μg timolol maleate at room temperature for 5 hours, then timolol maleate nanoparticle mixtures were transferred to the oven at 80 ºC overnight. The drug loaded silica-PMAA nanoparticles were washed twice with phosphate buffer solution (10 mM, pH 2.5) to remove timolol maleate that was adsorbed on the surface. The timolol maleate concentration in washing solution was determined via UV-Vis spectrophotometry at a wavelength of 294 nm (SpectraMax i3, Molecular Devices, Sunnyvale, CA).

6.1.7 Timolol maleate *in vitro* release study from oven drying post loading nanoparticles

Kinetic release study: timolol maleate loaded silica-PMAA nanoparticles were suspended in 0.5 mL phosphate buffer (10 mM, pH 2.5) and simulated tear fluid (pH 7.5) under room temperature. At predetermined time intervals, all release samples were centrifuged (14800 rpm) for 10 min, and 0.5 mL supernatant was withdrawn and replaced with 0.5 mL fresh release

medium. After the release study, nanoparticles were dissolved in 1 mL NaOH (1 M) to detect timolol maleate left inside the nanoparticles. The concentrations of timolol maleate in all release mediums were detected by UV-Vis spectrophotometry (SpectraMax i3, Molecular Devices, Sunnyvale, CA) at a wavelength of 294 nm. The percentage of cumulative released timolol maleate was determined from the calibration curve. All samples were analyzed in triplicate.

Equilibrium to kinetic release study: timolol maleate loaded silica-PMAA nanoparticles were suspended in 1 mL phosphate buffer (10 mM, pH 2.5) under room temperature to start the equilibrium release study. At predetermined time intervals, all release samples were centrifuged (14800 rpm) for 10 min, and 0.2 mL supernatant was withdrawn and the concentrations of timolol maleate in all release mediums were detected by UV-Vis spectrophotometry (SpectraMax i3, Molecular Devices, Sunnyvale, CA) at a wavelength of 294 nm, then the same solution was added back to each release sample. After 26 days, changed the equilibrium release study to kinetic release study in simulated tear fluid (pH 7.5) At predetermined time intervals, all release samples were centrifuged (14800 rpm) for 10 min, and 0.5 mL supernatant was withdrawn and replaced with 0.5 mL fresh phosphate buffer. After the release study, nanoparticles were dissolved in 1mL NaOH (1 M) to detect timolol maleate left inside the nanoparticles. The concentrations of timolol maleate in all release mediums were detected by UV-Vis spectrophotometry at a wavelength of 294 nm. The percentage of cumulative released timolol maleate was determined from the calibration curve. All samples were analyzed in triplicate.

6.2 Results and discussions

6.2.1 Timolol maleate *in vitro* release study from *in situ* loading silica-PMAA nanoparticles

In this study, timolol maleate was loaded into silica-PMAA nanoparticles during the silica sol-gel encapsulation process in water-in-oil microemulsion system in the same way as in silica-alginate nanoparticles (Chapter 5.2.2). The same result was also observed, no timolol maleate was detected by UV-Vis spectrophotometry at a wavelength of 294 nm during the *in vitro* release study for 24 hours. In addition, there was no timolol maleate detected even after dissolving the silica-PMAA nanoparticles. In summary, *in situ* loading method through water-in-oil microemulsion method showed low loading efficiency, almost to zero in this case. This could be due to the small molecular weight of timolol maleate, which is 432.49 g/mol, and timolol maleate diffused out of water phase during the reaction as well as washed away during multiple washing steps as the high solubility of timolol maleate in both isopropyl alcohol and deionized water.

6.2.2 Timolol maleate loading and release study from silica-PMAA nanoparticles

Two types of silica-PMAA nanoparticles were used in this study. PMAA-3: silica – PMAA nanoparticles made by 3 wt% PMAA solution for the water-in-oil microemulsion, and PMAA-1: silica-PMAA nanoparticles made by 1 wt% PMAA solution for the water-in-oil microemulsion. Table 6.1 lists the loading efficiency. PMAA-3 showed a higher loading ability than PMAA-1, so more PMAA also could improve the loading ability, which was the same as alginate.

Table 6.1 Loading efficiency for silica-PMAA nanoparticles

Nanoparticles	Nanoparticles dry weight(mg)	Initial TM* (μg)	Loaded TM (μg)	Loaded TM per NPs (μg)/(mg)
PMAA-3	16.23 ± 0.69	500	214.90 ± 5.12	13.25 ± 0.43
PMAA-1	15.15 ± 0.59	500	77.14 ± 6.23	5.09 ± 0.41

* TM: timolol maleate

Figure 6.1 shows the *in vitro* release profiles of timolol maleate from both types of silica-PMAA nanoparticles. For PMAA-1, there was no strong difference of release performance between pH 2.5 phosphate buffer and pH 7.5 simulated tear fluid. In pH 2.5 phosphate buffer, 77 % timolol maleate was released over 27 days; and 79 % timolol maleate was released over the same time in pH 7.5 simulated tear fluid. In addition, burst release profiles were observed in both conditions, 60 % timolol maleate released at pH 2.5 in 1 day and 57 % timolol maleate release at

pH 7.5 during the same time. This release performance was similar to silica-alginate nanoparticles. However, for PMAA-3, there was a significantly different in release profiles at pH 2.5 phosphate and pH 7.5 simulated tear fluid. In pH 2.5 phosphate buffer, 26 % timolol maleate was released over 27 days, whereas, 46 % timolol maleate was released over the same time in pH 7.5 simulated tear fluid. Moreover, burst release was also reduced compared to PMAA-1.

Figure 6.2 shows the mathematical modeling for timolol maleate *in vitro* release from silica-PMAA nanoparticles. Two models were used in this study, Peppas equation and sphere monolithic solutions model, as listed in Table 5.1. As shown in Figure 6.2 (C&D), for PMAA-1, rapid burst release ($\frac{M_t}{M_\infty} > 0.6$) was observed in 1 day. In addition, monolithic solution modeling did not show good fit with the experimental release data. Therefore, timolol maleate was not homogeneously distributed inside those nanoparticles, and most of the timolol maleate should be in the surface level of nanoparticles. However, as shown in Figure 6.2 (A&B), for PMAA-3, both modeling had better fit with the experimental data. For Peppas equation modeling, in pH 2.5 phosphate buffer n = 0.27 and in pH 7.5 simulated tear fluid n = 0.20. Both were smaller than 0.43. Therefore, the release mechanism should be Fickian diffusion in both conditions. For monolithic solution modeling, PMAA-3 showed better homogeneously distribution of timolol maleate than PMAA-1. The experimental data showed higher release compared to modeling in the first 2 days, this should be due to the surface adsorbed timolol maleate.

These results showed that the concentration of PMAA solution used in water-in-oil microemulsion played an important role for the loading and release performance of timolol maleate.

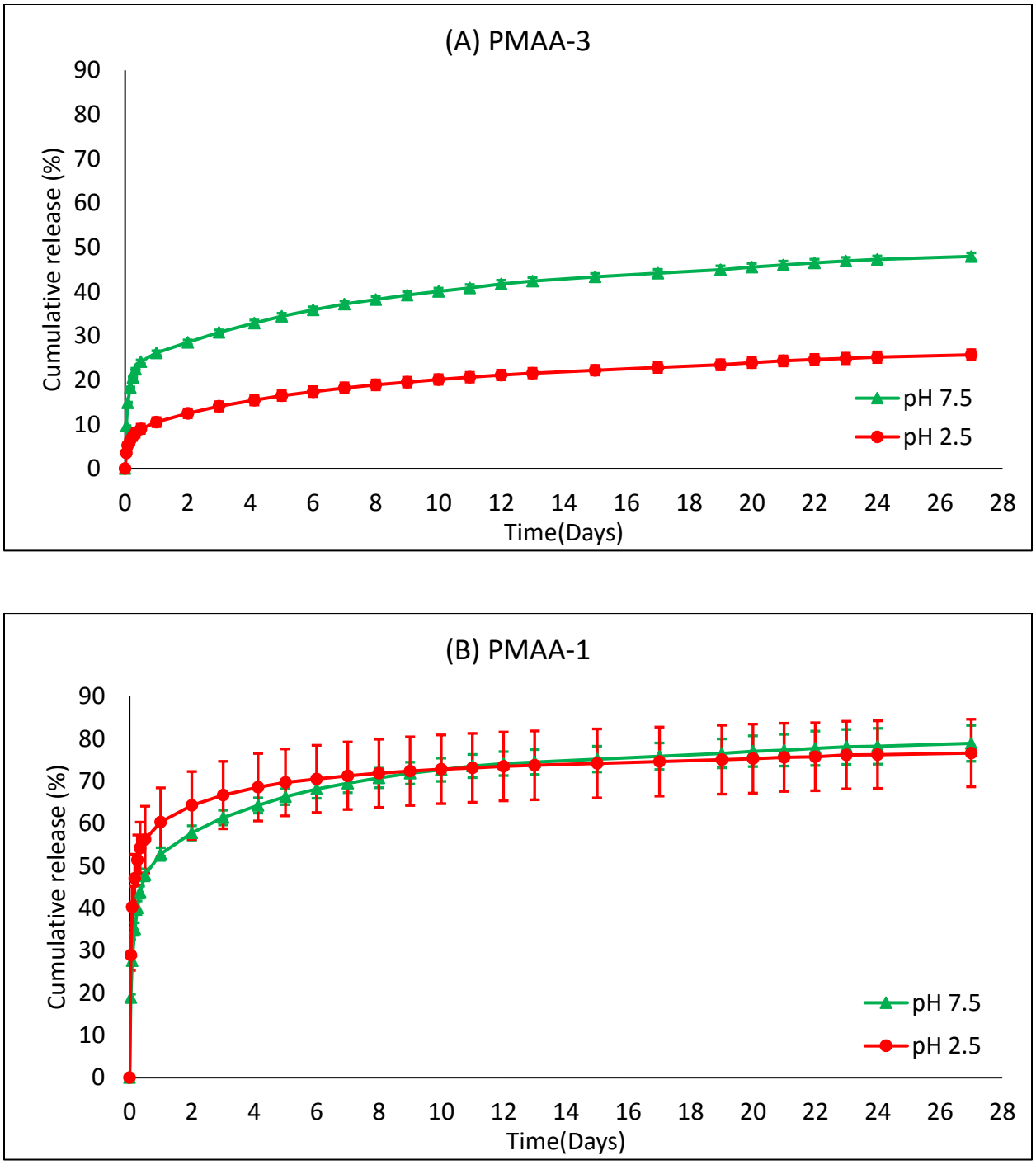

Figure 6.1 Timolol maleate release from silica-PMAA nanoparticles in phosphate buffer (pH 2.5) and simulated tear fluid (pH 7.5). (A) PMAA-3; (B) PMAA-1.

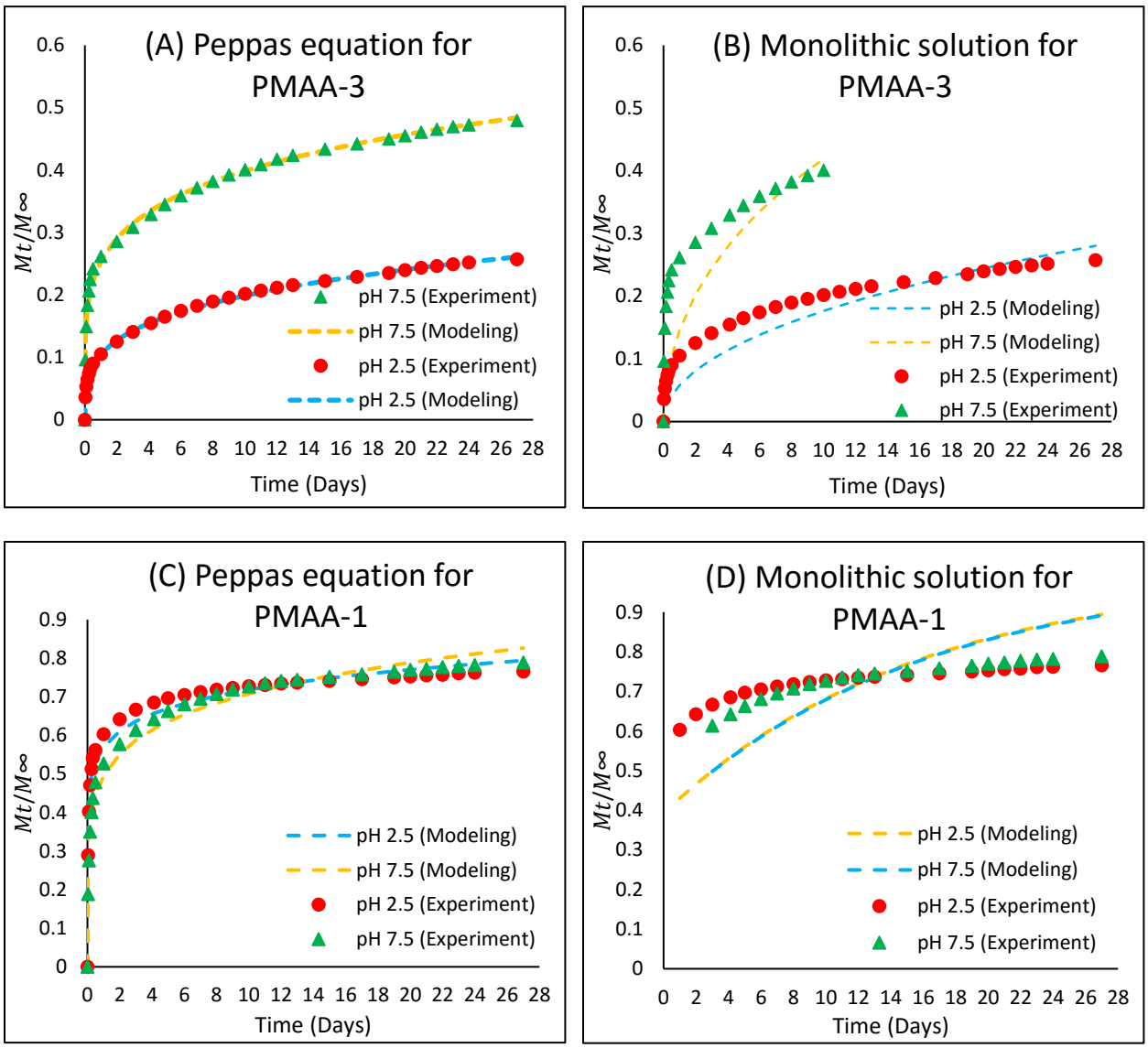

Figure 6.2 Mathematical models used for timolol maleate release from silica-PMAA nanoparticles (A&B: PMAA-3), (C&D: PMAA-1) in phosphate buffer (pH 2.5) and simulated tear fluid (pH 7.5). (A) Peppas equation modeling: pH 2.5 (R^2= 0.9986); pH 7.5 (R^2= 0.9910), (B) Monolithic solutions modeling: pH 2.5 (R^2= 0.7971); pH 7.5 (R^2= 0.2917), (C) Peppas equation modeling: pH 2.5 (R^2= 0.9294); pH 7.5 (R^2= 0.9607). (D) Monolithic solutions modeling: pH 2.5 (R^2= -5.5240); pH 7.5 (R^2= -1.2850)

In order to simulate the release process of timolol maleate from PMAA-3 nanoparticles under storage condition first, followed by being applied to the eye, an equilibrium release study, where the incubation solution remains unchanged, followed by a kinetic release study, where sink conditions were maintained through refreshing of the incubation buffer, was performed.. Silica nanoparticles were used as the control group.

As shown in Figure 6.3, the equilibrium release study was conducted in phosphate buffer (pH 2.5) for 26 days, during this time 37% timolol maleate was released from silica nanoparticles but only 14% timolol maleate was released from silica-PMAA nanoparticles. In next stage of kinetic release study, the release medium was changed from phosphate buffer solution (pH 2.5) to simulated tear fluid (pH 7.5). Both nanoparticles showed sustained release profiles for over 40 days, but silica-PMAA nanoparticles showed a more constant sustained release than silica nanoparticles. After a period of 40 days in simulated tear fluid (70 days total), approximately 50% of the drug was still remained within the nanoparticle and showed a trend of continuing release in an apparently linear manner.

The results showed that the silica-PMAA nanoparticle was a better carrier for pH-responsive release of timolol maleate compared to silica-alginate nanoparticle. One possible reason may be that PMAA has higher carboxyl group density than alginate. Therefore, the interactions of PMAA molecules as well as of PMAA molecules and timolol maleate molecules should be stronger than the ones of alginate molecules.

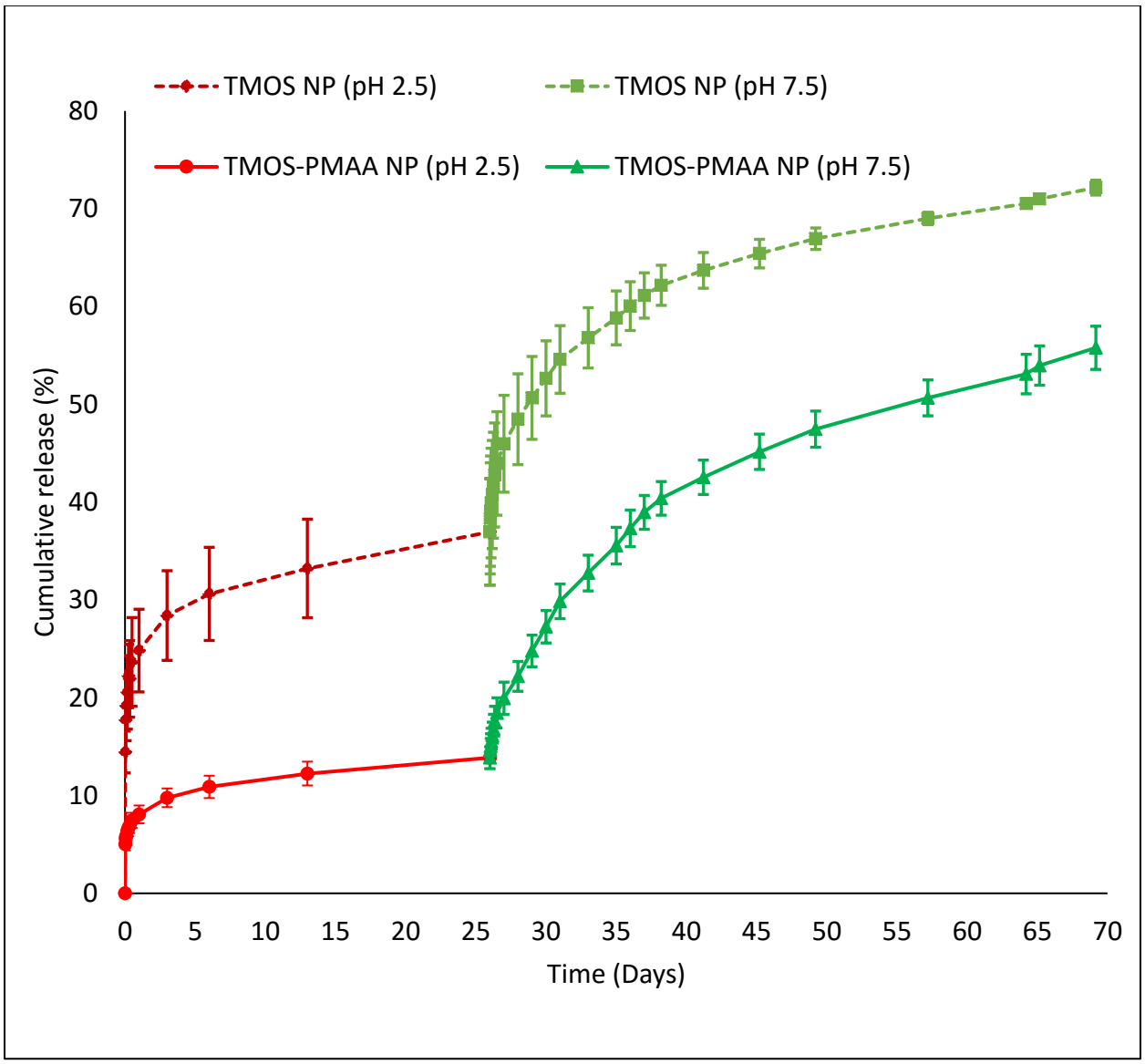

Figure 6.3 Timolol maleate equilibrium to kinetic release study. First 26 days, equilibrium release in phosphate buffer (pH 2.5), and then kinetic release in simulated tear fluid (pH 7.5). TMOS NP: silica nanoparticles (dash line); TMOS-PMAA NO: silica-PMAA nanoparticles (solid line)

6.3 Conclusions

Silica-PMAA nanoparticles have the potential to be a pH-responsive delivery vehicle for timolol maleate. With only a fraction of drug released at low pH condition and then continuous, sustained release at physiological pH condition, these nanoparticles demonstrated the concept of ON/OFF triggered release with < 15% drug released under pH 2.5 condition and a long, sustained release of drug in simulated tear fluid. In addition, the concentration of PMAA solution used in water-in-oil microemulsion played an important role for the loading and release performance of timolol maleate. More characterizations are needed to be done to further understand this performance.

Chapter 7 Contact lens loaded with nanoparticles

Contact lens has been used in drug delivery application in different ways. Commercial contact lenses are first used to absorb and release medications, but the release rate is rapid and limited drug is eluted after the first several hours.[189] To extend the duration of drug release, novel contact lens designs have been developed. For example, molecularly-imprinted,[126] vitamin E barriers,[190], nanoparticles,[191] drug polymer films,[192] liposomes,[193] and β-cyclodextrins[194] have been incorporated into contact lens and have demonstrated varying drug release profiles within *in vitro* release studies. However, storage stability is a major issue for the application of drug loaded contact lens. More specifically, while sustained release for up to a month has been demonstrated, the lenses continue to release encapsulated drugs, even while in their packaging. This limits the commercial feasibility and provides unacceptable variability in efficacy.

Soft contact lenses should have excellent optical transparency, show good stability under packing and storage. In addition, since the material directly contacts with the eye, it should be tear wettable, biofouling resistant, and have high ion and oxygen transmission. The cornea has no blood vessels, so it has to obtain oxygen from the atmosphere. Insufficient oxygen transport causes corneal edema with excessive corneal swelling in overnight wear.[195] Water content and good mechanical properties are also important parameters of soft contact lenses performance. Water content also affects the oxygen permeability and comfortable of wearing.[196] For the mechanical properties, soft contact lenses should not only be flexible enough to provide comfort to the wearer but also needs to be rigid enough to maintain overall shape and withstand multiple stress cycles in storage environments.[197]

To keep the advantages of the soft contact lenses, the loaded nanoparticles should have a very low effect on the contact lessee properties, like optical clarity, water content, ion and oxygen permeability, and mechanical properties. Therefore, it is necessary to compare these properties between soft contact lenses and silica-based nanoparticles loaded soft contact lenses.

7.1 Materials and methods

7.1.1 Materials

Timolol maleate, N,N-dimethylacrylamide, 2,2'-azobis-(2-methylpropionitrile) (AIBN) and poly (methacrylic acid, sodium salt) solution (30 wt%) were purchased from Sigma Aldrich; Triton X-100, sodium phosphate dibasic heptahydrate, sodium phosphate monobasic monohydrate, sodium chloride, potassium chloride, sodium bicarbonate, and calcium chloride dehydrate were purchased from AMRESCO; cyclohexane, ethanol, aqueous ammonia solution (29 wt% ammonia), isopropyl alcohol (70 %), hydrochloric acid (37 %), were purchased from BDH Chemicals; n-hexanol, ethylene glycol dimethacrylate were purchased from Alfa Aesar; hydroxyethyl methacrylate and providone K-90 were purchased from Spectrum Chemicals. 3 -methacryloxy-2 -hydroxypropyloxy) propylbis (trimethylsiloxy) methylsilane (SiGMA) was purchased from Pharnorcia. All chemicals were used without further purification. Deionized water used throughout the experiments was purified with an ELGA PURELAB Flex water purification system.

7.1.2 Preparation of soft contact lens

The soft contact lenses were prepared by polymerizing 2-hydroxyethyl methacrylate (HEMA) along with high oxygen permeability silicone monomer SiGMA, n-hexanol, N.N-dimethylacrylamide, n-hexanol, 2,2'-azobis-(2-methylpropionitrile) AIBN, providone K-90 and ethylene glycol dimethacrylate (EGDMA). This monomer mixed solution was injected into a plastic contact lens mold. After curing at 120 ºC for 2 hours, contact lenses were washed with isopropanol (50 %v/v) and water to remove initiator residue and unreacted monomers. For

nanoparticle loaded contact lenses, nanoparticles were added into monomer mixed solution before curing. All the other process were the same.

7.1.3 Optical clarity of soft contact lens

Optical clarity of the contact lenses was determined through transmission measurements using UV-Vis spectrophotometer (SpectraMax i3, Molecular Devices, Sunnyvale, CA). Each contact lens sample was placed in one well of 24 well plate with 1 mL pH 7.4 phosphate buffer solution. The well plate was placed in the spectrophotometer and transmittance was measured at wavelengths ranging from 400 nm to 750 nm.

7.1.4 Water content of soft contact lens

The weights of wet contact lenses (W_{wet}). were measured after washing with water. Then, the dried lens weighed (W_{dry}) were obtained by drying the contact lenses at 100 °C for overnight. The equilibrium water content (EWC) was calculated by:

$$EWC = \frac{W_{wet} - W_{dry}}{W_{wet}} \times 100$$

7.1.5 Synthesis of silica-PMAA nanoparticles

Silica-PMAA nanoparticles were prepared in water-in-oil microemulsion system. Initially, 20 mL n-hexanol was dissolved in 60 mL cyclohexane, followed by adding 6 mL PMAA (10 wt%) solution. After 5 min, 25 mL Triton X-100 was added dropwise until the mixed solution became optically transparent. After 10 min of vigorous stirring, 500 μL aqueous ammonia solution (29 wt%) was added, followed by adding 1.5 mL TMOS. The reaction was

allowed to stir for 24 hours at room temperature. 100 mL acetone was added to break the stability of microemulsion and the nanoparticles were recovered by centrifuge (4500 rpm, 10 min). In the end, nanoparticles were washed three times with isopropyl alcohol and deionized water to remove the excess surfactant and cosurfactant.

7.1.6 Timolol maleate loading process into nanoparticles

Timolol maleate was first dissolved in deionized water to make a 2 mg/mL solution. Then silica-PMAA nanoparticles were added into timolol maleate solution. This mixed solution was sonicated to get well dispersed nanoparticles and kept at room temperature for 5 hours, and then transferred to the oven with 80 ºC overnight to remove water.

7.1.7 Preparation of buffers

Phosphate buffer (pH 2.5, 10 mM) was prepared by dissolving 1.380 g sodium phosphate monobasic monohydrate to 1000 mL deionized water. Then adjusted the pH to 2.5 by hydrochloric acid (1 M).

Simulated tear fluid (pH 7.5) was prepared by dissolving 6.78 g sodium chloride, 1.38 g potassium chloride, 2.18 g sodium bicarbonate, 0.084 g calcium chloride dehydrate to 1000 mL deionized water. Then adjusted the pH to 7.5 by hydrochloric acid (1 M).

7.1.7 *In vitro* release study of timolol maleate loaded nanoparticle incorporated contact lens

Timolol maleate loaded nanoparticles were added into contact lens monomer solution. This monomer mixture was injected into a plastic contact lens mold. After curing at 120ºC for 2 hours, the contact lenses were washed with isopropanol (50 %v/v) and water to remove initiator

residue and unreacted monomers. *In vitro* release study was performed with two groups of contact lens. For the first group of contact lens, equilibrium release study was studied in 1 mL simulated tear fluid (pH 7.5) for 8 days for each lens, at predetermined time intervals, 0.2 mL release medium was withdrawn to detect the concentration of timolol maleate at 294 nm by UV-Vis spectrophotometry (SpectraMax i3, Molecular Devices, Sunnyvale, CA). Then this same 0.2 mL release medium was added back to the release container. After 8 days, changed all the release medium to 1 mL fresh simulated tear fluid (pH 7.5) for a second equilibrium release study. For the other group of contact lens, the first equilibrium study was performed in phosphate buffer (pH 2.5), and the second equilibrium study was performed in simulated tear fluid (pH 7.5). All samples were analyzed in triplicate.

7.2 Results and discussions

7.2.1 Optical clarity of contact lens

Optical clarity of silica nanoparticle incorporated contact lenses was determined through transmission measurements using UV-Vis spectrophotometer. Each contact lens was placed in one well of 24 well plate with 1 mL pH 7.4 phosphate buffer solution. Transmittance was measured at wavelengths from 400 nm to 750 nm. Phosphate buffer solution (pH 7.4) was used as the 100 % transmittance control. As shown in Figure 7.1, all tested contact lenses showed good transmission (> 90%). Contact lenses without nanoparticles showed the highest transmission with a minimum of 92 %; contact lenses with 0.2 wt% nanoparticles showed minimum 91 % transmission; contact lenses with 0.5 wt% nanoparticles showed minimum 90 % transmission. A photographic image of the nanoparticle incorporated lenses as shown Figure 7.1 shows that the loaded of particles caused no reduction of the visual clarity. Therefore, the addition of silica nanoparticles caused no strong visible alterations in the contact lens optical characteristics. This may be due to the low light absorbance of silica materials and the small size of silica nanoparticles.

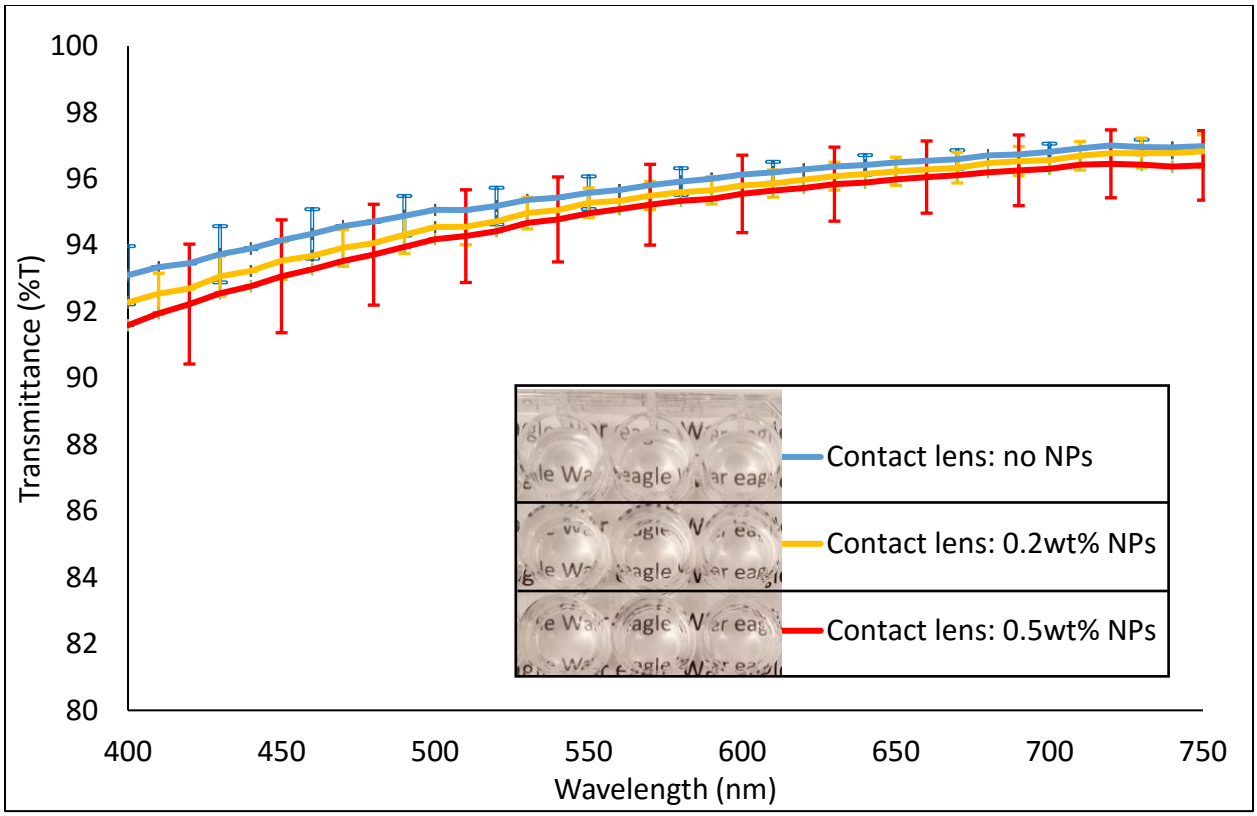

Figure 7.1 Transmittance of contact lens and nanoparticle incorporated contact lens. (Insert photographic image shows the visual clarity of different contact lenses)

7.2.2 Water content of contact lens

The contact lenses used in this study were the same ones for optical clarity test. The wet contact lens weight (W_{wet}) and dry the contact lens weight (W_{dry}) were measured. And the equilibrium water content (EWC) was calculated by $EWC = (W_{wet} - W_{dry})/ W_{wet} \times 100$. Table 7.1 lists the EWC for normal soft contact lenses and nanoparticle incorporated lenses. Without nanoparticle, the average EWC was 66.61 % for soft lens. Contact lens with 0.2 wt% nanoparticle inside had a 65.32 % average EWC, and lens with 0.5 wt% nanoparticle inside had a 67.45 % average EWC. Therefore, this result shows that the addition of silica nanoparticles almost caused no effect on the water content of contact lenses.

Table 7.1 Water content of contact lens and nanoparticle incorporated contact lens

Nanoparticle wt% in lens	EWC
0	66.61 ± 1.98
0.2	65.32 ± 1.82
0.5	67.45 ± 1.86

7.2.3 *In vitro* release of contact lens

In order to test the performance of silica-PMAA nanoparticles inside contact lenses for *in vitro* release study. Timolol maleate was first loaded into silica-PMAA nanoparticles, and then those nanoparticles were added into the monomer solution of contact lens. In the end, silica-PMAA nanoparticle incorporated contact lenses were prepared with timolol maleate loaded inside the nanoparticles. For the *in vitro* release study, the equilibrium release in 1 mL of phosphate buffer solution (pH 2.5) and simulated tear fluid (pH 7.5) was studied, this was a study to mimic the storage condition before contact lenses were applied to the eyes. As shown in Figure 7.2, after 8 days, only 3 µg timolol maleate released per lens in phosphate buffer solution (pH 2.5), however, 8 µg timolol maleate released per lens in simulated tear fluid (pH 7.5). This was due to the pH-responsive timolol maleate release ability of silica-PMAA nanoparticles as shown in previously studies. After 8 days of equilibrium release study, a second equilibrium study was performed by using simulated tear fluid (pH 7.5) in both sets of contact lenses. Initial burst release was observed in all lenses, this was due to the exchange of the fresh release medium. However, lenses initially in phosphate buffer solution (pH 2.5) released more timolol maleate compared to lenses initially in simulated tear fluid (pH 7.5). Eventually, all the lenses reached the similar release amount of timolol maleate. This result showed that silica-PMAA nanoparticles maintained their pH-responsive timolol maleate release ability even inside contact lens. This result also provided the information that silica-PMAA nanoparticle inside the contact lenses can limit the timolol maleate release amount under acidic solution to reduce the drug leakage during packing and storage condition. In addition, this nanoparticle laden lenses showed pH-responsive trigger release profile once in simulated tear film solution.

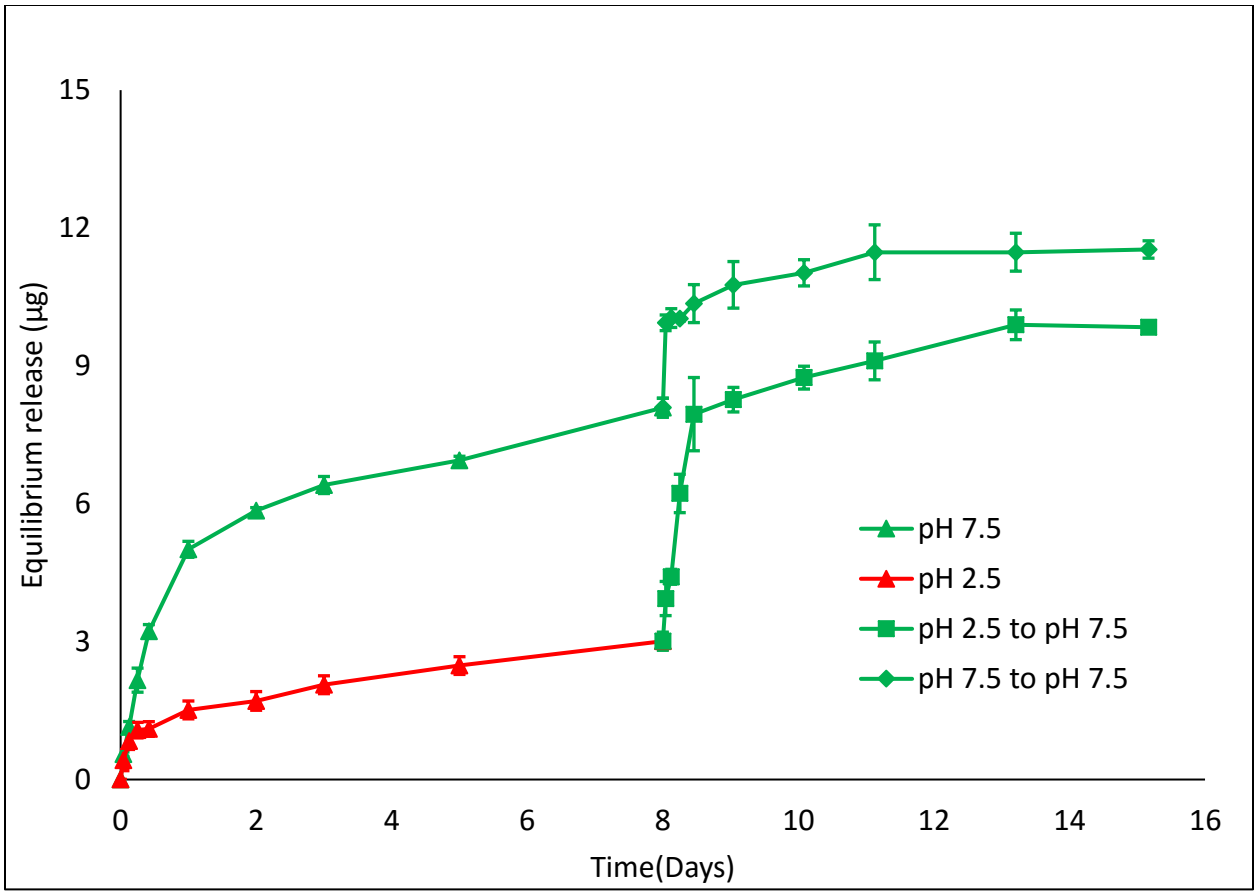

Figure 7.2 Timolol maleate *in vitro* equilibrium release from silica-PMAA nanoparticle incorporated contact lenses. (First equilibrium release study: 0-8 days, one set of contacts lenses were in phosphate buffer (pH 2.5)); the other set of contact lenses were in simulated tear fluid (pH 7.5): second equilibrium release study: 8-15 days, both sets of contact lenses were in simulated tear fluid (pH 7.5).)

7.3 Conclusions

Silica-based nanoparticles showed limited visible alterations in the contact lens optical characteristics, as well as negligible influence on the water content. This showed the potential for using silica-based nanoparticles for contact lens to control delivery drug molecules, as these nanoparticles would not undermine the physical properties of soft contact lens. *In vitro* equilibrium release showed that silica-PMAA nanoparticles inside the contact lens could limit the release of timolol maleate under acidic solution. In addition, the nanoparticle laden contact lenses showed pH-responsive trigger release profile once in simulated tear film solution. This promising pH-responsive release performance of silica-PMAA nanoparticle incorporated contact lens could lead to the production of commercial contact lens drug delivery vehicles.

Chapter 8 Summary

This dissertation was mainly concerned with the development of silica-polymer composite nanoparticle for pH-responsive drug release application. This type of composite nanoparticles could be produced by water-in-oil microemulsion method with the ability to control the size and composition of the nanoparticles. The pH-responsive drug release ability of silica-alginate composite material and silica-PMAA composite particles were studied. The results showed that silica-alginate composite material had potential to pH-responsive delivery the drug molecular similar to rhodamine B, and it could be used in biomedical applications such as wound healing or oral drug delivery. Silica-PMAA composite particles showed pH-responsive release ability for timolol maleate, which is a common used drug for glaucoma treatment. In addition, encouraging pH-responsive release profile was observed for the silica-PMAA nanoparticle incorporated contact lens.

The composites developed in this work could provide significant improvements for the application of contact lens drug delivery. Moving forward, more studies need to be done to get to the next stage. For example, more characterizations of the silica-based nanoparticles need to be done to better understand the control factors for the pH-responsive ability of composite nanoparticles. And how to fine control the release from silica-based nanoparticles, may be by controlling the particles size or polymer weight ratio. In addition, how to load more nanoparticles into contact lens without sacrificing the optical clarity, and the oxygen permeability and mechanical property of nanoparticle loaded contact lens also need to be studied. Moreover, it is important to develop an *in vitro* release system with a better prediction for the real drug delivery process in the eye. This *in vitro* release system should consider the tear production rate, tear

turnover rate and tear film volume with the wear of contact lens. More types of drug also can be studied such as bimatoprost for glaucoma treatment and cyclosporine A for dry eye treatment. Eventually, animal study is needed for testing the treatment performance of the contact lens.

References

1. Quigley, H.A. and A.T. Broman, *The number of people with glaucoma worldwide in 2010 and 2020.* Br J Ophthalmol, 2006. **90**(3): p. 262-7.
2. Casson, R.J., et al., *Definition of glaucoma: clinical and experimental concepts.* Clin Exp Ophthalmol, 2012. **40**(4): p. 341-9.
3. *Glaucoma Facts and Stats*. http://www.glaucoma.org/glaucoma/glaucoma-facts-and-stats.php.
4. Friedman, D.S., et al., *Prevalence of open-angle glaucoma among adults in the United States.* Arch Ophthalmol, 2004. **122**(4): p. 532-8.
5. Lee, D.A. and E.J. Higginbotham, *Glaucoma and its treatment: A review.* American Journal of Health-System Pharmacy, 2005. **62**(7): p. 691-699.
6. Schwartz, G.F. and H.A. Quigley, *Adherence and Persistence with Glaucoma Therapy.* Survey of Ophthalmology, 2008. **53**(6): p. S57-S68.
7. Taniguchi, E.V., et al., *Clinicians' perspectives on the use of drug-eluting contact lenses for the treatment of glaucoma.* Therapeutic Delivery, 2014. **5**(10): p. 1077-1083.
8. Patel, A., et al., *Ocular drug delivery systems: An overview.* World journal of pharmacology, 2013. **2**(2): p. 47-64.
9. Boone, A., A. Hui, and L. Jones, *Uptake and release of dexamethasone phosphate from silicone hydrogel and group I, II, and IV hydrogel contact lenses.* Eye Contact Lens, 2009. **35**(5): p. 260-7.
10. Ciriminna, R., et al., *The Sol–Gel Route to Advanced Silica-Based Materials and Recent Applications.* Chemical Reviews, 2013. **113**(8): p. 6592-6620.

11. Jaganathan, H. and B. Godin, *Biocompatibility assessment of Si-based nano- and micro-particles.* Advanced Drug Delivery Reviews, 2012. **64**(15): p. 1800-1819.

12. Vivero-Escoto, J.L., R.C. Huxford-Phillips, and W. Lin, *Silica-based nanoprobes for biomedical imaging and theranostic applications.* Chemical Society Reviews, 2012. **41**(7): p. 2673-2685.

13. McCarthy, S.A., G.-L. Davies, and Y.K. Gun'ko, *Preparation of multifunctional nanoparticles and their assemblies.* Nat. Protocols, 2012. **7**(9): p. 1677-1693.

14. Graham, T., *XXXV.-On the properties of silicic acid and other analogous colloidal substances.* Journal of the Chemical Society, 1864. **17**(0): p. 318-327.

15. Schubert, U. and H. Nicola, *Synthesis of inorganic materials*. 2012: John Wiley & Sons.

16. Hench, L.L. and J.K. West, *The sol-gel process.* Chemical Reviews, 1990. **90**(1): p. 33-72.

17. Buckley, A.M. and M. Greenblatt, *The Sol-Gel Preparation of Silica Gels.* Journal of Chemical Education, 1994. **71**(7): p. 599.

18. Shchipunov, Y.A., *Entrapment of Biopolymers into Sol—Gel-derived Silica Nanocomposites*, in *Bio-inorganic Hybrid Nanomaterials*. 2008, Wiley-VCH Verlag GmbH & Co. KGaA. p. 75-112.

19. David, A.E., et al., *Immobilized thermolysin for highly efficient production of low-molecular-weight protamine—An attractive cell-penetrating peptide for macromolecular drug delivery applications.* Journal of Biomedical Materials Research Part A, 2012. **100A**(1): p. 211-219.

20. Tan, S.C. and B.C. Yiap, *DNA, RNA, and Protein Extraction: The Past and The Present.* Journal of Biomedicine and Biotechnology, 2009. **2009**: p. 574398.

21. Axelrod, E., et al., *Negative dielectric loss phenomenon in porous sol–gel glasses.* Journal of Non-Crystalline Solids, 2006. **352**(40): p. 4166-4173.

22. Keefer, K.D., *Structure and Growth of Silica Condensation Polymers*, in *Silicon-Based Polymer Science*. 1989, American Chemical Society. p. 227-240.

23. SAVKO, N., *The Role of Inverse Nonionic Microemulsion in the Synthesis of SiO_2 Particles*. 2010, Università degli studi di Trieste.

24. Brinker, C.J. and G.W. Scherer, *Sol-Gel Science: The Physics and Chemistry of Sol-Gel Processing*. 1990: Academic press. Boston, USA.

25. Ciriminna, R., et al., *From Molecules to Systems: Sol−Gel Microencapsulation in Silica-Based Materials.* Chemical Reviews, 2011. **111**(2): p. 765-789.

26. Dickey, F.H., *Specific Adsorption.* The Journal of Physical Chemistry, 1955. **59**(8): p. 695-707.

27. Johnson, P. and T.L. Whateley, *On the use of polymerizing silica gel systems for the immobilization of trypsin.* Journal of Colloid and Interface Science, 1971. **37**(3): p. 557-563.

28. Braun, S., et al., *Biochemically active sol-gel glasses: The trapping of enzymes.* Materials Letters, 2007. **61**(14): p. 2843-2846.

29. Shchipunov, Y.A. and T.y.Y. Karpenko, *Hybrid Polysaccharide−Silica Nanocomposites Prepared by the Sol−Gel Technique.* Langmuir, 2004. **20**(10): p. 3882-3887.

30. Singh, V., et al., *Polysaccharide-Silica Hybrids: Design and Applications.* Polymer Reviews, 2016. **56**(1): p. 113-136.

31. Vecchione, R., et al., *Multilayered silica-biopolymer nanocapsules with a hydrophobic core and a hydrophilic tunable shell thickness.* Nanoscale, 2016. **8**(16): p. 8798-8809.

32. Shchipunov, Y.A., *Sol–gel-derived biomaterials of silica and carrageenans.* Journal of colloid and interface science, 2003. **268**(1): p. 68-76.

33. Prokopowicz, M. and A. Przyjazny, *Synthesis of sol-gel mesoporous silica materials providing a slow release of doxorubicin.* J Microencapsul, 2007. **24**(7): p. 682-701.

34. Barbé, C., et al., *Sol–gel matrices for controlled release: from macro to nano using emulsion polymerisation.* Journal of Sol-Gel Science and Technology, 2008. **46**(3): p. 393-409.

35. Kocak, G., C. Tuncer, and V. Butun, *pH-Responsive polymers.* Polymer Chemistry, 2017. **8**(1): p. 144-176.

36. Rapoport, N., *Physical stimuli-responsive polymeric micelles for anti-cancer drug delivery.* Progress in Polymer Science, 2007. **32**(8): p. 962-990.

37. Schmaljohann, D., *Thermo- and pH-responsive polymers in drug delivery.* Advanced Drug Delivery Reviews, 2006. **58**(15): p. 1655-1670.

38. Thevenot, J., et al., *Magnetic responsive polymer composite materials.* Chemical Society Reviews, 2013. **42**(17): p. 7099-7116.

39. Chen, W. and J. Du, *Ultrasound and pH Dually Responsive Polymer Vesicles for Anticancer Drug Delivery.* 2013. **3**: p. 2162.

40. Jochum, F.D., et al., *Thermo- and Light-Responsive Polymers Containing Photoswitchable Azobenzene End Groups.* Macromolecules, 2009. **42**(20): p. 7854-7862.

41. Dai, S., P. Ravi, and K.C. Tam, *pH-Responsive polymers: synthesis, properties and applications.* Soft Matter, 2008. **4**(3): p. 435-449.

42. Zhao, B. and J.S. Moore, *Fast pH- and Ionic Strength-Responsive Hydrogels in Microchannels.* Langmuir, 2001. **17**(16): p. 4758-4763.

43. Matsumoto, A., R. Yoshida, and K. Kataoka, *Glucose-Responsive Polymer Gel Bearing Phenylborate Derivative as a Glucose-Sensing Moiety Operating at the Physiological pH.* Biomacromolecules, 2004. **5**(3): p. 1038-1045.

44. Hu, J., G. Zhang, and S. Liu, *Enzyme-responsive polymeric assemblies, nanoparticles and hydrogels.* Chemical Society Reviews, 2012. **41**(18): p. 5933-5949.

45. Murakami, Y. and M. Maeda, *DNA-Responsive Hydrogels That Can Shrink or Swell.* Biomacromolecules, 2005. **6**(6): p. 2927-2929.

46. Hoffman, A.S., *Hydrogels for biomedical applications.* Advanced Drug Delivery Reviews, 2012. **64**: p. 18-23.

47. Hu, J., et al., *Stimuli-responsive tertiary amine methacrylate-based block copolymers: Synthesis, supramolecular self-assembly and functional applications.* Progress in Polymer Science, 2014. **39**(6): p. 1096-1143.

48. Jin, X. and Y.-L. Hsieh, *pH-responsive swelling behavior of poly(vinyl alcohol)/poly(acrylic acid) bi-component fibrous hydrogel membranes.* Polymer, 2005. **46**(14): p. 5149-5160.

49. Peng, T. and Y.-L. Cheng, *pH-responsive permeability of PE-g-PMAA membranes.* Journal of Applied Polymer Science, 2000. **76**(6): p. 778-786.

50. Liu, F. and M.W. Urban, *Dual Temperature and pH Responsiveness of Poly(2-(N,N-dimethylamino)ethyl methacrylate-co-n-butyl acrylate) Colloidal Dispersions and Their Films.* Macromolecules, 2008. **41**(17): p. 6531-6539.

51. Lu, J., et al., *Fabrication of pH-sensitive poly(2-(diethylamino)ethyl methacrylate)/palygorskite composite microspheres via Pickering emulsion*

polymerization and their release behavior. Journal of Applied Polymer Science, 2015. **132**(26): p. 42179-42186.

52. Fares, M.M. and A.M. Al-Shboul, *Stimuli pH-responsive (N-vinyl imidazole-co-acryloylmorpholine) Hydrogels; Mesoporous and Nanoporous Scaffolds.* Journal of Biomedical Materials Research Part A, 2012. **100A**(4): p. 863-871.

53. González, N., C. Elvira, and J.S. Román, *Novel Dual-Stimuli-Responsive Polymers Derived from Ethylpyrrolidine.* Macromolecules, 2005. **38**(22): p. 9298-9303.

54. Lin, Y.-H., et al., *Physically crosslinked alginate/N,O-carboxymethyl chitosan hydrogels with calcium for oral delivery of protein drugs.* Biomaterials, 2005. **26**(14): p. 2105-2113.

55. Lim, Y.-M., et al., *Synthesis and properties of hyaluronic acid containing copolymers crosslinked by γ-ray irradiation.* Macromolecular Research, 2011. **19**(5): p. 436-441.

56. Soppimath, K.S., A.R. Kulkarni, and T.M. Aminabhavi, *Chemically modified polyacrylamide-g-guar gum-based crosslinked anionic microgels as pH-sensitive drug delivery systems: preparation and characterization.* Journal of Controlled Release, 2001. **75**(3): p. 331-345.

57. Lohani, A., et al., *Tailored-interpenetrating polymer network beads of κ-carrageenan and sodium carboxymethyl cellulose for controlled drug delivery.* Journal of Drug Delivery Science and Technology, 2016. **31**: p. 53-64.

58. Kamiński, K., et al., *pH-Sensitive Genipin-Cross-Linked Chitosan Microspheres For Heparin Removal.* Biomacromolecules, 2008. **9**(11): p. 3127-3132.

59. Rehm, B.H.A., *Bacterial polymers: biosynthesis, modifications and applications.* Nat Rev Micro, 2010. **8**(8): p. 578-592.

60. Gao, T., W. Wang, and A. Wang, *A pH-sensitive composite hydrogel based on sodium alginate and medical stone: Synthesis, swelling, and heavy metal ions adsorption properties.* Macromolecular Research, 2011. **19**(7): p. 739-748.

61. Coradin, T., *Silica/alginate bio-nanocomposites*, in *Nanocomposites with Biodegradable Polymers*, V. Mittal, Editor. 2011, Oxford University Press Inc. : New York, United States. p. 166-188.

62. Liu, G., et al., *The pH-responsive alginate hydrogel prepared through solution extrusion and the release behavior for different drugs.* Frontiers in Bioengineering and Biotechnology, 10th World Biomaterials Congress (2016)

63. Velings, N.M. and M.M. Mestdagh, *Physico-chemical properties of alginate gel beads.* Polymer Gels and Networks, 1995. **3**(3): p. 311-330.

64. Thu, B., et al., *Alginate polycation microcapsules: I. Interaction between alginate and polycation.* Biomaterials, 1996. **17**(10): p. 1031-1040.

65. Fukushima, Y., et al., *A new immobilization technique of whole cells and enzymes with colloidal silica and alginate.* Biotechnol Bioeng, 1988. **32**(5): p. 584-94.

66. Patil, M.B., et al., *Preparation and characterization of filled matrix membranes of sodium alginate incorporated with aluminum-containing mesoporous silica for pervaporation dehydration of alcohols.* Separation and Purification Technology, 2007. **54**(1): p. 34-43.

67. Xu, S., et al., *Silica nanotubes-doped alginate gel for yeast alcohol dehydrogenase immobilization.* Journal of Molecular Catalysis B: Enzymatic, 2006. **43**(1–4): p. 68-73.

68. Heichal-Segal, O., S. Rappoport, and S. Braun, *Immobilization in Alginate-Silicate Sol-Gel Matrix Protects [beta]-Glucosidase Against Thermal and Chemical Denaturation.* Nat Biotech, 1995. **13**(8): p. 798-800.

69. Kawakami, K. and S.-Y. Furukawa, *Alcohol-oxidation activity of whole cells ofpichia postons entrapped in hybrid gels composed of Ca-alginate and organic silicate.* Applied Biochemistry and Biotechnology, 1997. **67**(1): p. 23-31.

70. Dai, Y.N., et al., *Swelling characteristics and drug delivery properties of nifedipine-loaded pH sensitive alginate-chitosan hydrogel beads.* J Biomed Mater Res B Appl Biomater, 2008. **86**(2): p. 493-500.

71. González-Rodríguez, M.L., et al., *Alginate/chitosan particulate systems for sodium diclofenac release.* International Journal of Pharmaceutics, 2002. **232**(1): p. 225-234.

72. Hu, L., et al., *Alginate encapsulated mesoporous silica nanospheres as a sustained drug delivery system for the poorly water-soluble drug indomethacin.* Asian Journal of Pharmaceutical Sciences, 2014. **9**(4): p. 183-190.

73. Bal, A., B. Özkahraman, and Z. Özbaş, *Preparation and characterization of pH responsive poly(methacrylic acid-acrylamide-N-hydroxyethyl acrylamide) hydrogels for drug delivery systems.* Journal of Applied Polymer Science, 2016. **133**(13): p. 43226-43233.

74. Lochhead, R.Y., *The Role of Polymers in Cosmetics: Recent Trends*, in *Cosmetic Nanotechnology*. 2007, American Chemical Society. p. 3-56.

75. Zelikin, A.N., J.F. Quinn, and F. Caruso, *Disulfide Cross-Linked Polymer Capsules: En Route to Biodeconstructible Systems.* Biomacromolecules, 2006. **7**(1): p. 27-30.

76. Wei, F., M. Zhang, and Y.-Q. Feng, *Application of poly(methacrylic acid-ethylene glycol dimethacrylate) monolith microextraction coupled with capillary zone electrophoresis to the determination of opiates in human urine.* Electrophoresis, 2006. **27**(10): p. 1939-1948.

77. Wiogo, H.T.R., et al., *Insight into Serum Protein Interactions with Functionalized Magnetic Nanoparticles in Biological Media.* Langmuir, 2012. **28**(9): p. 4346-4356.

78. Okamoto, H. and Y. Wada, *Viscoelastic study of the conformational transition of poly(methacrylic acid) in dilute aqueous solution.* Journal of Polymer Science: Polymer Physics Edition, 1974. **12**(12): p. 2413-2422.

79. Lando, J.B., J.L. Koenig, and J. Semen, *Conformational studies of poly(methacrylic Acid). II. Laser-excited Raman studies of the conformational transition in aqueous solution.* Journal of Macromolecular Science, Part B, 1973. **7**(2): p. 319-343.

80. Heitz, C., M. Rawiso, and J. François, *X-ray scattering study of a poly(methacrylic acid) sample as a function of its neutralization degree.* Polymer, 1999. **40**(7): p. 1637-1650.

81. Mandel, M., *The potentiometric titration of weak polyacids.* European Polymer Journal, 1970. **6**(6): p. 807-822.

82. Wang, X., X. Ye, and G. Zhang, *Investigation of pH-induced conformational change and hydration of poly(methacrylic acid) by analytical ultracentrifugation.* Soft Matter, 2015. **11**(26): p. 5381-5388.

83. Pristinski, D., V. Kozlovskaya, and S.A. Sukhishvili, *Fluorescence correlation spectroscopy studies of diffusion of a weak polyelectrolyte in aqueous solutions.* The Journal of Chemical Physics, 2005. **122**(1): p. 014907.

84. Ruiz-Pérez, L., et al., *Conformation of Poly(methacrylic acid) Chains in Dilute Aqueous Solution.* Macromolecules, 2008. **41**(6): p. 2203-2211.

85. Swift, T., et al., *The pH-responsive behaviour of poly(acrylic acid) in aqueous solution is dependent on molar mass.* Soft Matter, 2016. **12**(9): p. 2542-2549.

86. Sharma, A., et al., *Constant pH simulations of pH responsive polymers.* The Journal of Chemical Physics, 2016. **145**(23): p. 234906.

87. Zhang, J. and N.A. Peppas, *Synthesis and Characterization of pH- and Temperature-Sensitive Poly(methacrylic acid)/Poly(N-isopropylacrylamide) Interpenetrating Polymeric Networks.* Macromolecules, 2000. **33**(1): p. 102-107.

88. Liu, Y., et al., *pH-sensitive polymeric micelles triggered drug release for extracellular and intracellular drug targeting delivery.* Asian Journal of Pharmaceutical Sciences, 2013. **8**(3): p. 159-167.

89. Min, K.H., et al., *Tumoral acidic pH-responsive MPEG-poly(β-amino ester) polymeric micelles for cancer targeting therapy.* Journal of Controlled Release, 2010. **144**(2): p. 259-266.

90. Luo, Y.-L., W. Yu, and F. Xu, *pH-responsive PMAA-b-PEG-b-PMAA triblock copolymer micelles for prednisone drug release and release kinetics.* Polymer Bulletin, 2012. **69**(5): p. 597-620.

91. Lay, C.L., et al., *pH-Responsive Poly(methacrylic acid)-Grafted Hollow Silica Vesicles.* Chemistry – A European Journal, 2011. **17**(8): p. 2504-2509.

92. Han, J., et al., *"Graft to" Synthesis and Ibuprofen-Loading Performance of pH-Sensitive PMAA–Silica Hybrid Nanoparticles with Controlled Bimodal Mesopores.* Journal of Pharmaceutical Sciences, 2015. **104**(12): p. 4299-4306.

93. Danielsson, I. and B. Lindman, *The definition of microemulsion.* Colloids and Surfaces, 1981. **3**(4): p. 391-392.

94. Talegaonkar, S., et al., *Microemulsions: a novel approach to enhanced drug delivery.* Recent Pat Drug Deliv Formul, 2008. **2**(3): p. 238-57.

95. Lawrence, M.J. and G.D. Rees, *Microemulsion-based media as novel drug delivery systems.* Advanced Drug Delivery Reviews, 2000. **45**(1): p. 89-121.

96. Malik, M.A., M.Y. Wani, and M.A. Hashim, *Microemulsion method: A novel route to synthesize organic and inorganic nanomaterials.* Arabian Journal of Chemistry, 2012. **5**(4): p. 397-417.

97. Bowcott, J.E. and J.H. Schulman, *Emulsions Control of droplet size and phase continuity in transparent oil-water dispersions stabilized with soap and alcohol.* Zeitschrift für Elektrochemie, Berichte der Bunsengesellschaft für physikalische Chemie, 1955. **59**(4): p. 283-290.

98. Akhtar, M., *Microemullsions Formation, Stability and their Characterisations*, in *Department of Chemistry*. 1996, Brunel University (The university of West London).

99. Prince, L.M., *A theory of aqueous emulsions: II. Mechanism of film curvature at the oil/water interface.* Journal of Colloid and Interface Science, 1969. **29**(2): p. 216-221.

100. Paul, B.K. and S.P. Moulik, *Microemulsions: an overview.* Journal of Dispersion Science and Technology, 1997. **18**(4): p. 301-367.

101. Moulik, A.K.R.S.P., *Physicochemistry of W/O Microemulsions: Formation, Stability, and Droplet Clustering*, in *Microemulsions: Properties and Applications*, M. Fanun, Editor. 2008, CRC Press: Boca Raton, USA.

102. Moulik, S.P., A.K. Rakshit, and I. Capek, *Microemulsions as Templates for Nanomaterials,* in *Microemulsions*. 2009, John Wiley & Sons, Ltd. p. 180-210.

103. Bagwe, R.P., et al., *Optimization of Dye-Doped Silica Nanoparticles Prepared Using a Reverse Microemulsion Method.* Langmuir, 2004. **20**(19): p. 8336-8342.

104. Jin, Y., et al., *Silica Nanoparticles with Continuously Tunable Sizes: Synthesis and Size Effects on Cellular Contrast Imaging.* Chemistry of Materials, 2008. **20**(13): p. 4411-4419.

105. Chang, S.-Y., L. Liu, and S.A. Asher, *Preparation and Properties of Tailored Morphology, Monodisperse Colloidal Silica-Cadmium Sulfide Nanocomposites.* Journal of the American Chemical Society, 1994. **116**(15): p. 6739-6744.

106. Chu, M., Y. Sun, and S. Xu, *Silica-coated quantum dots fluorescent spheres synthesized using a quaternary 'water-in-oil' microemulsion system.* Journal of Nanoparticle Research, 2008. **10**(4): p. 613-624.

107. Zhu, L., J. Meng, and X. Cao, *Synthesis and photoluminescent properties of silica-coated LaCeF3:Tb nanocrystals.* Journal of Nanoparticle Research, 2008. **10**(2): p. 383-386.

108. Zhao, X., R.P. Bagwe, and W. Tan, *Development of Organic-Dye-Doped Silica Nanoparticles in a Reverse Microemulsion.* Advanced Materials, 2004. **16**(2): p. 173-176.

109. Peng, C.-C., J. Kim, and A. Chauhan, *Extended delivery of hydrophilic drugs from silicone-hydrogel contact lenses containing Vitamin E diffusion barriers.* Biomaterials, 2010. **31**(14): p. 4032-4047.

110. Gulsen, D. and A. Chauhan, *Ophthalmic drug delivery through contact lenses.* Invest Ophthalmol Vis Sci, 2004. **45**(7): p. 2342-7.

111. Beatriz, R., et al., *Dry Eye Characterization by Analyzing Tear Film Images*, in *Ophthalmological Imaging and Applications*. 2014, CRC Press. p. 449-476.

112. Nichols, J.J. and P.E. King-Smith, *Thickness of the pre- and post-contact lens tear film measured in vivo by interferometry.* Invest Ophthalmol Vis Sci, 2003. **44**(1): p. 68-77.

113. Wang, J., et al., *In situ visualization of tears on contact lens using ultra high resolution optical coherence tomography.* Eye Contact Lens, 2009. **35**(2): p. 44-9.

114. Muntz, A., et al., *Tear exchange and contact lenses: A review.* Journal of Optometry, 2015. **8**(1): p. 2-11.

115. Carney, L.G. and R.M. Hill, *Human tear pH. Diurnal variations.* Arch Ophthalmol, 1976. **94**(5): p. 821-4.

116. Yamada, M., et al., *Fluorophotometric measurement of pH of human tears in vivo.* Curr Eye Res, 1997. **16**(5): p. 482-6.

117. Lattimore Jr, M.R., *Contact lens anterior surface pH.* International Contact Lens Clinic, 1990. **17**(9–10): p. 228-231.

118. Tomlinson, A., *Complications of contact lens wear*. Tear film changes with contact lens wear. 1992, Mosby, St.Louis.

119. Mann, A. and B. Tighe, *Contact lens interactions with the tear film.* Exp Eye Res, 2013. **117**: p. 88-98.

120. Creech, J.L., A. Chauhan, and C.J. Radke, *Dispersive Mixing in the Posterior Tear Film Under a Soft Contact Lens.* Industrial & Engineering Chemistry Research, 2001. **40**(14): p. 3015-3026.

121. Hillman, J.S., *Management of acute glaucoma with pilocarpine-soaked hydrophilic lens.* The British Journal of Ophthalmology, 1974. **58**(7): p. 674-679.

122. Schultz, C.L., T.R. Poling, and J.O. Mint, *A medical device/drug delivery system for treatment of glaucoma.* Clinical and Experimental Optometry, 2009. **92**(4): p. 343-348.

123. Alvarez-Lorenzo, C., et al., *Imprinted soft contact lenses as norfloxacin delivery systems.* Journal of Controlled Release, 2006. **113**(3): p. 236-244.

124. Alvarez-Lorenzo, C., et al., *Soft contact lenses capable of sustained delivery of timolol.* J Pharm Sci, 2002. **91**(10): p. 2182-92.

125. White, C.J., et al., *Extended release of high molecular weight hydroxypropyl methylcellulose from molecularly imprinted, extended wear silicone hydrogel contact lenses.* Biomaterials, 2011. **32**(24): p. 5698-5705.

126. Hiratani, H., et al., *Ocular release of timolol from molecularly imprinted soft contact lenses.* Biomaterials, 2005. **26**(11): p. 1293-1298.

127. Jung, H.J. and A. Chauhan, *Temperature sensitive contact lenses for triggered ophthalmic drug delivery.* Biomaterials, 2012. **33**(7): p. 2289-2300.

128. Kim, H.-J., et al., *Diamond Nanogel-Embedded Contact Lenses Mediate Lysozyme-Dependent Therapeutic Release.* ACS Nano, 2014. **8**(3): p. 2998-3005.

129. Siepmann, J., et al., *Calculation of the Dimensions of Drug-Polymer Devices Based on Diffusion Parameters.* Journal of Pharmaceutical Sciences, 1998. **87**(7): p. 827-832.

130. Siepmann, J., F. Lecomte, and R. Bodmeier, *Diffusion-controlled drug delivery systems: calculation of the required composition to achieve desired release profiles.* Journal of Controlled Release, 1999. **60**(2): p. 379-389.

131. Siepmann, J. and F. Siepmann, *Mathematical modeling of drug release from lipid dosage forms.* International Journal of Pharmaceutics, 2011. **418**(1): p. 42-53.

132. Glaessl, B., et al., *Deeper insight into the drug release mechanisms in Eudragit RL-based delivery systems.* International Journal of Pharmaceutics, 2010. **389**(1): p. 139-146.

133. Brandl, F., et al., *Hydrogel-based drug delivery systems: Comparison of drug diffusivity and release kinetics.* Journal of Controlled Release, 2010. **142**(2): p. 221-228.

134. Lecomte, F., et al., *pH-Sensitive Polymer Blends Used as Coating Materials to Control Drug Release from Spherical Beads: Elucidation of the Underlying Mass Transport Mechanisms.* Pharmaceutical Research, 2005. **22**(7): p. 1129-1141.

135. Arifin, D.Y., L.Y. Lee, and C.-H. Wang, *Mathematical modeling and simulation of drug release from microspheres: Implications to drug delivery systems.* Advanced Drug Delivery Reviews, 2006. **58**(12): p. 1274-1325.

136. Gallagher, K.M. and O.I. Corrigan, *Mechanistic aspects of the release of levamisole hydrochloride from biodegradable polymers.* Journal of Controlled Release, 2000. **69**(2): p. 261-272.

137. Berchane, N.S., et al., *Effect of mean diameter and polydispersity of PLG microspheres on drug release: Experiment and theory.* International Journal of Pharmaceutics, 2007. **337**(1): p. 118-126.

138. Chirico, S., et al., *Analysis and modeling of swelling and erosion behavior for pure HPMC tablet.* Journal of Controlled Release, 2007. **122**(2): p. 181-188.

139. Abdekhodaie, M.J. and X.Y. Wu, *Drug release from ion-exchange microspheres: Mathematical modeling and experimental verification.* Biomaterials, 2008. **29**(11): p. 1654-1663.

140. Siepmann, J. and F. Siepmann, *Mathematical modeling of drug delivery.* International Journal of Pharmaceutics, 2008. **364**(2): p. 328-343.

141. Siepmann, J. and F. Siepmann, *Modeling of diffusion controlled drug delivery.* Journal of Controlled Release, 2012. **161**(2): p. 351-362.

142. Siepmann, J. and N.A. Peppas, *Modeling of drug release from delivery systems based on hydroxypropyl methylcellulose (HPMC).* Advanced Drug Delivery Reviews, 2001. **48**(2): p. 139-157.

143. Higuchi, T., *Rate of Release of Medicaments from Ointment Bases Containing Drugs in Suspension.* Journal of Pharmaceutical Sciences, 1961. **50**(10): p. 874-875.

144. Siepmann, J. and N.A. Peppas, *Higuchi equation: Derivation, applications, use and misuse.* International Journal of Pharmaceutics, 2011. **418**(1): p. 6-12.

145. Ritger, P.L. and N.A. Peppas, *A simple equation for description of solute release I. Fickian and non-fickian release from non-swellable devices in the form of slabs, spheres, cylinders or discs.* Journal of Controlled Release, 1987. **5**(1): p. 23-36.

146. Peppas, N.A. and J.J. Sahlin, *A simple equation for the description of solute release. III. Coupling of diffusion and relaxation.* International Journal of Pharmaceutics, 1989. **57**(2): p. 169-172.

147. Zhang, H.-Y., et al., *pH-responsive mesoporous silica nanocarriers based on layer-by-layer self-assembly.* Bio-medical materials and engineering, 2014. **24**(6): p. 2211-2218.

148. Sun, Y.-L., et al., *Cucurbit[7]uril Pseudorotaxane-Based Photoresponsive Supramolecular Nanovalve.* Chemistry – A European Journal, 2012. **18**(30): p. 9212-9216.

149. Chen, C., et al., *Stimuli-responsive controlled-release system using quadruplex DNA-capped silica nanocontainers.* Nucleic Acids Res, 2011. **39**(4): p. 1638-44.

150. Kim, B. and Y. Shin, *pH-sensitive swelling and release behaviors of anionic hydrogels for intelligent drug delivery system.* Journal of Applied Polymer Science, 2007. **105**(6): p. 3656-3661.

151. Guo, W., et al., *A General pH-Responsive Supramolecular Nanovalve Based on Mesoporous Organosilica Hollow Nanospheres.* Chemistry – A European Journal, 2010. **16**(29): p. 8641-8646.

152. Shilpa, A., S.S. Agrawal, and A.R. Ray, *Controlled Delivery of Drugs from Alginate Matrix.* Journal of Macromolecular Science, Part C, 2003. **43**(2): p. 187-221.

153. Pittman, J.L., K.F. Schrum, and S.D. Gilman, *On-line monitoring of electroosmotic flow for capillary electrophoretic separations.* Analyst, 2001. **126**(8): p. 1240-1247.

154. Maurya, N.S., et al., *Biosorption of dyes using dead macro fungi: Effect of dye structure, ionic strength and pH.* Bioresource Technology, 2006. **97**(3): p. 512-521.

155. Zhang, R., et al., *Real time monitoring of the drug release of rhodamine B on graphene oxide.* Carbon, 2011. **49**(4): p. 1126-1132.

156. Wang, J., et al., *Silica-based nanocomposites via reverse microemulsions: classifications, preparations, and applications.* Nanoscale, 2014. **6**(9): p. 4418-4437.

157. López-Quintela, M.A., *Synthesis of nanomaterials in microemulsions: formation mechanisms and growth control.* Current Opinion in Colloid & Interface Science, 2003. **8**(2): p. 137-144.

158. Wang, J., et al., *Reverse Microemulsion-Mediated Synthesis of SiO2-Coated ZnO Composite Nanoparticles: Multiple Cores with Tunable Shell Thickness.* ACS Applied Materials & Interfaces, 2010. **2**(4): p. 957-960.

159. Arriagada, F.J. and K. Osseo-Asare, *Synthesis of Nanosize Silica in a Nonionic Water-in-Oil Microemulsion: Effects of the Water/Surfactant Molar Ratio and Ammonia Concentration.* Journal of Colloid and Interface Science, 1999. **211**(2): p. 210-220.

160. Auger, A., et al., *A comparative study of non-covalent encapsulation methods for organic dyes into silica nanoparticles.* Nanoscale Research Letters, 2011. **6**(1): p. 328.

161. Gao, F., et al., *Preparation of aminated core-shell fluorescent nanoparticles and their application to the synchronous fluorescence determination of γ-globulin.* Luminescence, 2008. **23**(6): p. 392-396.

162. Coradin, T., D. Eglin, and J. Livage, *The silicomolybdic acid spectrophotometric method and its application to silicate/biopolymer interaction studies.* Spectroscopy, 2004. **18**(4).

163. Gill, I. and A. Ballesteros, *Bioencapsulation within synthetic polymers (Part 1): sol–gel encapsulated biologicals.* Trends in Biotechnology, 2000. **18**(7): p. 282-296.

164. Finnie, K.S., et al., *Formation of Silica Nanoparticles in Microemulsions.* Langmuir, 2007. **23**(6): p. 3017-3024.

165. Yong, C.P. and L.M. Gan, *Microemulsion Polymerizations and Reactions*, in *Polymer Particles: -/-*, M. Okubo, Editor. 2005, Springer Berlin Heidelberg: Berlin, Heidelberg. p. 257-298.

166. Sager, W.F.C., *Controlled formation of nanoparticles from microemulsions.* Current Opinion in Colloid & Interface Science, 1998. **3**(3): p. 276-283.

167. Jaramillo, N., C. Paucar, and C. García, *Influence of the reaction time and the Triton x-100/Cyclohexane/Methanol/H2O ratio on the morphology and size of silica nanoparticles synthesized via sol–gel assisted by reverse micelle microemulsion.* Journal of Materials Science, 2014. **49**(9): p. 3400-3406.

168. Soares, J.P., et al., *Thermal behavior of alginic acid and its sodium salt.* Eclética Química, 2004. **29**: p. 57-64.

169. Zhuravlev, L.T., *The surface chemistry of amorphous silica. Zhuravlev model.* Colloids and Surfaces A: Physicochemical and Engineering Aspects, 2000. **173**(1–3): p. 1-38.

170. Osseo-Asare, K. and F.J. Arriagada, *Preparation of SiO2 nanoparticles in a non-ionic reverse micellar system.* Colloids and Surfaces, 1990. **50**: p. 321-339.

171. Ab Rahman, I. and V. Padavettan, *Synthesis of Silica Nanoparticles by Sol-Gel: Size-Dependent Properties, Surface Modification, and Applications in Silica-Polymer Nanocomposites-A Review*. Journal of Nanomaterials, 2012. p. 132424-15

172. Thibaud, C., et al., *Sol-Gel Biopolymer/Silica Nanocomposites in Biotechnology.* Current Nanoscience, 2006. **2**(3): p. 219-230.

173. Lal, J. and L. Auvray, *Perturbations of microemulsion droplets by confinement and adsorption of polymer*. Journal de Physique II, 1994. **4**(12): p. 2119-2125.

174. Stubenrauch, C., *Microemulsions: Background, New Concepts, Applications, Perspectives*. 1 edition ed. 2008: Wiley-Blackwell. 140.

175. Ikeda, H., T. Murata, and S. Fujino, *Preparation and photoluminescence of monolithic silica glass doped with Tb3+ ions using SiO2–PVA nanocomposite.* Optical Materials, 2014. **36**(7): p. 1119-1122.

176. Constantin, S. and R. Freitag, *One-Step Synthesis of Monolithic Silica Nanocomposites in Fused Silica Capillaries.* Journal of Sol-Gel Science and Technology, 2003. **28**(1): p. 71-80.

177. Wang, S., et al., *Synthesis of magnetite–silica core–shell nanoparticles via direct silicon oxidation.* Journal of Colloid and Interface Science, 2014. **432**: p. 43-46.

178. Sun, Y., et al., *Water-Based Synthesis of Ultrasmall PEGylated Gold–Silica Core–Shell Nanoparticles with Long-Term Stability*. Chemistry of Materials, 2014. **26**(18): p. 5201-5207.

179. Ow, H., et al., *Bright and Stable Core−Shell Fluorescent Silica Nanoparticles.* Nano Letters, 2005. **5**(1): p. 113-117.

180. Gao, X., et al., *Synthesis and characterization of functionalized rhodamine B-doped silica nanoparticles.* Optical Materials, 2009. **31**(11): p. 1715-1719.

181. Bae, S.W., W. Tan, and J.-I. Hong, *Fluorescent dye-doped silica nanoparticles: new tools for bioapplications.* Chemical Communications, 2012. **48**(17): p. 2270-2282.

182. Wang, Y., et al., *Rhodamine B doped silica nanoparticle labels for protein microarray detection.* Science China Chemistry, 2010. **53**(4): p. 747-751.

183. Li, L., et al., *Effect of formulation variables on in vitro release of a water-soluble drug from chitosan–sodium alginate matrix tablets.* Asian Journal of Pharmaceutical Sciences, 2015. **10**(4): p. 314-321.

184. Cuomo, F., et al., *Loading and Protection of Hydrophilic Molecules into Liposome-Templated Polyelectrolyte Nanocapsules.* Langmuir, 2014. **30**(27): p. 7993-7999.

185. Chen, J., et al., *The Preparation of Capsaicin-Chitosan Microspheres (CCMS) Enteric Coated Tablets.* International Journal of Molecular Sciences, 2013. **14**(12): p. 24305.

186. Inoue, K., *Managing adverse effects of glaucoma medications.* Clinical Ophthalmology (Auckland, N.Z.), 2014. **8**: p. 903-913.

187. Rathore, K.S., R. Nema, and S. Sisodia, *Preparation and characterization of timolol maleate ocular films.* Int J PharmTech Res, 2010. **2**(3): p. 1995-2000.

188. Tan, B. and S.E. Rankin, *Study of the Effects of Progressive Changes in Alkoxysilane Structure on Sol−Gel Reactivity.* The Journal of Physical Chemistry B, 2006. **110**(45): p. 22353-22364.

189. Jung Jung, H. and A. Chauhan, *Ophthalmic drug delivery by contact lenses.* Expert Review of Ophthalmology, 2012. **7**(3): p. 199-201.

190. Hsu, K.-H., et al., *Dual drug delivery from vitamin E loaded contact lenses for glaucoma therapy.* European Journal of Pharmaceutics and Biopharmaceutics, 2015. **94**: p. 312-321.

191. Jung, H.J., et al., *Glaucoma therapy by extended release of timolol from nanoparticle loaded silicone-hydrogel contact lenses.* Journal of Controlled Release, 2013. **165**(1): p. 82-89.

192. Ciolino, J.B., et al., *In vivo performance of a drug-eluting contact lens to treat glaucoma for a month.* Biomaterials, 2014. **35**(1): p. 432-439.

193. Gulsen, D., C.-C. Li, and A. Chauhan, *Dispersion of DMPC Liposomes in Contact Lenses for Ophthalmic Drug Delivery.* Current Eye Research, 2005. **30**(12): p. 1071-1080.

194. Xu, J., X. Li, and F. Sun, *Cyclodextrin-containing hydrogels for contact lenses as a platform for drug incorporation and release.* Acta Biomaterialia, 2010. **6**(2): p. 486-493.

195. Harvitt, D.M. and J.A. Bonanno, *Re-evaluation of the oxygen diffusion model for predicting minimum contact lens Dk/t values needed to avoid corneal anoxia.* Optom Vis Sci, 1999. **76**(10): p. 712-9.

196. Nicolson, P.C. and J. Vogt, *Soft contact lens polymers: an evolution.* Biomaterials, 2001. **22**(24): p. 3273-3283.

197. Chyasnavichyus, M., S.L. Young, and V.V. Tsukruk, *Mapping micromechanical properties of soft polymer contact lenses.* Polymer, 2014. **55**(23): p. 6091-6101.